ORNL-3238
UC-80 – Reactor Technology
TID-4500 (17th ed.)

MARITIME REACTOR PROGRAM

ANNUAL PROGRESS REPORT

FOR PERIOD ENDING NOVEMBER 30, 1961

OAK RIDGE NATIONAL LABORATORY
operated by
UNION CARBIDE CORPORATION
for the
U.S. ATOMIC ENERGY COMMISSION

DISCLAIMER

Printed in USA. Price $2.50 cents. Available from the

Office of Technical Services
U. S. Department of Commerce
Washington 25, D. C.

ORNL-3238

UC-80 — Reactor Technology
TID-4500 (17th ed.)

Contract No. W-7405-eng-26

MARITIME REACTOR PROGRAM
ANNUAL PROGRESS REPORT

For Period Ending November 30, 1961

H. C. McCurdy, Program Coordinator

DATE ISSUED

MAR 9 - 1962

OAK RIDGE NATIONAL LABORATORY
Oak Ridge, Tennessee
operated by
UNION CARBIDE CORPORATION
for the
U. S. ATOMIC ENERGY COMMISSION

THIS PAGE

WAS INTENTIONALLY

LEFT BLANK

CONTENTS

1. INTRODUCTION AND SUMMARY

The Laboratory has, since September 1957, provided technical assistance to the AEC Division of Reactor Development (Office of Maritime Reactors) on certain aspects of the NS SAVANNAH program. The NS SAVANNAH, which will be the first nuclear-powered merchant ship, was built by New York Shipbuilding Corporation of Camden, New Jersey. The 63-Mw (thermal) pressurized-water reactor and the propulsion equipment were supplied by The Babcock & Wilcox Company of Lynchburg, Virginia. States Marine Lines, Inc., will operate the ship as an agent for the Maritime Administration following completion of the sea trials by the builder. Over-all program direction is exercised for the Government by the Maritime Administration-Atomic Energy Commission Joint Group.

Construction of the NS SAVANNAH was complete as of May 1, 1961. Following extensive public hearings, which were held March 6–8 and April 12, 1961, the Atomic Energy Commission on July 24, 1961, authorized, subject to certain conditions, the fueling, startup, and operation of the NS SAVANNAH's reactor for test and demonstration purposes at Camden, New Jersey, and at Yorktown, Virginia. An extended precritical test program culminated in a coordinated systems test, or "dummy run," which was completed on October 18. Fueling was authorized by the AEC on November 24, 1961. Fuel loading was carried out during a 30-hr period November 27–28, 1961. Assembly of the reactor vessel head and control drives was under way at the end of this report period.

Tests at power levels up to 10% of rated power will be conducted at Camden. The NS SAVANNAH will then be moved by auxiliary power to Yorktown for additional dockside testing up to full power and for sea trials by the builder, using Yorktown as an operational base.

The Laboratory's Maritime Program is determined to a considerable extent by needs which develop in the NS SAVANNAH project; the specialized facilities and personnel of the Laboratory often can be employed advantageously to supplement the efforts of the principal participants. Thus, the nature of the ORNL program is supplemental, resulting in diversified, but somewhat disconnected, activities whose common tie is that they are

in support of some aspect of the NS SAVANNAH project. In general, the experimental and theoretical investigations are limited in scale and scope and are intended to meet specific needs.

NS SAVANNAH Project – General Support

During the current report period the Laboratory continued to act as an inspection agency for the AEC, witnessing inspections and tests during fabrication of nuclear components. The principal components involved were the replacement control rod drives, the spare reactor vessel head, and Core II fuel elements.

Consultation and design review services were provided as requested. The bulk of this effort was concerned with the replacement control rod drive program and with the NS SAVANNAH startup tests. Laboratory personnel participated in the public hearings.

Preparations were completed for a survey of the exterior of the reactor compartment shield. The survey will be made under the direction of ORNL personnel when the reactor can be operated at full power.

An experimental program was initiated to develop a procedure for in situ measurement of the iodine-removal efficiency of the reactor compartment filter unit. A facility for testing prototype charcoal units was constructed and put into operation. In a related program the iodine collection efficiency of the charcoal cartridges which are to be used for environmental monitoring on the ship is being determined. A preliminary test gave an efficiency of 99.4%, but the iodine concentrations were much higher than desired. Methods of producing iodine concentrations in air in the maximum permissible concentration $(MPC)_a$ range are being studied.

Assistance was given to the NS SAVANNAH Medical Department in the development of a shipboard bioassay program. Experimental studies were carried out to determine the lowest detectable limits of a representative corrosion product (Co^{58}) in raw urine specimens. External body counting experiments using a man-simulating phantom indicated that the detection of about 0.1 μc of either Fe^{59} or Co^{60} or a combination of both in either spleen or lung appears to be feasible. Tests in counting samples of serum

from neutron-irradiated blood showed that a 2- by 2-in. NaI(Tl) crystal is much less satisfactory for detection of Na^{24} than a 3- by 3-in. crystal. NS SAVANNAH counting equipment was used in these experiments.

Charpy impact specimens from excess material used to fabricate the reactor vessel upper closure head were irradiated in the ORR pressurized-water in-pile loop and tested by the Naval Research Laboratory. The results showed an increase in the nil-ductility-transition (NDT) temperature of 190°F for a fast-neutron (>1 Mev) dosage of 2.6×10^{19} neutrons/cm^2. The dose rate was about two orders of magnitude higher than is expected in the NS SAVANNAH reactor vessel wall.

ORNL personnel assisted in an investigation of possible corrosion consequences as a result of the thermal insulation on the NS SAVANNAH primary piping becoming wet during precritical testing. Metallographic examination of a section of suspect piping showed evidences of incipient chloride stress-corrosion cracking. Procedures were developed for cleaning, inspecting, and reinsulating the affected piping.

Pressurized-Water In-Pile Loop

The Maritime-ORR pressurized-water in-pile loop continued to operate in a satisfactory and essentially trouble-free manner. Some improvements were made in instrumentation for flux-monitoring and for analysis of dissolved oxygen in the water.

Water chemistry studies were initiated to investigate the transport and deposition of corrosion products ("crud") and of long-lived water-borne activity. During the period of normal loop operation the level of water-borne long-lived activity is relatively low, being about 2×10^4 disintegrations per second per liter. The level increases by a factor of about 50 during loop startup, primarily because of an increase in crud level. Studies of the characteristics of the crud showed nearly complete absence of crud particles in the 0.01- to 0.5-μ range and indicated that magnetite (Fe_3O_4) is present in the crud as well-developed crystallites. The implication is that recrystallization of the magnetite occurs, and this implies that appreciable radiochemical exchange takes place between

activated and nonactivated crud. These studies support the view that magnetite may be a desirable material for use as a high-temperature filter ion-exchange medium for pressurized-water reactor systems, and therefore exploratory tests were started.

Advanced Core Development

An evaluation of the substitution of Zircaloy for stainless steel in the fuel-element containers was completed, and a final report is being prepared. Physics calculations indicated that replacement of the stainless steel fuel container in a 4.2 wt % U^{235} enriched core (the enrichment of the inner zone of Core I) by a Zircaloy fuel container could increase the cold, clean reactivity of the core by $\Delta k = 0.065$, the worth of the 21 control rods by $\Delta k = 0.04$, and the reactivity lifetime by a factor of 2. If the enrichment of the Zircaloy fuel container core were reduced to 3.86 wt % U^{235}, the same shutdown control margin could be obtained and 0.9 full-power years longer life. For the same reactivity lifetime the enrichment could be reduced to 3.38 wt % U^{235}.

From a detailed stress analysis it was determined that a wall thickness of 0.140 in. would be adequate for a fuel container fabricated from 20% cold-worked Zircaloy provided certain design modifications were made. An evaluation of the compatibility of Zircaloy with NS SAVANNAH operating conditions indicated that Zircaloy-4 would be adequate for long-term service in the reactor. Zircaloy-4 is preferred over Zircaloy-2 because of a lower tendency for hydrogen absorption.

A fuel-cycle cost analysis was performed to estimate the cost savings that would result from the Zircaloy substitution. A 30% reduction in fuel-cycle cost is indicated if the Zircaloy is utilized to extend core lifetime as much as possible without decreasing the shutdown control margin. It was found that the relative cost savings are somewhat insensitive to uncertainties in the absolute magnitude of fuel-cycle cost components.

Additional lifetime calculations were made using the CANDLE code to investigate the effects of various fuel-management schemes on the burnup of an initial two-zone Core I (4.2 wt % U^{235} inner zone, 4.6 wt % U^{235}

outer zone). The schemes examined were: (1) switch inner and outer fuel zones at the end of Core I burnup; (2) remove the burned inner zone, replace it by the burned outer zone, and insert a fresh outer zone; and (3) leave the burned Core I fuel in place but replace the stainless steel fuel container by a Zircaloy fuel container. Of the three fuel-management schemes studied, the Zircaloy substitution (scheme 3) was found to be the most attractive from the point of view of increased reactivity lifetime.

Fuel rod swaging studies demonstrated that nonstoichiometric UO_2 can be utilized to produce high-density UO_2 fuel rods by subjecting the rods to a postswaging sintering treatment. Corrosion-erosion tests of intentionally defected UO_2 fuel rods were carried out in high-temperature water. Swaged rods showed weight increases which appeared to result from oxidation of the UO_2 to a higher oxide. Weight changes in rods containing UO_2 pellets were essentially negligible. The coefficient of thermal expansion of swaged fuel rods containing UO_2 was determined. Measured expansion coefficients were intermediate between values for the individual materials, indicating that some interaction between the fuel and cladding occurs under isothermal conditions. The fission-gas-release rate parameter, D', was determined for fused-and-ground UO_2 powder, which is a possible fuel for Core III of the NS SAVANNAH. The measured values are of the same order of magnitude as reported earlier for the UO_2 pellets used in Core I.

Irradiation test specimens were fabricated for ORR pressurized-water in-pile loop experiments Nos. 4, 5, and 6, using both swaging and vibratory-compaction techniques. Brazing procedures were developed and a full-size prototype bundle for a proposed Vallecitos Boiling-Water Reactor test was brazed and found to be within the required dimensional tolerances. Fabrication studies on vibratory-compacted fuel defined the particle-size distributions which would yield high bulk densities. A maximum density of about 87.5% of theoretical was obtained using mixtures of two particle-size fractions. Maximum densities about 1% higher were obtainable with three-fraction mixtures.

An investigation of gas evolution from fused-and-ground UO_2 was carried out to determine the source and nature of gas which could cause the fuel-rod swelling sometimes observed when clusters of swaged fuel-rods

were brazed in hydrogen at 1010°C. It was found that the swelling problem could be eliminated by outgassing the oxide for 24 hr at 1000°C in vacuum prior to use. It was also learned that the major fraction of the gases released was nitrogen, probably present in the UO_2 as adsorbed gas or as an organic compound.

Irradiation tests of swaged and vibratory-compacted UO_2 fuel in stainless steel rods are being conducted in the ORR pressurized-water in-pile loop. The program presently planned consists of six experiments involving a total of 24 fuel rods which are being irradiated in clusters of three. Each test fuel rod is 0.5 in. in diameter and has an approximately 16-in. fueled length; the clad material is 0.035-in.-thick type 304 stainless steel. The maximum heat flux ranges from 90 000 to 550 000 Btu/hr·ft^2, and the expected peak burnup ranges from 900 to 11 000 Mwd/MT of UO_2.

Irradiation of three of the experimental assemblies was completed; two others are being irradiated. Postirradiation examination of the six swaged fuel rods making up experimental assembly No. 1 was completed at the General Electric Company's Vallecitos Atomic Laboratory. The peak heat flux in this assembly is estimated to have been 115 000 Btu/hr·ft^2, and the peak burnup was measured to be 1050 Mwd/MT of UO_2. No appreciable dimensional changes or other deleterious effects were noted. Little, if any, sintering of the fuel body could be detected. The Kr^{85} released was measured for each rod, and values ranging from 0.7 to 6.1% were obtained.

2. NS SAVANNAH PROJECT — GENERAL SUPPORT

Shield Survey

T. V. Blosser

A proposed survey of the exterior of the NS SAVANNAH reactor compartment shield was described in the previous report in this series.[1] In that report the extremely low permissible levels of radiation (in some regions as low as 0.5 rem/yr) were listed, the design of suitable instrumentation for measurement of such levels was projected, and a series of measurements using a mockup of the NS SAVANNAH shield at the Bulk Shielding Facility (BSF) was proposed. The progress of the experimental program and the development of the required instrumentation are described here.

Design Dose Rates

For convenience the design dose rates for the NS SAVANNAH shield, unchanged since the previous report, are repeated in Table 2.1. The 0.5 rem/yr dose rates permitted in passenger and crew areas obviously govern the design of the shielding. Of this dose rate 10% is assumed to be contributed by fast neutrons, while the remainder is assumed to be from gamma rays. A sectional view of the ship, the reactor, and the associated shields is shown in Fig. 2.1.

Measurements at the BSF

The measurements at the BSF have now been completed. The primary purpose of these experiments was to calibrate the radiation-detection instruments to be used in the NS SAVANNAH survey in radiation fields, the spectra of which would be fair approximations of the spectra expected from the NS SAVANNAH shield. To this end, data were obtained behind two mockups constructed in the BSF pool.[2] Both mockups are compared with a schematic representation of the actual shield in Fig. 2.2.

---

[1] Maritime Reactor Project Ann. Prog. Rep. Nov. 30, 1960, ORNL-3046, pp. 5–11.

[2] The Illmenite concrete slabs utilized in the mockup were fabricated by ORNL under the supervision of the Prepakt Co. who supplied the aggregate.

Table 2.1. Design Dose Rates for the NS SAVANNAH Shield

Location	Operating Conditions	Type of Access	Control Area	Design Dose Rate
Access spaces outside secondary shield (passenger spaces)	Full power	Normal	Yes (initial operations)	5.0 rem/yr
			No (ultimately)	0.5 rem/yr
Access spaces outside secondary shield (crew spaces)	Full power	Normal	Yes	5.0 rem/yr
Cargo holds	One-fifth of full power	Limited	Yes	0.5 rem/yr
Inside containment vessel	Reactor operating	Not permitted	Yes	
	Reactor shut down 1/2 hr or longer; no fission products in primary loops	Limited	Yes	200 mr/hr
Locations occupied during fuel transfer operations	Reactor shut down 3 days or longer	Limited	Yes	200 mr/hr (transient conditions)
				10 mr/hr (continuing conditions)

The gate in the BSF pool that permits selectively draining one part of the pool while retaining the water in the other proved convenient in these experiments. The reactor, pressure vessel, and water annulus portions of the NS SAVANNAH shield were mocked up on the water side of the gate, while the secondary shield was mocked up in the dry area. However, a background gamma-ray activity of 2 to 10 mr/hr remaining from a previous and unrelated experiment necessitated shielding of nearby structural components with 2-in. slabs of lead. For all measurements, complete background traverses were made at the same positions as the data traverses. In addition, the streaming around the mockup edges was assayed and corrected for. It will be noted that various compressions were required in the mockups because of the much lower power of the Bulk Shielding Reactor (BSR) compared with the NS SAVANNAH reactor (1 Mw versus 69 Mw) and the space limitations of the BSF pool. These compressions are not believed to have significantly affected the simulation of the expected spectra or to have disturbed the equilibrium between fast-neutron and thermal-neutron fluxes.

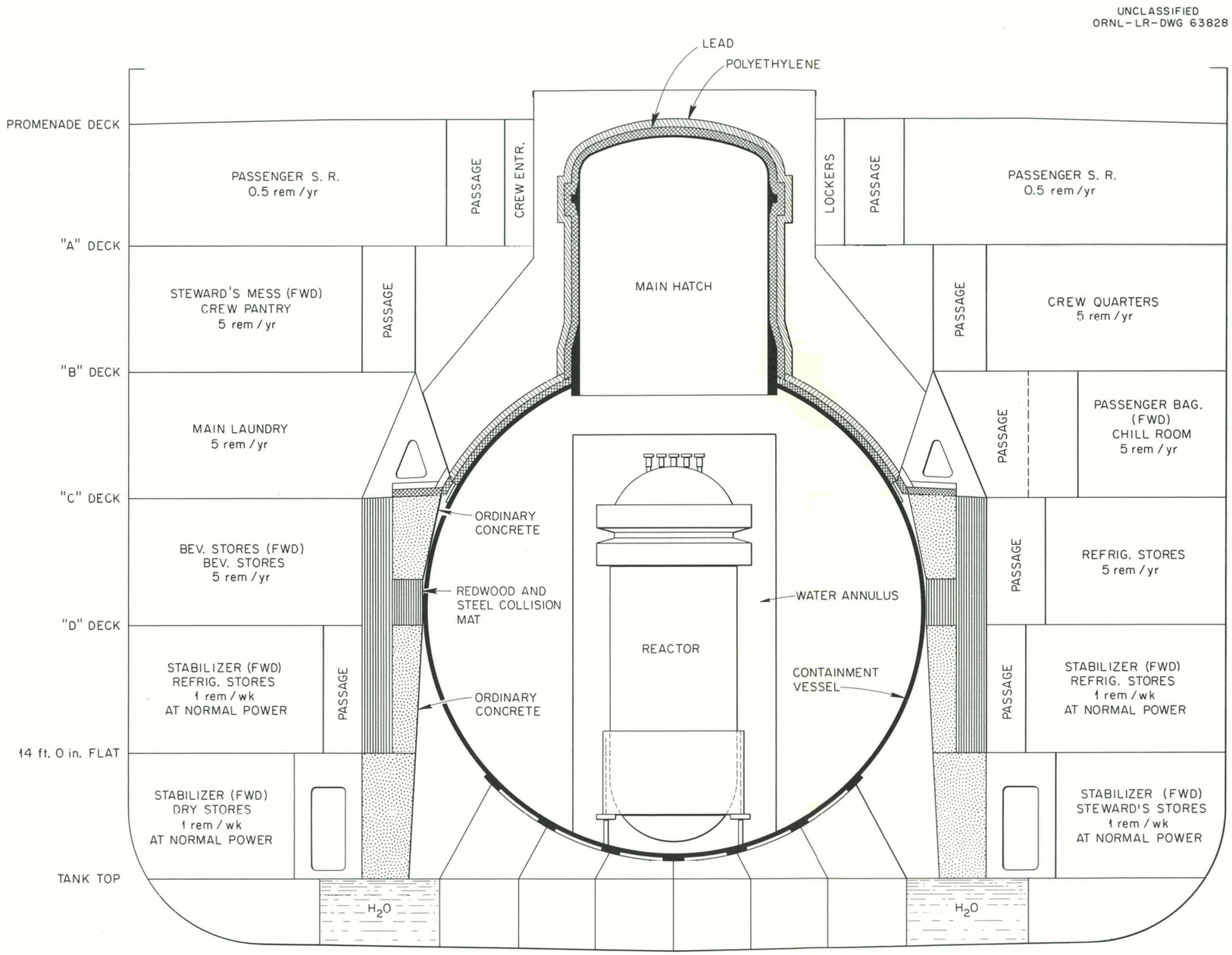

Fig. 2.1. Cross Section of NS SAVANNAH, Reactor, and Shield, Looking Forward.

UNCLASSIFIED
ORNL-LR-DWG 63827

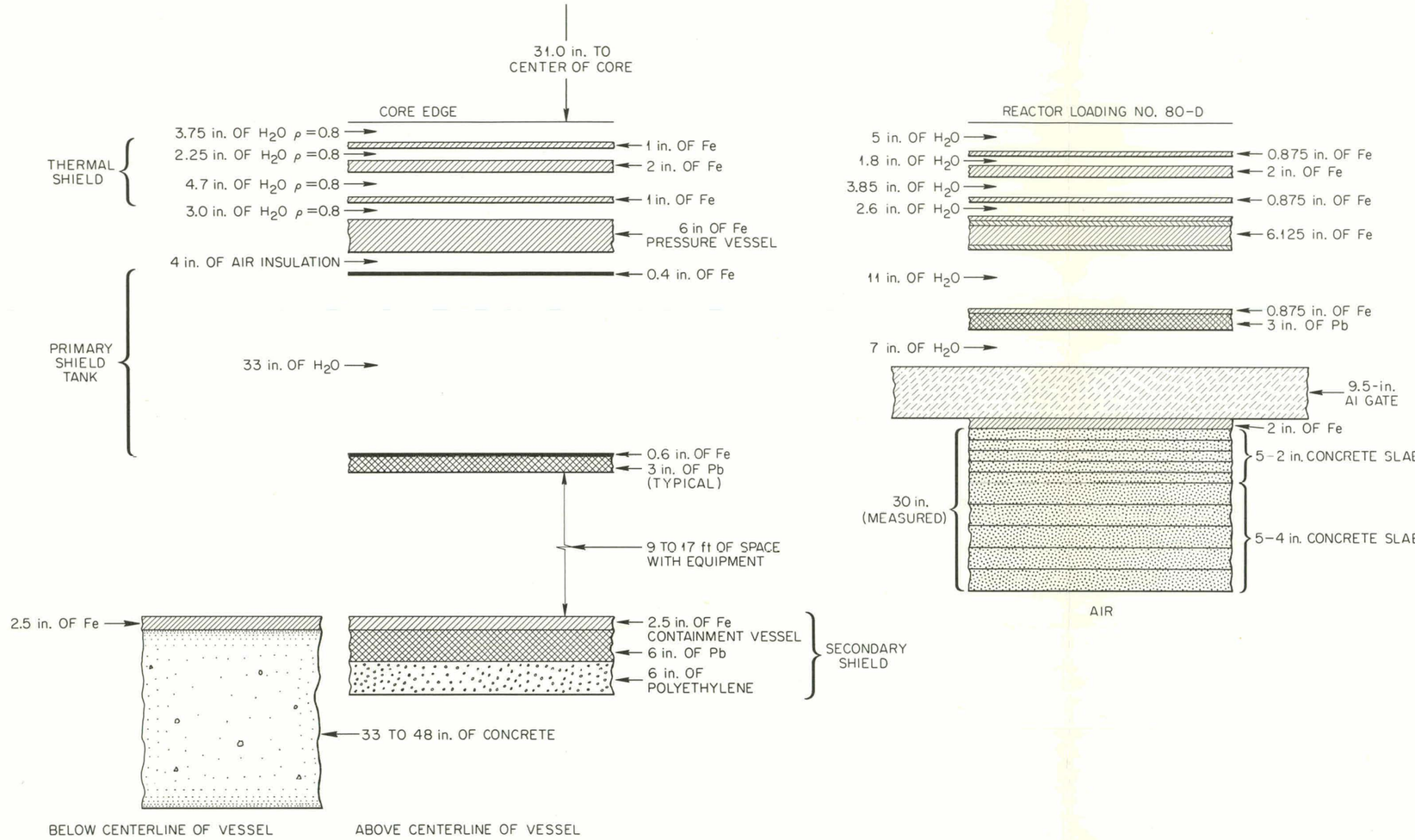

Fig. 2.2. Comparison of Schematic NS SAVANNAH Shield with Mockups Used in BSF Tests.

Prior to the start of the BSF experiments, the dose rate anticipated behind the mockup was calculated by using the design parameters of the actual shield, corrected for the modifications required by the mockup and the geometrical R^2 attenuation, in conjunction with the known dose per watt at the surface of the BSR-1 core, as plotted by Maienschein et al.[3] The results gave ~0.3 mrad/hr as the fast-neutron dose rate at a reactor power of 100 kw, and 2.1 mr/hr as the gamma-ray dose rate at a reactor power of 100 kw. The thermal flux was not estimated. Because of the various approximations involved and the use of graphs to obtain certain values, the accuracy of these numbers was not expected to be better than a factor of about 2.

Dose rates actually measured behind one of the mockups in the BSF pool by various instruments are compared with the results of calculations in Table 2.2. The agreement may be seen to be well within expectations.

[3]F. C. Maienschein et al., ORNL Dwg. 2-01-058-0-366.

Table 2.2. Comparison of the Response of Various Instruments to Radiation Leaking from NS SAVANNAH Mockup Shield[a] in BSF

Detector	Reactor Power (kw)	Dose Rate
Gamma Rays (computed rate = ~2.1 mr/hr)		
900-cm^3 ion chamber	100	1.15 mr/hr
Anthracene crystal	100	1.50 mr/hr
	10	0.155 mr/hr
Fast Neutrons (computed rate = 0.3 mrad/hr)		
Hurst-type dosimeter	100	(b)
Modified long counter	100	0.5 mrad/hr
	10	0.056 mrad/hr

[a]This was the version of the mockup which contained a 30-in. slab of concrete. Instruments were uniformly positioned 10 cm behind the mockup.

[b]Count rate too low to measure dose with this instrument.

Radiation-Detection Instruments

The instrumentation required for the NS SAVANNAH survey has been essentially perfected and installed in the Vanette truck previously pictured.[4] Calibrations have been completed and the entire complex has been thoroughly tested by field studies of two land-based reactors.

Since the quantity to be evaluated in the NS SAVANNAH survey will be the biological effectiveness of its shield, a prime requirement of the detection equipment, in addition to high sensitivity, is that the detectors be capable of calibration in terms of dose to human tissue. The dose is obtained separately for gamma rays, fast neutrons, thermal neutrons, and intermediate-energy neutrons. Because the biological dose from fast neutrons and gamma rays is proportional to the energy lost by the radiation in passing through tissue, the gamma-ray and fast-neutron detectors should have absorptive characteristics similar to human tissue. On the other hand, the biological dose from thermal neutrons is proportional to the number of thermal neutrons absorbed in the tissue, and thus an instrument measuring thermal-neutron flux is suitable. The instruments presently in use are described below.

Gamma-Ray Detectors. Two gamma-ray detectors are included in the present equipment. The first is a 900-cm^3, CO_2-filled, carbon-walled ionization chamber of a type that has been commonly employed at several ORNL shielding facilities. Its reliability is a matter of record, but since the minimum gamma-ray dose that can be measured with this instrument is ~10 mr/hr, its use will be restricted to detector intercalibrations and to measurements of the dose in excess of 50 mr/hr that are permitted (according to Table 2.1) in certain limited-access areas of the ship.

The primary gamma-ray measuring instrument is an anthracene-crystal scintillation counter. In the usual method of operating such a detector, the total current output of its associated photomultiplier is read by an electrometer-type of circuit. In the present application sensitivity has

[4]Maritime Reactor Project Ann. Prog. Rep. Nov. 30, 1960, ORNL-3046, pp. 12–14, Figs. 2.3, 2.4, 2.5.

been increased by using a pulse-counting technique, which permits measurement of dose rates as low as ~0.01 mr/hr.

The theory on which this technique is based may be briefly outlined. If a plot is made of the integral count rate as a function of energy (or pulse height) of the gamma rays impinging on a detector, then the area under the resulting curve will be a measure of the tissue dose rate at the detector, provided the response of the detector relative to tissue is sensibly constant over the range of energies involved. Carr and Hine[5] have reported that the dosage measurements with anthracene crystals show a tissue equivalence for gamma rays from 0.2 to 3.0 Mev. From the plot of the first-collision dose rate as a function of energy, shown in Fig. 2.3 for tissue and anthracene, it can be seen that the response of anthracene is theoretically tissue-equivalent within ±1% from 100 kev to at least 7.0 Mev.

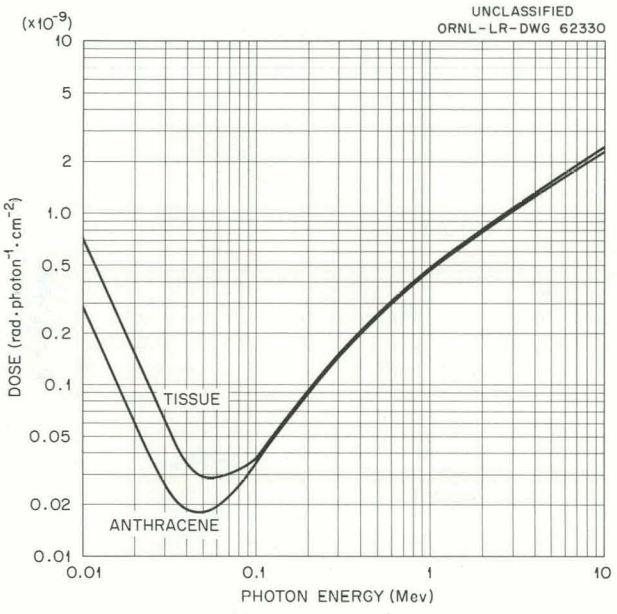

Fig. 2.3. First-Collision Dose Rates in Tissue and Anthracene as Functions of Photon Energy.

The apparent difficulty in the application of the method lies in the fact that for each point where a dose measurement is desired a gamma-ray spectrum must be plotted, unless the gamma-ray field is such that the energy spectrum does not vary appreciably. Under these circumstances the count rate at a fixed energy bias can be related to the area under the spectrum, which in turn is a measure of the dose rate. In the present application, however, the spectrum may not remain constant, since the shield may be penetrated by tubes, cooling circuits, etc.

---

[5]R. T. Carr and G. J. Hine, Nucleonics, 11: 53 (1953).

The pulse-counting method has been made applicable, however, by the development of a small, transistorized integrator, having the equivalent of 80 input channels, which can be mounted within a standard AID amplifier. The response of the integrator is linear to within ±5% over the entire pulse-height range of interest. Its design is such that dose rates as high as 100 mr/hr can be measured without significant errors from counting losses.

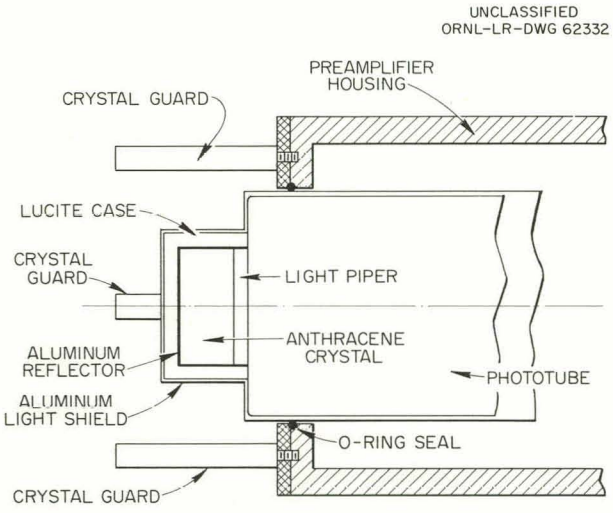

Fig. 2.4. Arrangement of the Anthracene Crystal.

The construction of the dosimeter proper is shown in Fig. 2.4. It consists of a 1-in.-diam, 1/2-in.-thick, anthracene crystal wrapped in an aluminum-coated Mylar reflecting foil 200 $\mu g/cm^2$ thick and installed in a 3-mm-thick Lucite case and light piper in contact with the cathode of a low-dark-current type-RCA-6655 photomultiplier tube. A light-tight, 5-mil-thick, aluminum jacket protects the crystal.

The 3-mm-thick Lucite cover serves to balance the loss in light yield which would result from energetic photoelectrons and Compton electrons escaping from the crystal without losing all their energy to a scintillation. The Lucite scatters a portion of these electrons back into the crystal.

The dosimeter has been calibrated against known-strength gamma-ray sources of various energies. The strengths of the sources were known to ±3% from measurements in a calibrated gas ionization chamber. From the calibrations against the known-strength sources, two quantities were obtained. The first was the pulse height corresponding to the photopeak, plotted in Fig. 2.5 as a function of maximum recoil electron energy. The excellent linearity of the curve shows that over this energy range, at

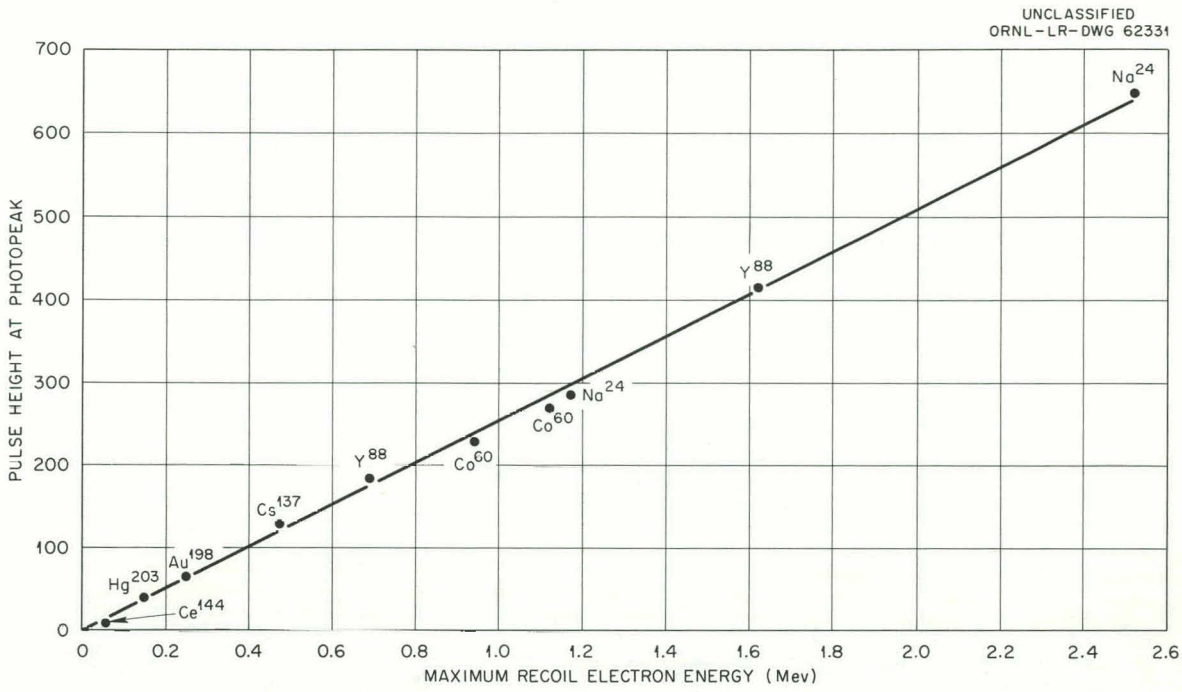

Fig. 2.5. Pulse Height at Photopeak as a Function of Maximum Recoil Energy.

least, the height of the pulse is directly proportional to the electron energy.

The second quantity of interest, the pulse-height spectrum, was obtained for all the sources, and the area under the integral count rate versus pulse-height curve was obtained numerically. Dose rates were computed for each of the known sources, and a ratio of dose rate to the area under the corresponding pulse-height spectrum was computed. These results are shown in Table 2.3.

It may be seen that with the exception of Hg^{203}, all sources give a figure for the dose rate per unit area that is independent of source energy to within ±5%. The behavior of Hg^{203} results from an appreciable portion of its dose rate coming from pulses that are not energetic enough to overcome the energy bias (~50 kev) of the detector. From the tabulated data it is clear that the dose in tissue, in mrad/hr, can be expressed as 5.1×10^{-7} A, where A is the area under a curve of integral counts per minute as a function of pulse-height settings such that the maximum pulse-height setting is taken as 1000.

Table 2.3. Ratio of Computed Dose Rate from Various Gamma-Ray Sources to Area Under Observed Pulse-Height Spectra

Source	Energy (Mev)	Ratio of Dose to Area
		$\times 10^{-7}$
Hg^{203}	0.279	6.94[a]
Au^{198}	0.412	5.24
Cs^{137}	0.662	5.30
Ra	~1.0 (av)	5.04
Co^{60}	1.17	4.94
	1.33	
Na^{24}	1.38	5.00
	2.76	
	Average	5.1

[a]Excluded from average.

The neutron sensitivity of the detector was checked with a polonium-beryllium source. It was found that the detector senses only about 2% of the actual neutron dose.

Thermal-Neutron Flux Measurements. Thermal-neutron fluxes will be measured with a highly sensitive BF_3 proportional counter. A diagram of this counter is shown in Fig. 2.6. The fill gas is BF_3, enriched to 96% in B^{10}, at a pressure of 76 cm Hg, that is, essentially 1 atm. Such a pressure, several times that customarily used, not only increases sensitivity but also makes the counter better able to withstand accidental damage during field use.

The BF_3 counters have been calibrated by comparison with absolute flux measurements made with foils. The vertical thermal column of the ORNL Graphite Reactor was used for the calibrations, which were made in both water and air.

Such calibrations involve only straightforward comparisons, and in the present case the single difficulty involved the assignment of a location for the center of detection of the counter tube. The most simple approach, of course, is to assume that the center of detection is the geometrical axis of the counter. Since the flux varies logarithmically

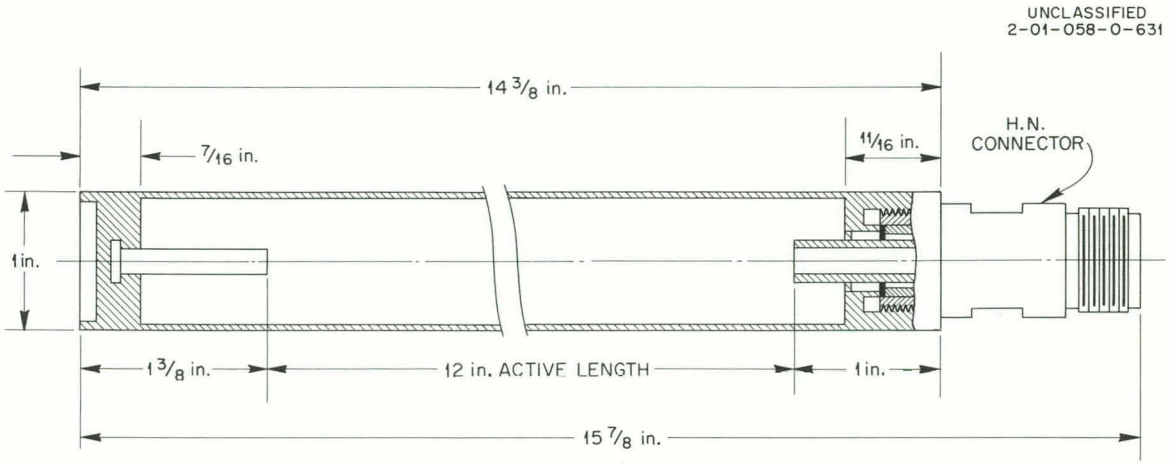

NOTE: BODY MATERIAL: TYPE-1100 ALUMINUM
FILL GAS: BF_3
0.002-in. TUNGSTEN ANODE
INSULATOR MATERIAL: 96-98 % Al_2O_3
CONNECTOR MATERIAL: BRASS

Fig. 2.6. Diagram of BF_3 Proportional Counter.

with z, a more sophisticated approach is to assume that the center of detection is at the logarithmic mean between the z's of the leading and trailing edges of the tube. With the present counter this point is 0.4 cm before the geometric axis. For the present application, however, a numerical method was devised. The counter tube was assumed to be divided into 20 longitudinal strips, and the response of each strip in a 2.71-cm relaxation length field was separately evaluated. By this method the center of detection falls 0.7 cm before the counter axis. Results for all three methods are shown in Table 2.4. The numerical method is believed to be the most physically realistic of the three, and the response of 275 cpm per unit flux obtained by its use will be accepted in practice. This value is for the counter when used in water. A value for air, obtained by comparison with foil measurements within and above an 8-in.-diam, air-filled tube placed in the thermal column, is 355 cpm per unit flux.

Fast-Neutron Detectors. Proton recoil proportional counters of the Hurst type have been widely used for fast-neutron detection at various ORNL shielding facilities. Present techniques, however, place a lower limit of ~1 mrad/hr on the measurable dose rate with such counters, and the lower energy bias level is approximately 0.2 Mev. In order to cover

Table 2.4. BF_3 Counter Response in Water for Three Assumptions of Center of Detection

Assumed Center of Detection of Counter	Distance of Center Above Bottom of Thermal Column (cm)	Average Flux from Gold-Foil Data (neutrons/cm^2·sec)	Counter Response (cpm per unit flux)
On geometrical axis	32.57	77.5	282
At logarithmic mean of edges	32.2	88.9	246
0.7 cm before geometric axis[a]	32.5	79.6	275

[a]Computed by numerical method described in text.

the energy range below this cutoff and to achieve a greater degree of sensitivity, a modified long counter will be used. This modified long counter essentially consists of a high-pressure BF_3 counter enclosed in a cadmium-covered polyethylene cylinder, with the polyethylene thicknesses adjusted to give a counter response proportional to the physical dose. Another cylinder in which the polyethylene thickness has been adjusted to give a response proportional to the biological dose is also available. A detailed description of the modified long counter and its calibration is presently being prepared.

Iodine Adsorption Studies

R. E. Adams W. E. Browning, Jr.

Reactor Compartment Unit

An activated-charcoal iodine adsorption unit will be used to process the radioiodine which may be present in the ventilation gases from the reactor containment vessel of the NS SAVANNAH under normal and emergency conditions before release of these gases to the environment. While existing experimental data are sufficient to demonstrate the feasibility of a design utilizing activated charcoal for the removal of iodine vapor from moist air streams,[6] additional study is needed to ensure that the iodine

[6]R. E. Adams and W. E. Browning, Jr., Removal of Radioiodine from Air-Steam Mixtures, ORNL-CF-60-11-39, November 14, 1960.

adsorbers specified for the NS SAVANNAH will provide the required iodine-removal efficiency under the operating conditions peculiar to the reactor compartment emergency ventilation system.

Laboratory studies are under way on samples of the activated charcoal used in the full-size iodine adsorbers (Pittsburgh BPL) and on prototype charcoal units (11 in. × 11 in. × 1.125 in.) manufactured by the same process as was used in the production of the full-size iodine adsorbers. The experimental facility for testing the prototype units under specified operating conditions is essentially complete. Initial operation of the test system indicated that several minor deficiencies exist, and these are being corrected.

The efficiency of an iodine adsorber unit depends upon the form in which iodine exists in the gas stream. It may be in the form of vapor or an iodide or it may be adsorbed on very small particles present in the gas stream. For laboratory tests simulating shipboard conditions to be valid the iodine in each case must be adequately characterized as to form. Special equipment has been fabricated for determining the character or form of radioiodine in gas systems, and initial calibration or familiarization tests are under way.

Environmental Monitors

Environmental monitoring for the presence of radioiodine in the various inhabited compartments of the ship will be accomplished by passing a measured volume of air through an activated-charcoal cartridge. Iodine radioactivity in the cartridge will then be determined by one of several types of radiation detection instruments, that is, a G-M survey meter, a G-M scaler, or a multichannel gamma-ray spectrometer. Iodine-131 "standards" were fabricated at ORNL and supplied to New York Shipbuilding Corporation for determining the response of these instruments. These standards contained amounts of I^{131} equivalent to 0.1, 1.0, 10, and 100 times the $(MPC)_a$, maximum permissible concentration in air, for continuous exposure to I^{131}. The standards were constructed to represent an air sample volume of 2.25 m^3. Tests were conducted to determine the

volume flow rate which could be drawn through charcoal cartridges by the air samplers which will be used on the NS SAVANNAH. With a modified cartridge designed to optimize the sampling flow rate, a 2.25 m^3 volume of air could be processed in 10 min. The multichannel gamma-ray spectrometer was able to detect I^{131} equivalent to the $(MPC)_a$ in a 10-min sample, while the G-M survey meter and scaler were applicable to the 10 to 100 times the $(MPC)_a$ range.

It is necessary to know the adsorption or collection efficiency under conditions of high gas velocity through the charcoal mass and very low mass concentrations of iodine in air in order to successfully monitor iodine with activated charcoal cartridges. A 1-in.-diam, 1.25-in.-deep column of Pittsburgh PCB charcoal, 6/16 mesh, was studied at 24°C with a linear air velocity through the charcoal of 298 fpm. For a test period of 40 min, the iodine collection efficiency was determined to be 99.40%. This test was run with iodine concentrations much larger than desired, since it is difficult to produce in the laboratory a concentration of iodine in air that is equivalent to $(MPC)_a$ conditions. Several methods of producing the desired conditions are being studied.

Bioassay Development Program

B. R. Fish G. W. Royster, Jr.

Shipboard bioassay procedures are being developed for the NS SAVANNAH Medical Department. Initial efforts have been directed toward establishing procedures with which significant internal exposures may be recognized. This screening process must be reliable, and it must be capable of selecting a few significant exposures from among a relatively large number of candidates. Because of space and equipment limitations, a procedure requiring a minimum of sample processing is desired.

One promising method for shipboard use is direct counting of raw urine specimens using an NaI crystal and a multichannel analyzer. The crystal and analyzer that will be installed aboard the NS SAVANNAH have been used in all the developmental work.

Urinalysis for Radioactive Corrosion Products

It is believed at this time that the most probable internal exposure incident aboard the NS SAVANNAH would involve radioactive corrosion products. For this reason, initial efforts have been directed toward establishing the lowest detectable limits of a representative corrosion product (Co^{58}) in raw urine specimens. It is expected that by finding the Co^{58} content in urine at a known time after an exposure, the Co^{58} exposure can be calculated. Then, the total exposure can be estimated on the basis of the amount of Co^{58} taken into the body and the a priori knowledge of the corrosion-product mixture.

Initial efforts to establish the lowest detectable amounts of Co^{58} in raw urine specimens were begun during the first week of June 1961. Because Co^{58} was not readily available, Mn^{54} (0.84-Mev γ) was used to simulate Co^{58} (0.81-Mev γ). Since Co^{60} will also be present in the urine, an effort was made to determine the lowest detectable counting rate of Co^{58} in the presence of Co^{60}. The relative amounts of the two isotopes used in these studies correspond to the proportions predicted to be found in the primary coolant water after 30 days of reactor operation. Scattered gamma rays from Co^{60} are recorded in the same group of channels in which gamma rays emitted by Co^{58} are detected. Thus, it is necessary to determine the background in the Co^{58} band that is due to scatter from Co^{60}. For a given counting arrangement, there is a constant ratio of the net counting rate in the Co^{60} photopeaks to the net counting rate that is due to scatter into the energy band which includes the Co^{58} photopeak. This ratio was determined for samples of various volumes. Samples containing Co^{58} or Co^{60} or both were counted and analyzed using the 2-in. by 2-in. well-type NaI crystal which will be installed on the NS SAVANNAH, a 3-in. by 3-in. well-type crystal, and a 4-in. by 2-in. solid crystal. The RCLiac 128-channel analyzer was used with each of the crystals. Counting efficiencies for samples of various volumes are listed in Table 2.5, and the spectra of a 50-ml sample containing both Mn^{54} and Co^{60} are presented in Fig. 2.7. The channel shifts and nonlinearities evident in Fig. 2.7 are representative of the equipment problems experienced in the

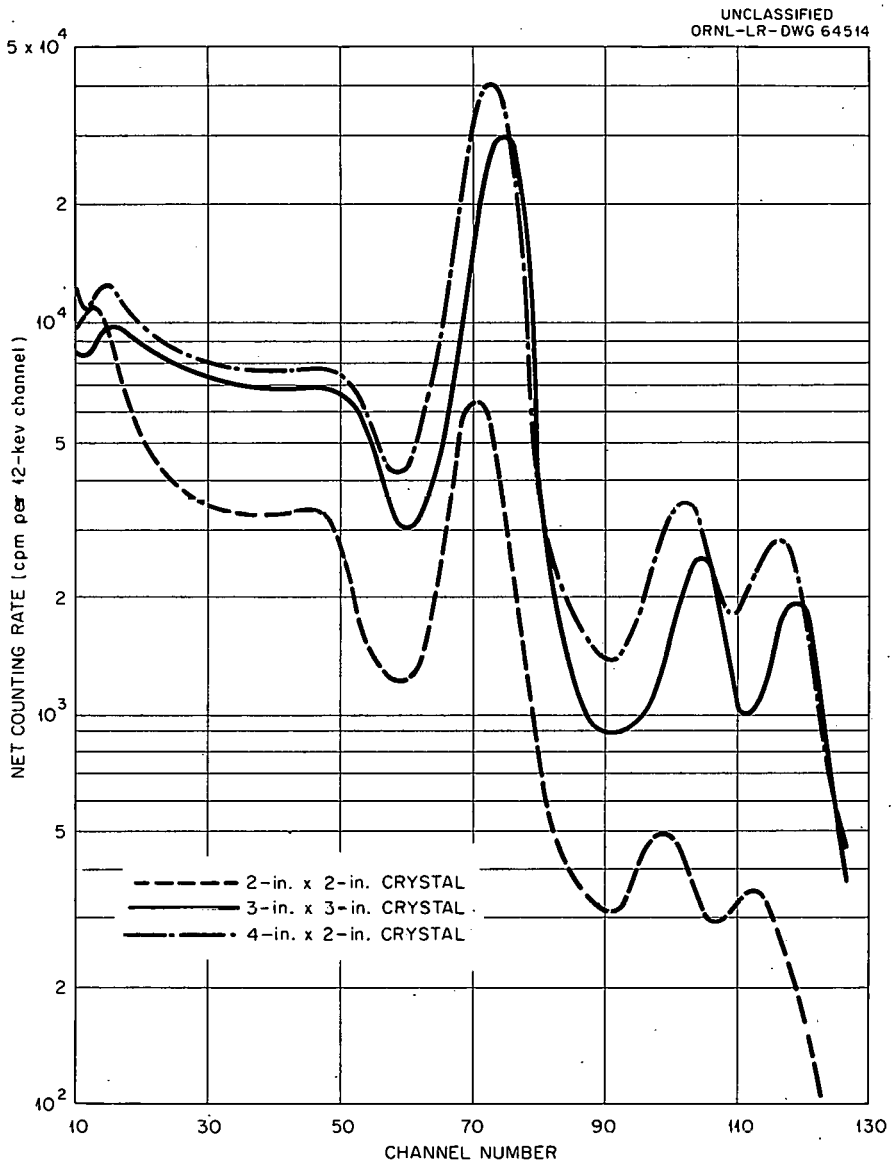

Fig. 2.7. Spectra of Mn^{54} and Co^{60} Obtained from a 50-ml Urine Specimen in a 2-in.-diam Plastic Box Placed on Top of NaI Crystals of Various Sizes.

early part of the program. By September most of the instrumental difficulties had been resolved. The lowest detectable amounts of Mn^{54} (or Co^{58}) per urine sample for various sample volumes are given in Table 2.6. Clearly, any estimate of least detectable quantity depends directly upon the background at the time and place where the counting is carried out.

Table 2.5. Counting Efficiencies of NaI Crystals for Mn^{54} and Co^{60} in Urine Samples of Various Sizes

Sample Volume (ml)	Average Counting Efficiencies (%)			
	Mn^{54}		Co^{60}	
	2-in. by 2-in. Crystal	3-in. by 3-in. Crystal	2-in. by 2-in. Crystal	3-in. by 3-in. Crystal
1	7.9[a]	23.5[a] 7.8	5.8[a]	5.8
2	7.7[a]	22.2[a] 6.8	5.7[a]	12.1[a] 5.1
3	7.2[a]	5.9	5.3[a]	4.6
4	6.5[a]	5.2	5.0[a]	4.1
50	1.1	5.1	0.98	4.0
100	0.78	4.8	0.70	3.8
200	0.61	3.8	0.57	3.2
300	0.52	3.3	0.48	2.7

[a]Counted in well (other samples counted on top of crystal).

Table 2.6. Lowest Detectable Activity in Urine Samples Measured with a 2-in. by 2-in. NaI Crystal

RCLiac Channels 65 Through 79 at 12 kev per Channel

Sample Volume (ml)	Lowest Detectable Mn^{54} Activity Per Sample (dpm)	Estimated Equivalent Daily[a] Rate of Urinary Excretion of Mn^{54} or Co^{58} (dpm per day)
1	410[b]	610 000
2	430[b]	330 000
3	460[b]	230 000
4	510[b]	190 000
50	3000[c]	90 000
100	4200[c]	63 000
200	5200[c]	39 000
300	6100[c]	30 000

[a]Assumed urine output of 1500 ml/day.

[b]Sample in crystal well.

[c]Sample on top of crystal.

External Scanning of Body-Organ Deposits

External body-counting experiments for the detection of Fe^{59} in the spleen and Co^{60} in the lungs were carried out with a man-simulating phantom. The NS SAVANNAH counting equipment was used by removing the crystal from the shield and placing the crystal over the organ in question while the phantom was in a prone position on a cot. The Fe^{59} in the spleen was in the form of a homogeneous aqueous solution. The Co^{60} was contained in four small plastic vials of equal activity, and one of these was placed in each of the four lung compartments of the phantom.

Agreement between determinations performed on consecutive days was rather poor, primarily because of the large variations in background experienced with the unshielded detector; however, based on these preliminary experiments, the detection of about 0.1 μc of either Fe^{59} or Co^{60} or a combination of both in either spleen or lung appears to be feasible. Use of a collimated detector to reduce background should improve the reliability of this technique.

Blood Analysis for Na^{24}

Samples of serum from neutron-irradiated blood were counted using the 2-in. by 2-in. NaI(Tl) crystal with the RCLiac 128-channel analyzer and a 3-in. by 3-in. crystal with a Radiation Instrument Development Laboratory 200-channel analyzer. The 2-in. by 2-in. crystal was much less satisfactory for detection of Na^{24} than the 3-in. by 3-in. crystal. For the 2.75-Mev photopeak of Na^{24}, the peak-to-valley ratio is 1.1 using the 2-in. by 2-in. crystal, whereas this ratio is 4.7 for the 3-in. by 3-in. crystal.

Correlation of Urine Excretion and Body Burden

Whole-body counter and urinalysis data of humans accidentally exposed to radioactive corrosion products are being collected and analyzed. These data will aid in relating the cobalt concentration in urine to an order-of-magnitude estimate of the total corrosion-product exposure.

Replacement Control Rod Drives

S. I. Kaplan E. R. Mann

A replacement control rod drive system is being prepared for the NS SAVANNAH reactor as a part of an upgrading program. Assistance has been provided in the following aspects of this program:

1. development (by the Marvel-Schebler Division, Borg-Warner Corporation) of a set of canned control rod drives actuated by a solid-state, pulse-type control system that positions the rods according to a preset program,
2. preparation of a control rod withdrawal sequence for core I that is intended to introduce an essentially uniform reactivity increment per unit rod withdrawal over the major portion of the total rod worth,
3. analog computations by The Babcock & Wilcox Company to examine the safety aspects of the Marvel-Schebler design and the compatibility of the design with the ship's operating requirements.

The more basic recommendations submitted in reviews of the Marvel-Schebler work concerned the incorporation of rod position information which could be automatically compared with the position input signal, the need for a means of checking the rod withdrawal patterns without moving the rods, the reliability of the scram circuitry, and the use of analog simulation of the Marvel-Schebler system to observe any control and safety problems peculiar to the new rod drives. Portions of the draft material for the supplementary safeguards report covering installation of the Marvel-Schebler equipment were also reveiwed to assist The Babcock & Wilcox Company (B&W) in its responsibility for compiling and presenting this document.

In the proposed control rod positioning program, the order of rod withdrawal approximates that specified by B&W for the original rod drives and the Bailey controller. While the rod program requires simultaneous motion of more than one rod bank, B&W investigations predict that no local hot spots will be generated by this mode of operation. The rate of reactivity addition provided is adequate to meet all NS SAVANNAH maneuvering

specifications, contingent upon the realization of a power reactivity deficit of 1.32% Δk between zero and full power, as was assumed for the core I reference design. If high-power operating experience reveals a significantly different reactivity deficit, the program can be readily modified to match the existing conditions. A comparable scheme will be generated for core II, based upon data from the core II zero power experiments.

The analog simulation of the Marvel-Schebler system was started in March 1961 by B&W personnel under the direction of the ORNL Reactor Controls Department. The ORNL analog computer facility was utilized pending preparations to use the computer portion of the NS SAVANNAH training simulator at Lynchburg College, Lynchburg, Virginia. The work was transferred to Lynchburg in May 1961 and is continuing under the direction of B&W personnel, with advice and assistance furnished by ORNL as requested.

Irradiation Testing of Pressure-Vessel Steel

V. O. Haynes W. C. Thurber

An evaluation of the neutron-irradiation-induced changes in steel obtained from scrap from the NS SAVANNAH pressure vessel has been completed. The procedures employed and the results obtained are summarized in the following paragraphs. A report on this topic is being prepared.

Irradiation Conditions

Charpy impact specimens were machined from scrap material identified as A212, grade B, carbon-silicon steel obtained from the slab used for the upper closure head. Thirty-two specimens were irradiated in the pressurized-water loop in the Oak Ridge Research Reactor. The irradiation specimens were canned in groups of eight in stainless steel, as shown in Fig. 2.8. Nickel wires were included at each of the notch positions for neutron-dose monitoring. Two cans were interconnected so that two groups of eight specimens could be inserted into each leg of the hairpin loop facility. The as-fabricated assemblies are shown in Fig. 2.9. The

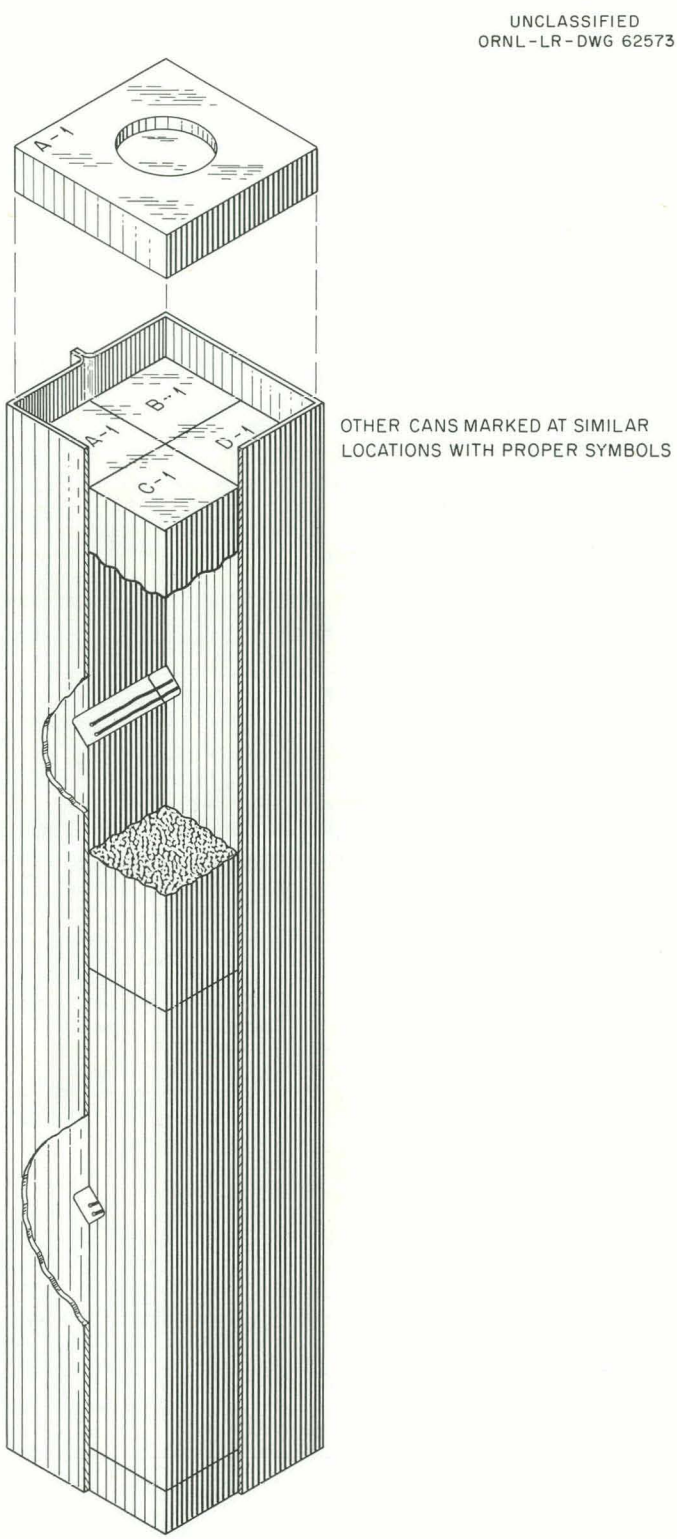

Fig. 2.8. Arrangement and Identification of Charpy Impact Specimens Within Upper Can of the Irradiation Assembly, A-1 Leg.

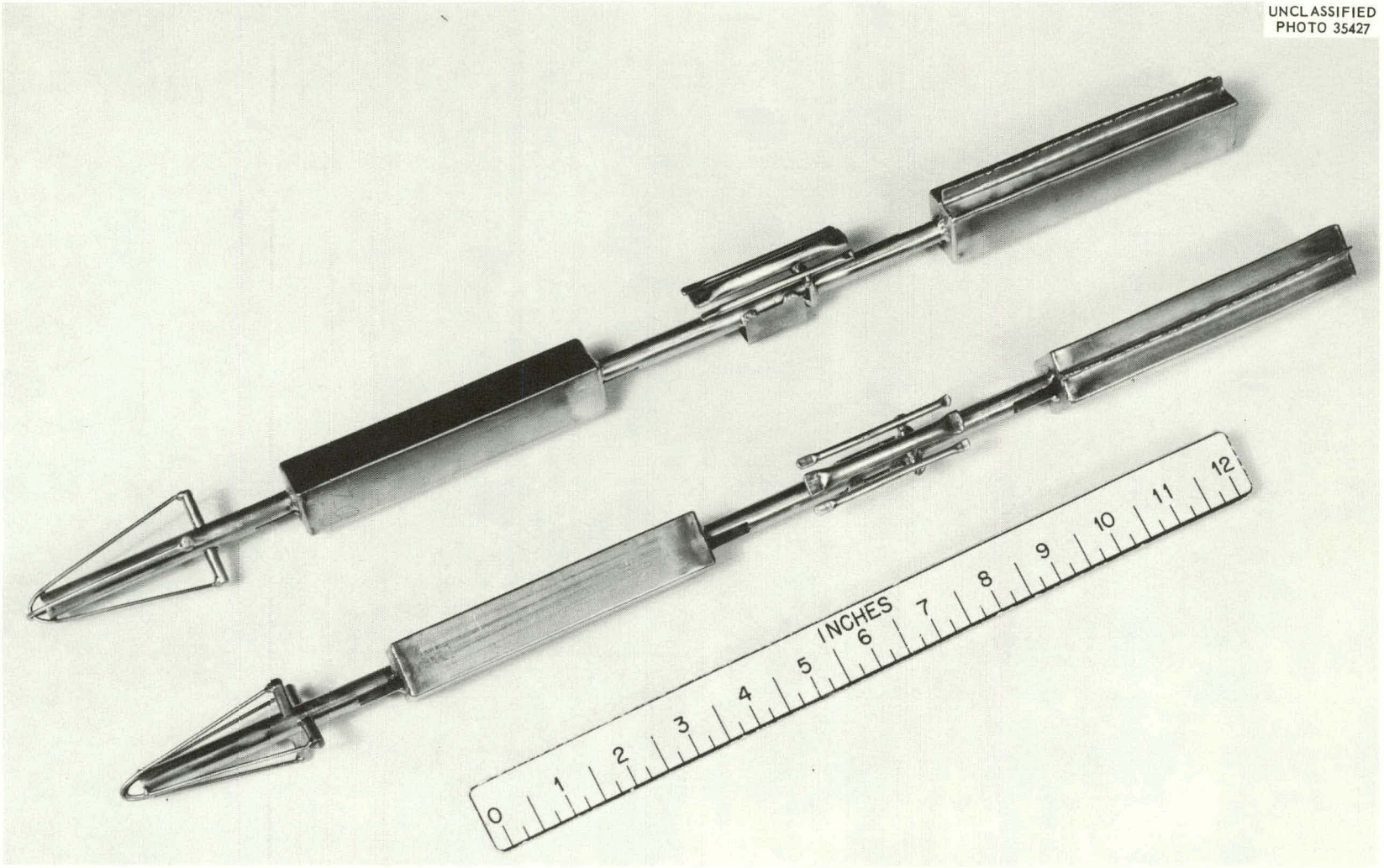

Fig. 2.9. As-Fabricated Charpy Impact Specimen Irradiation Assemblies.

small tubes between groups of specimens contained additional neutron-flux monitors. The position of the specimens relative to the reactor is shown by Fig. 2.10.

One cycle of ORR operation, which consisted of three weeks at a nominal 20-Mw reactor power, was used for the irradiation. During this time the loop water was maintained at 475°F and 1750 psi. The pressure was important to the experiment only in that it was utilized to compress the can walls against the specimens for better heat transfer between the specimens and the can.

The dose received by the specimens was obtained by analysis of the Co^{58} activity induced in the nickel wires, and temperature was computed based on estimates of the gamma heating in the specimens. Generalized results of these computations are given by Table 2.7.

Table 2.7. Neutron Irradiation Data for Tests of Charpy Impact Specimens

Specimen Group	Fast Neutron (>1 Mev) Dose (neutrons/cm^2)	Irradiation Temperature (°F)
	$\times 10^{19}$	
I	0.44	495
II and III	1.1	505
IV	2.6	515

Test Results

The irradiated specimens were broken at the Naval Research Laboratory along with nine unirradiated control specimens which had received a 500°F, 23-day heat treatment. The reported impact energy fracture values are plotted in Fig. 2.11 to show the nil-ductility-transition (NDT) temperatures of the various specimens.

A previous determination established 20 ft-lb as the best correlation energy between Charpy impact specimens of this material and NDT temperature

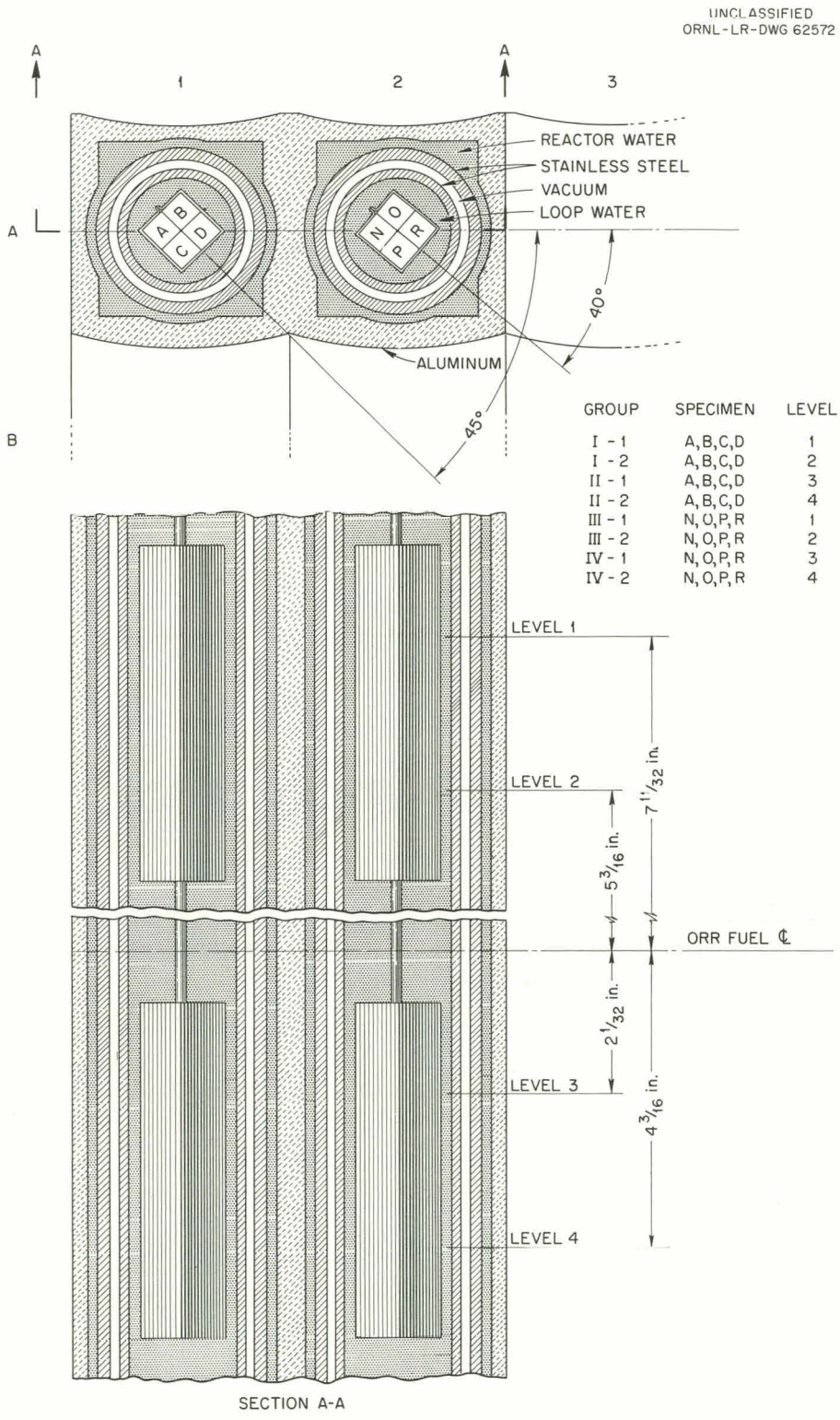

Fig. 2.10. Irradiation Position and Identification of Charpy Impact Specimens in the ORR.

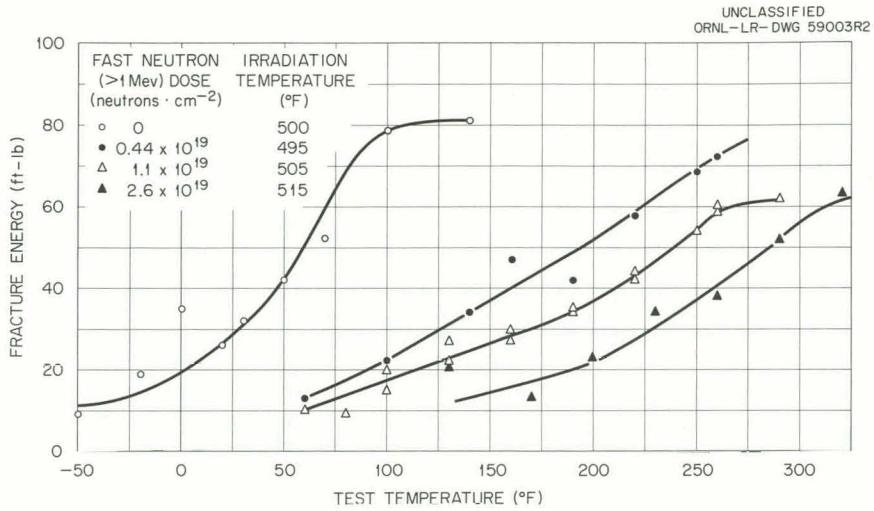

Fig. 2.11. Charpy Specimen Fracture Energy vs Test Temperature for Various Doses. Data are for A212B steel from the NS SAVANNAH pressure vessel.

as determined by drop-weight tests.[7] Based on this value, the data of Fig. 2.11 show the transition temperature increases summarized in Table 2.8.

Table 2.8. NDT Temperature Shifts of Irradiated Charpy Impact Specimens of NS SAVANNAH Pressure Vessel Steel

Specimen Group	NDT Temperature Shift (°F)	Fast Neutron (>1 Mev) Dose (neutrons/cm^2)
		$\times 10^{19}$
I	90	0.44
II and III	115	1.1
IV	190	2.6

The percentage of fibrous fracture as a function of temperature was also reported, and the data are plotted in Fig. 2.12. A change of this property in relation to fast-neutron dose may also be noted.

[7]W. C. Thurber and J. T. Lamartine, Determination of the Nil-Ductility-Transition Temperature for A212B Steel Used in the NS SAVANNAH Pressure Vessel, ORNL-CF-59-7-143, July 23, 1959.

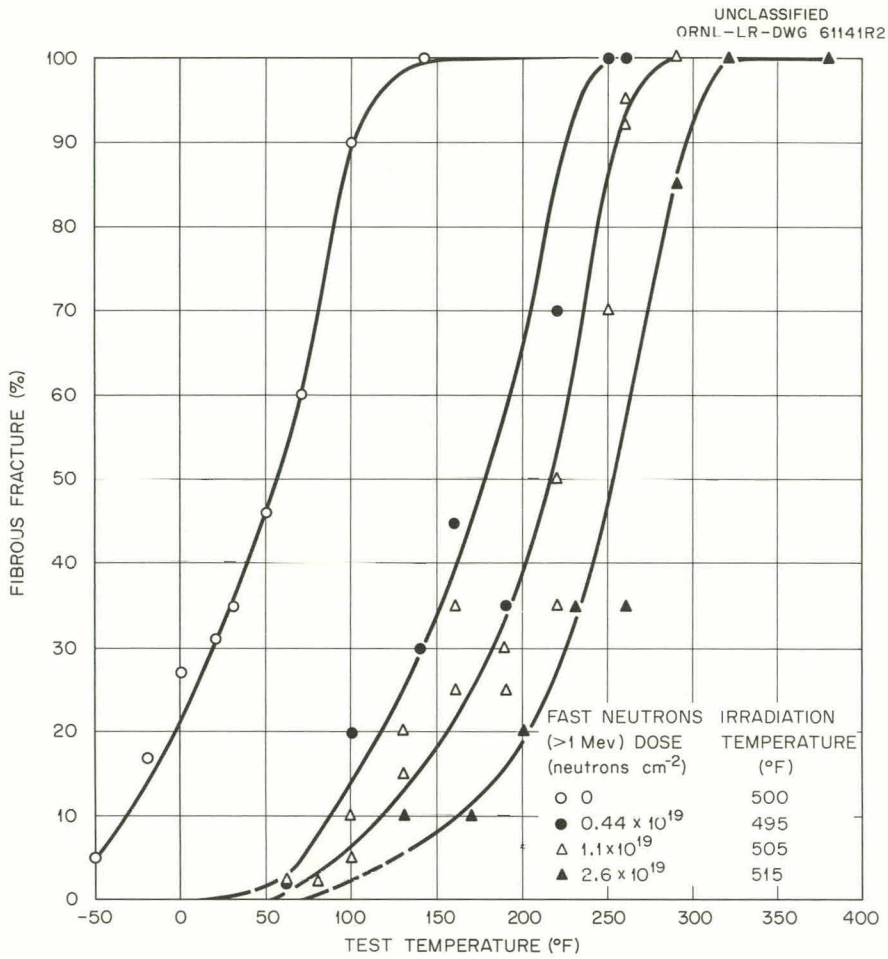

Fig. 2.12. Percentage Fibrous Fracture in Charpy Specimens vs Test Temperature for Various Doses. Data are for A212B steel from the NS SAVANNAH pressure vessel.

Thermal Insulation Investigation

L. D. Schaffer

During the precritical testing of the NS SAVANNAH primary water system, the piping was insulated to allow the temperature of the system to be raised so that the hot-flushing operation could be performed. Since the system was still under inspection for water integrity, all joints and areas of potential leaks were left uninsulated to permit observation during the hot-flushing operation. The applied insulation was not water-proofed because the insulating operation had not been completed. In the course of hot flushing, several leaks developed in the primary system and a valve

gasket failed. As a result, the insulation within the reactor compartment was wetted in several locations. The system was thermally cycled several times after the leaks developed.

Since it was known that the thermal insulation contained some chlorides, an investigation was initiated to determine whether the system had been damaged by chloride stress-corrosion cracking. Ebasco Services Incorporated inspectors removed the insulation and inspected the PP-IV line on the inlet side of the letdown coolers where water leakage was known to have been heavy. It was necessary during removal of the insulation to mechanically clean from the pipe a tightly adhering deposit which appeared to be the protective shipping tape baked in place. After cleaning, the pipe surface was dye-penetrant inspected for cracks. Defects were observed that varied in length from 1/16 to 3/4 in. They were mainly aligned with the longitudinal axis of the pipe, although some were irregular and transverse to the pipe axis. After an unsuccessful attempt to remove the defects by light grinding, a 6-in. section of this pipe, including a pipe elbow, was removed and sent to the Oak Ridge National Laboratory for metallographic examination. In addition, two 3-ft-long sections of as-received piping (2-in., sched-160, type 304 stainless steel) similar to that removed from the NS SAVANNAH primary system and samples of both dry insulation and insulation known to have been wetted were sent to the Oak Ridge National Laboratory for study.

The pipe removed from the NS SAVANNAH was badly battered as a result of the cutting operation at the Shipyard, as may be seen in Fig. 2.13, but many areas of definite, longitudinal, crackline defects were revealed by fluorescent-penetrant inspection. A total of six metallographic sections were taken of prominent and typical defects on the section of piping. Two sections showed defects which were either laps or stringered inclusions encountering the surface at a low angle, and two other sections showed only shallow grooves. However, two of the sections revealed defects which appeared to be intergranular and intragranular defects, 3 to 4 mils deep, normal to the surface. These defects, shown in Figs. 2.14 and 2.15, appeared as straight-line indications parallel to the longitudinal axis of

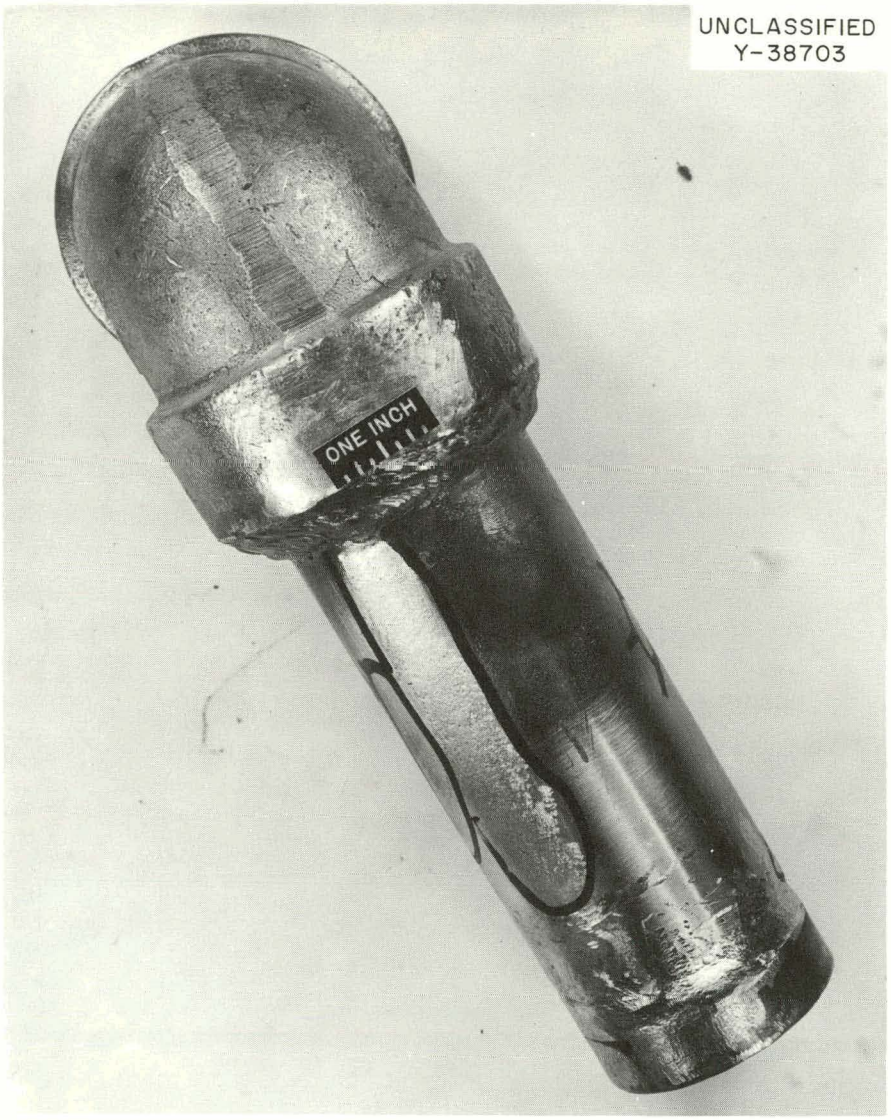

Fig. 2.13. Section of PP-1V Line After Cleaning.

the pipe, which could mean that they were originally created during fabrication and served in this instance as sites for the concentration of chlorides and as origins for chloride stress-corrosion cracking.

Fluorescent-penetrant inspection of the as-received piping sections showed that both the density and the intensity of the defect indications were less than had been observed on the PP-IV specimen. Two sections were examined in which defect indications were noted. Metallographic examination revealed that these flaws were laps or inclusions.

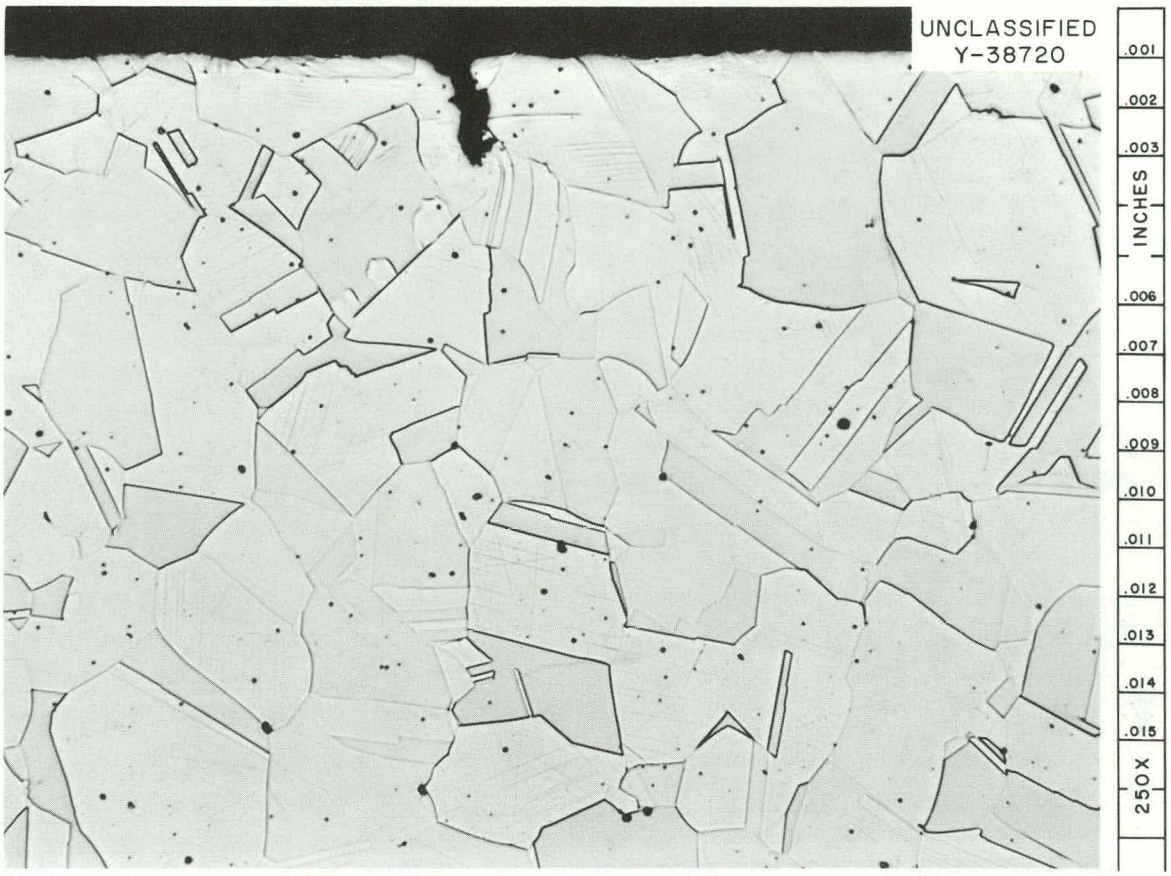

Fig. 2.14. Photomicrograph of Penetration Normal to Surface of Pipe PP-1V. Etchant: modified aqua regia. 250X

The thermal insulation received at ORNL was analyzed to determine the total chloride content and the amount of chloride that could be removed by water leaching. The insulation that had remained dry in the reactor compartment was found to contain 275 ppm chloride, and the insulation that had been wetted was found to contain 190 ppm chloride when analyzed by the same method. A block of the dry insulation was set in a beaker of cold water for 47 hr without agitation. After this period the water was analyzed and found to have leached 85 ppm chloride from the insulation block. In a parallel test the water was heated to boiling and the amount of chloride extracted rose to 200 ppm.

A third phase of this investigation was directed at establishing whether the fabrication stresses in the 2-in., sched-160, stainless steel pipe were of sufficient magnitude to induce cracking in a chloride-bearing

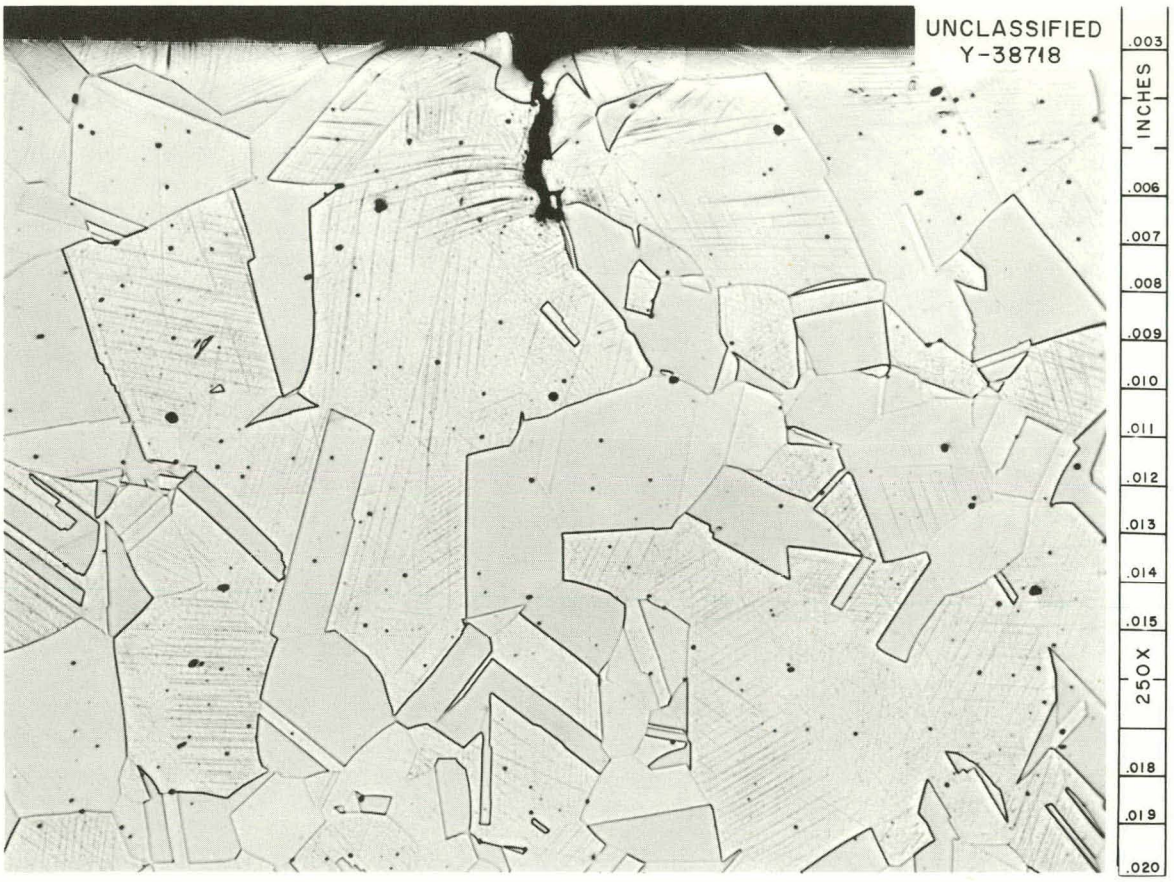

Fig. 2.15. Photomicrograph of Pentration Normal to Surface of Pipe PP-1V. Etchant: modified aqua regia. 250X

environment. Autoclave tests were performed in which a cross section of the stainless steel pipe taken from the reactor system was exposed at 250°C in deionized water containing 110 ppm chloride for 100 hr. As a result of this exposure the metal became heavily corroded, but no cracks were found. The corrosion rate amounted to 62 mpy.

In an attempt to reduce the excessive corrosion, the chloride concentration was reduced to 50 ppm, and the test was run, as before, on the same test specimen, along with an annealed control specimen. After the 100-hr test period, the sample and its control specimen were examined. The over-all corrosion rate was appreciably less severe. Microscopic examination showed several areas that appeared to contain fine cracks. These two specimens were then exposed during an additional 100-hr run to a fresh solution containing 50 ppm chloride.

After the tests, the specimens were studied metallographically. The control specimen showed no cracking, but the pipe section showed cracking on both the outer and inner surface of the pipe. Cracks typical of those found in the reactor piping section are shown in Fig. 2.16.

Three conclusions were reached on the basis of the laboratory tests. First, the insulation contained appreciable water-soluble chlorides which could be leached from the insulation and deposited on the primary piping at the thermal conditions that existed in the NS SAVANNAH primary system. Second, it was found that the residual stresses in the stainless steel piping under study were of sufficient magnitude to cause chloride stress-corrosion cracking when the pipe was exposed to chloride-containing water at elevated temperatures. Third, from the metallographic examination it appears that chloride stress-corrosion cracking was responsible for the two defects shown in Figs. 2.14 and 2.15 but that the attack was in an early stage. This view is supported by the conditions under which the piping had operated. The defects may have extended from initially shallow fabrication defects such as those seen in this examination and shown in Fig. 2.17.

Based on the inspection and laboratory work of Ebasco Services Incorporated and the Oak Ridge National Laboratory and the fact that the various locations of the wetted insulation could not be positively identified, all the thermal insulation within the containment vessel was removed. The piping was mechanically cleaned and then inspected by the fluorescent-penetrant method. The defects that were found by this inspection were ground out, after which the piping surfaces were cleaned with an Alconox solution, rinsed with demineralized water, and dried. The piping was then reinsulated with a thermal insulation containing sodium silicate, and the insulation was sealed. This investigation has been reported in detail.[8]

---

[8]L. D. Schaffer and J. A. Klapper, NS SAVANNAH Nuclear Merchant Ship Investigation of the Effects of Wet Chloride-Bearing Thermal Insulation on Austenitic Steel Pipe, ORNL-TM-14, November 1, 1961.

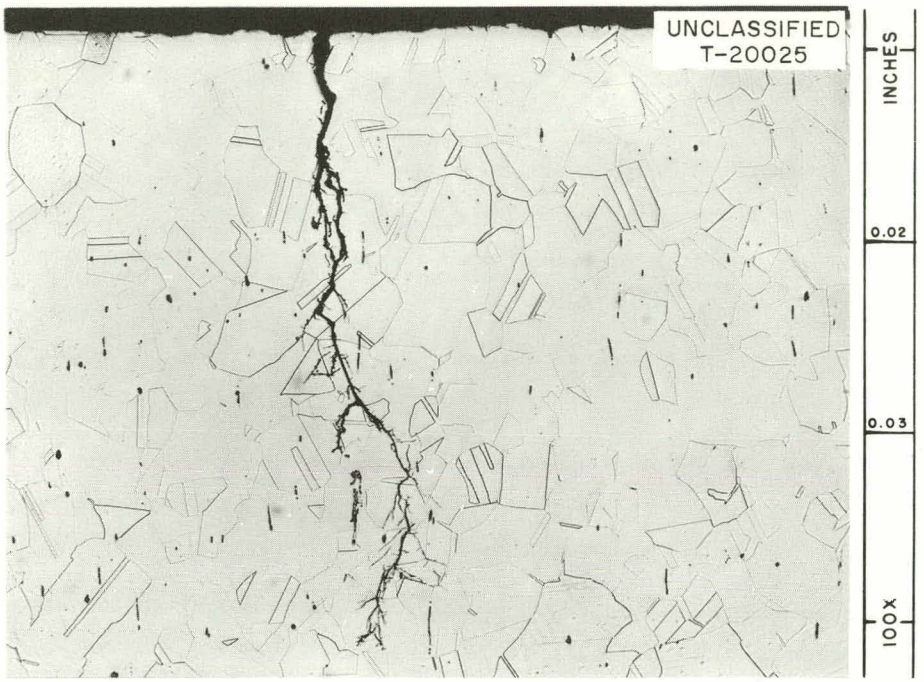

Fig. 2.16. Cracks in Type 304 Stainless Steel Pipe Specimen After 200 hr in Water Containing 50 ppm Chloride. Etchant: glyceria regia. 100X

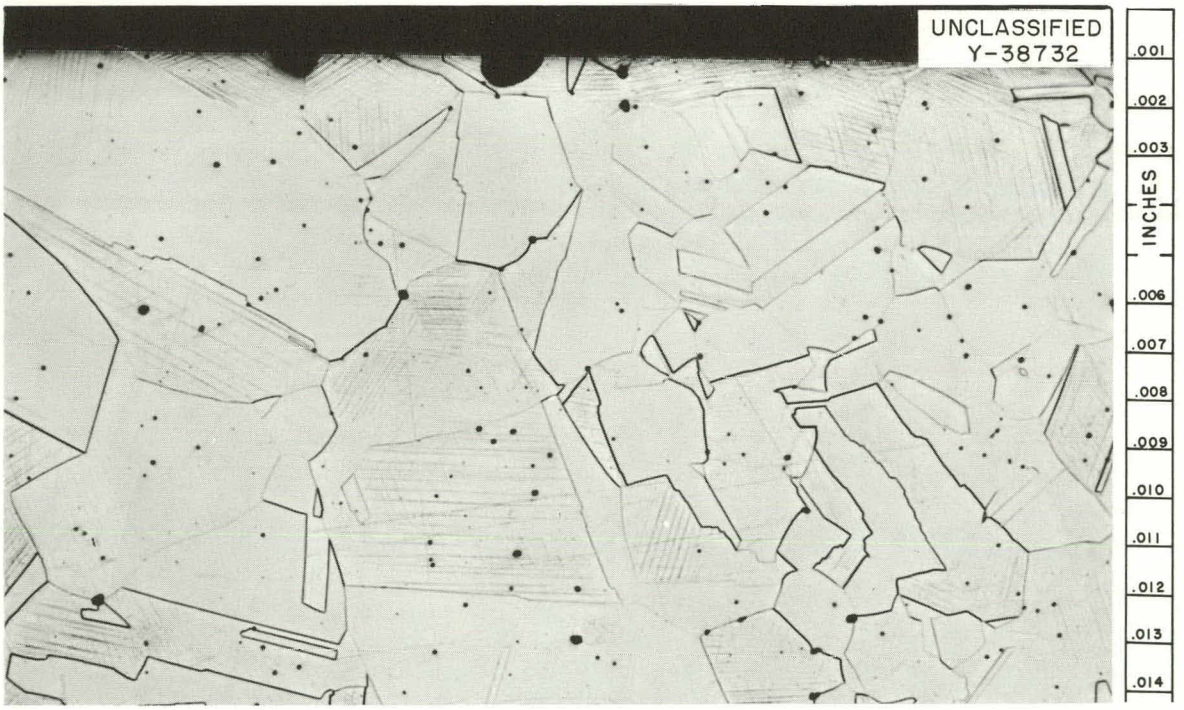

Fig. 2.17. Shallow Defect Area Observed in Type 304 Stainless Steel Piping Sample from NS SAVANNAH Reactor System.

Analysis of Primary System Components for Gamma-Emitting Elements

W. C. Thurber

Samples from several components[9] of the NS SAVANNAH primary coolant system were chemically analyzed for cobalt, tantalum, silver, antimony,

[9]Maritime Reactor Project Ann. Prog. Rep. Nov. 30, 1959, ORNL-2865, p. 64.

Table 2.9. Analysis of NS SAVANNAH Primary System Components for Gamma-Emitting Impurities

Component Description	Specimen Designation		Impurity Content (wt %)				
	Heat No.	Mark No.	Co	Ta	Ag	Sb	Zn
Lower plate, upper flow baffle	X22240-3T	220	0.11	<0.001	0.0002	<0.0001	<0.0001
Upper plate, upper flow baffle	X22260-3E	201	0.11	<0.001	<0.0001	<0.0001	<0.0001
Pad-lift lug, upper flow baffle	X22260-3E	208	0.11	<0.001	<0.0001	<0.0001	<0.0001
Cylinder, upper flow baffle	X22532-3B	202	0.076	<0.001	0.005	<0.0001	<0.0001
		209	0.076	<0.001	0.005	<0.0001	<0.0001
Gussets 2, 3, and 4, upper flow baffle	X22155-2H	207	0.16	<0.001	<0.0001	<0.0001	<0.0001
		210	0.16	<0.001	<0.0001	<0.0001	<0.0001
Upper grid plate and main hold-down spring components	X22305-1H	303	0.096	<0.001	0.001	<0.0001	<0.0001
		306	0.096	<0.001	0.001	<0.0001	<0.0001
		307	0.096	<0.001	0.001	<0.0001	<0.0001
		308	0.096	<0.001	0.001	<0.0001	<0.0001
		309	0.096	<0.001	0.001	<0.0001	<0.0001
		311	0.096	<0.001	0.001	<0.0001	<0.0001
		320	0.096	<0.001	0.001	<0.0001	<0.0001
		110	0.096	<0.001	0.001	<0.0001	<0.0001
		227	0.096	<0.001	0.001	<0.0001	<0.0001
Upper grid plate components	X22260-3D	318	0.074	<0.001	<0.0001	<0.0001	<0.0001
		325	0.074	<0.001	<0.0001	<0.0001	<0.0001
		416	0.074	<0.001	<0.0001	<0.0001	<0.0001
		417	0.074	<0.001	<0.0001	<0.0001	<0.0001
		507	0.074	<0.001	<0.0001	<0.0001	<0.0001
Cylinder, core support shield	X22505-1B	400	0.10	<0.001	0.0001	<0.0001	<0.0001
Fuel container assembly components	111146-4	414	0.057	<0.001	<0.0001	<0.0001	<0.0001
		415	0.057	<0.001	<0.0001	<0.0001	<0.0001
Base plate, fuel container assembly	114463-3	418	0.053	<0.001	<0.0001	<0.0001	<0.0001
Main brace, fuel container assembly	16943-14	425	0.076	<0.001	<0.0001	<0.0001	<0.0001
Doubler plate, fuel container assembly	X26099-11	458	0.073	<0.001	<0.0001	<0.0001	<0.0001
Cylinder, lower flow baffle	X22453-1T	500	0.088	<0.001	<0.0001	<0.0001	<0.0001
Lower plate, lower flow baffle	X22514-2B7	508	0.080	<0.001	<0.0001	<0.0001	<0.0001

and zinc. These elements, if present in the various stainless steel structures of the plant, could contribute significant amounts of long-lived gamma activity. Results of the analyses, which are summarized in Table 2.9, indicate that, with the exception of cobalt, the gamma-emitting elements, if present, were in quantities below the limit of detection.

3. PRESSURIZED-WATER IN-PILE LOOP

Operation

J. A. Conlin J. K. Franzreb
D. E. Tidwell

The ORR pressurized-water in-pile loop has operated satisfactorily in the period since the previous report.[1] Leakage has been remarkably low, with the result that the makeup requirement has been low, the purity of the water has remained high, and the equipment room has been free of contamination. After nearly two years of operation, all loop components continue to operate with minimum maintenance. The instruments and the automatic control equipment are functioning reliably.

Three experimental assemblies have been irradiated in the loop to date. The fueled test elements consisted of both swaged and vibratory-compacted UO_2 clad in type 304 stainless steel. The irradiation histories of these assemblies are presented in Table 3.1.

[1]Maritime Reactor Project Ann. Prog. Rep. Nov. 30, 1960, ORNL-3046, pp. 23–24.

Table 3.1. Irradiation Histories of Experimental Assemblies Exposed in the ORR Pressurized-Water In-Pile Loop

Experimental Assembly[a]	Reactor Cycles	Cycle Duration (weeks)	Reactor Power (Mw)
1	1	3	20
	2	3	16
	3	7	30
3	1	3	16
	2	3	16
	3	7	30
	4	7	30
	5	7	30
	6	7	30
4	1	7	30
	2	7	30

[a]Testing of experimental assembly No. 2 was cancelled.

Two other experimental assemblies are presently being irradiated (Nos. 5 and 6). The fueled elements include both vibratory-compacted and cold-swaged UO_2 clad in type 304 stainless steel. Each experimental assembly contains three fuel rods, and each assembly occupies one leg of the loop. Beginning with Experiment 4 all test assemblies have been equipped with a tube containing a flux-monitor wire. The flux-monitor wires are removed for counting at the end of each reactor cycle, and new wires are inserted.

A special containment vessel and associated remotely operated tools and equipment for use in the removal of ruptured fuel specimens were designed and fabricated during the past year, but there has been no occasion for their use. Radiation levels within the equipment room and at the sample station have been low. During normal operation, the equipment room activity is approximately 50 mr/hr. Contamination within the equipment room and at the sample station has also been low. This is attributed to the excellent leak tightness of the system. The aisles of the equipment room may usually be entered during reactor shutdowns without the use of contamination-zone clothing. A low contamination level, below normal tolerance, at the sample station has been maintained by use of proper sampling techniques and adequate measures to prevent the spread of contamination from the sample bottle connections.

The bypass loop fission-product-monitoring system, as originally designed, utilized N^{16} activity to indicate flow by determining the transit time from radioactive decay, but an orifice flowmeter was installed which indicates flow more accurately, especially when background activity is present from "crud" buildup.

It has been possible to maintain the desired water purity, and with one exception, the analytical techniques are adequate. The oxygen content is presently determined by the "Winkler" method, with a 0.05-ppm detection limit. The desired oxygen level in the loop water is <0.01 ppm, and therefore a more sensitive method of determination is needed. An oxygen analyzer capable of determinations in the range of 1 ppb has been ordered. The new analyzer will consist of a flow meter, an inlet ion-exchange column, a conductivity cell, a thallium column, a second conductivity

cell, and a cleanup ion-exchange column. In the new analyzer the dissolved oxygen in the water will combine with the thallium to form thallous hydroxide, which is a strong electrolyte. The conductivity of the water will be measured at the inlet and outlet of the thallium column. The difference between these two conductivity measurements will give a measure of the thallous hydroxide concentration, which will be calibrated in terms of the oxygen concentration in the water. The inlet ion-exchange column will lower the background conductivity of the water, and the outlet ion-exchange column will remove the thallous hydroxide from the water before it returns to the main loop. The new analyzer will be installed in a side stream of the loop purification system and, in addition to providing a more precise method, will provide for continuous analysis of the oxygen concentration of the loop.

Water Chemistry Studies

C. F. Baes, Jr. T. H. Handley

Water chemistry studies were initiated for determining the specific activities and the chemical compositions of filterable and nonfilterable impurities in the loop water. The studies include investigations of the transport and deposition of corrosion products (crud), which foul heat transfer surfaces and impair the operating reliability of mechanical systems exposed to the primary water, and the transport and deposition of the long-lived activity originating from the activation of the corrosion products in the reactor flux. The buildup of activated corrosion products causes long-term buildup of radiation levels throughout the primary system.

Behavior of Water-Borne Activity

The results of radiochemical and filtration tests conducted on water samples taken from the ORR loop side-stream purification system during a period of normal loop operation and during a period of loop startup are summarized in Tables 3.2 and 3.3. During the period of normal operation (constant temperature and flow rate) the level of water-borne activity

Table 3.2. Activity of Water in ORR Pressurized-Water Loop As Determined by Radiochemical Analysis

Activity	Sample Taken with Loop Operating[a] (dps/liter)		Sample Taken During Loop Startup[b] (dps/liter)	
	Sampled Ahead of Ion Exchanger	Sampled After Ion Exchanger	Sampled Ahead of Ion Exchanger	Sampled After Ion Exchanger
A^{41}	8×10^5			
Mn^{56}	9×10^4	2×10^3		
Fe^{59}	8×10^3	8×10^2	3×10^5	3×10^3
Co^{58}	6×10^3	5×10^2	2×10^5	3×10^3
Co^{60}	5×10^3	4×10^2	2×10^5	2×10^3
Mo^{99}	3×10^3	1×10^2		
Mn^{54}	2×10^3	1×10^2	3×10^4	6×10^2
Cr^{51}	2×10^3	2×10^2	1.3×10^5	5×10^3

[a]Samples taken on March 6, 1961.

[b]Samples taken on March 17, 1961.

Table 3.3. Activity Removed by Filtering Water in ORR Pressurized-Water Loop

Filter Pore Size (μ)	Activity Removed by Filtration with Loop Operating[a] (%)		Activity Removed by Filtration During Loop Startup[b] (%)	
	Filter Ahead of Ion Exchanger	Filter After Ion Exchanger	Filter Ahead of Ion Exchanger	Filter After Ion Exchanger
0.45[c]	65	58	95	93
0.05[d]	<0.01		0.1	
0.01[d]	<0.05			

[a]Samples taken on March 6, 1961.

[b]Samples taken on March 17, 1961.

[c]Gross activity (less A^{41}) removed by filter.

[d]Activity subsequently removed by filter.

was relatively low, the sum of the principal longer lived activities (Mn^{54} Fe^{59}, Co^{58}, and Co^{60}) being $\sim 2 \times 10^4$ dps/liter. Roughly two thirds of this activity was removed by a 0.45-μ filter (with a cellulose backing pad), and about 90% was removed by the purification system ion exchangers. The concentration of solids which could be removed by filtration at such

times was too low to be determined directly by weighing; however, from the activity which was retained by a 0.45-μ filter and from the specific activity of the crud (Table 3.4) determined during a period of disturbed loop operation (when weighable samples of crud could be collected on a filter), the crud level was estimated to have been <0.05 ppm during normal operation. In contrast, during loop startup, the water-borne activity level was ~50 times higher; 93% of this activity could be removed by a 5-μ filter; 98 to 99% was removed by the ion exchangers; and the crud content was often several ppm. Similar behavior was observed during other periods of disturbed loop operation (for example, temperature and flow-rate cycling).

Table 3.4. Results of Analyses Carried Out on May 17, 1961 of the Crud in the Water of the ORR Pressurized-Water Loop

Crud Sample Weight (mg)	Iron Content (wt %)	Nickel Content (wt %)	Sample Activity (dps/g)			
			Fe^{55}	Fe^{59}	Co^{58}	Co^{60}
			$\times 10^8$	$\times 10^7$	$\times 10^7$	$\times 10^7$
54.8	51	8.2	1.7	7.2	5.4	3.2
7.4	74	11	2.2	8.8	(a)	(a)
3.5	57	8.6	1.6	5.9	4.5	3.4

[a]Not determined.

The results of Table 3.3 show that there is a discontinuity in crud particle size. Virtually all the activity which can be removed by filtration is caught by a 0.45-μ filter, and very little additional material is stopped by a 0.01-μ filter.

These observations are in general agreement with the results[2] of a study of the water chemistry of the SM-1 pressurized-water reactor, which, like the ORR loop, is operated at a neutral pH and with a hydrogen overpressure. The total coolant activity and the crud level of the SM-1 are

[2]C. A. Bergmann, SM1 Research and Development Program: Long Lived Induced Activity Buildup in SM1 Core I Lifetime; Task XVIII-Phase I, APAE No. 77, Nov. 30, 1960.

similarly affected by reactor operation. At startup, shutdown, and during low-power operation, crud levels are usually >0.5 ppm. At steady-state full-power operation, crud levels are usually <0.1 ppm, and most of the activity is nonfilterable; that is, it is not held by a 0.45-μ filter.

Characteristics of Particulate Material

Electron micrographs of crud samples collected on a filter during a period of high crud level are shown in Fig. 3.1. Many of the particles may be seen to have pronounced geometrical form, suggesting that they are crystallites. Electron-diffraction patterns from such fields indicated the presence of magnetite; the appearance of these diffraction patterns confirmed that magnetite was present as relatively large crystals.[3]

Magnetic mixed oxides of iron and chromium of the magnetite structure have been reported by several investigators to be a principle constituent of crud.[4] Magnetite (Fe_3O_4) is the stable oxide of iron under the operating conditions of such pressurized-water systems as the ORR loop. It is formed at the interface between water and the protective, chromium-rich, oxide film present on the surface of corroding stainless steel. Atoms of iron which have diffused through the oxide film are oxidized by the water. As the oxide film grows, magnetite presumably is released as crud to the water. Its presence in crud as well-developed crystallites seems especially significant, however, in view of the apparent nearly complete absence of crud particles in the 0.01- to 0.05-μ range. The implication is that recrystallization of the magnetite occurs, and this implies, in turn, that appreciable radiochemical exchange can take place between activated and nonactivated crud.

Behavior of Colloidal and Dissolved Material

Several observations have been made which suggest strongly that the activity not removed from loop water samples by filtration through a 0.45-μ

---

[3]T. E. Wilmarth, Analytical Chemistry, ORNL, personal communication.

[4]D. J. DePaul, Corrosion and Wear Handbook, TID-7006, Chap. 2, pp. 11–20, March 1957.

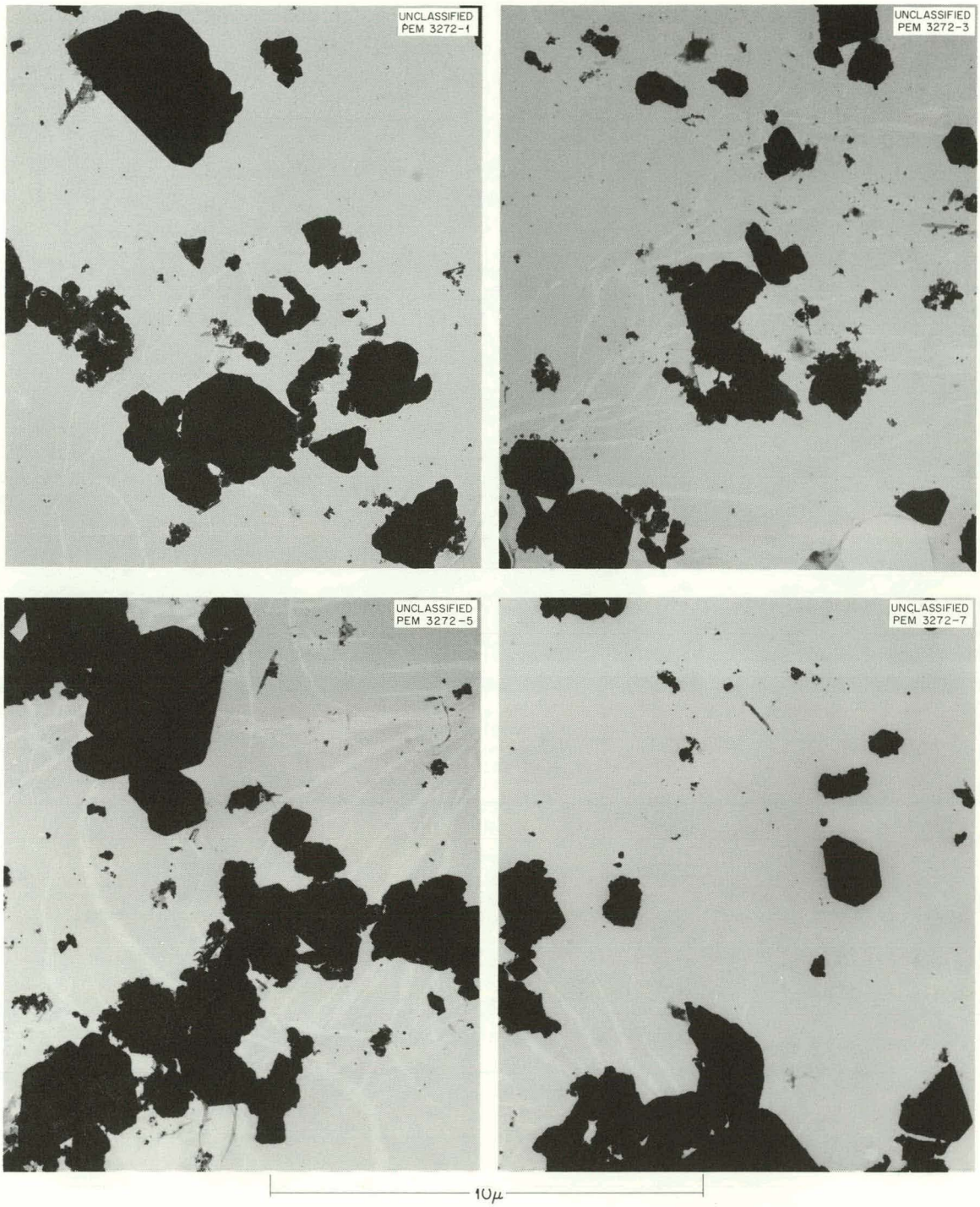

Fig. 3.1. Electron Micrographs of Solids Removed from ORR Pressurized-Water Loop.

filter is associated with dissolved (ionic) material. First, it was found, as indicated in Table 3.5, that appreciable portions of the manganese, iron, and cobalt activity were retained by cellulose backing pads, which initially were used to support the millipore filters. Mild pretreatment of the sample with dilute acid, dilute base, or half-neutralized Versene reduced this retention. This behavior suggests that the activity was retained by an ion-exchange process.

Table 3.5. Results of Pressurized-Water Loop Filtration Tests Conducted on April 12, 1961

Sample[a] Pretreatment	Distribution of Activity[b] (%)					
	Co^{58}			Mn^{56}		
	Filter	Backing	Filtrate	Filter	Backing	Filtrate
Untreated	21	77	2	3	77	21
0.01 M in HCl	31	<1	64	5	<1	95
0.01 M in NaOH	43	11	43	3	13	83
0.01 M in Versene, 0.01 M in NaOH	32	<1	69	4	<1	94

[a]Sample taken ahead of ion exchangers during normal loop operation.

[b]Values are percentages of the introduced activity found at the position indicated.

In paper electromigration tests, the activity which had passed through a 0.45-μ filter and had been absorbed on a backing pad was found to move toward the cathode, indicating that the activity was associated with cationic material. On comparing the velocity of migration with that observed for dissolved metal salts, it further appeared that the activity was present as the simple metal cations and not as colloidal particles.

The conductivity of loop water in the cooled side-stream purification system, upstream of the ion exchangers, was typically 0.2 μmhos/cm (at 37°C) during normal loop operation. This corresponds to a dissolved solids level of 0.027 ppm as $Fe(OH)_2$. If it is assumed that all the activity which cannot be filtered is associated with such ionic material, the

specific activity is found to be of the same magnitude as that of the water-borne crud (see Table 3.4). This, of course, is to be expected if the two kinds of material (filterable and nonfilterable) are in chemical exchange equilibrium.

The presence of such dissolved material provides a mechanism for the above-suggested recrystallization of crud particles. If such dissolved material is present at the operating temperature of the system, appreciable crystal growth of crud particles and activity exchange are to be expected. This emphasizes the potential value of a high-temperature filter–ion-exchange medium which would perform the same function as the low-temperature, organic, ion exchangers presently used in the side-stream purification system of the ORR loop (and used generally in pressurized-water reactors). At full flow, such a unit should be especially effective in reducing activity and crud transport during periods of disturbed operation when water-borne activity (at a relatively high level) is present largely in filterable crud. If a suitable inorganic ion-exchange material could be found for use in such a purification unit, it might be very effective in removing the ionic activity which, presumably, is being supplied to the loop water by dissolution and ion-exchange reactions involving crud and corrosion products throughout the system.

Magnetite as a High-Temperature Filter–Ion-Exchange Medium

Since magnetite (Fe_3O_4) is the stable oxide of iron in pressurized-water reactor systems and a principle constituent of crud, it is a possible high-temperature filter–ion-exchange medium. If, as is suggested here, this constituent of crud both supplies and exchanges with the ionic material in the high-temperature water, the introduction of a bed of non-activated magnetite into the system might well, by the same process that now contributes to the transport of activity, accumulate the dissolved activity without otherwise disturbing the chemical or nuclear behavior of the system. Magnetite has been shown to possess ion-exchange properties at ordinary temperatures.[5] While this is presumably due to surface exchange

[5]P. J. Anderson, The Ion Adsorption Properties of Synthetic Magnetite, AERE M/R 2046, 1956.

only, at the temperatures (~260°C) of pressurized-water systems, bulk-phase ion exchange may occur. Magnetite is an interstitial oxide in which the ferrous and ferric ions are dispersed in the interstices of a close-packed oxide lattice. Various studies on the high-temperature corrosion of ferrous alloys show that the diffusion of metal atoms and ions through the similar oxide lattice of the corrosion film is appreciable, it being a process in one of the generally accepted corrosion mechanisms.[4]

Engineering tests[6] at the Westinghouse Bettis Plant have already shown that magnetite beds are practical and effective as mechanical filters in removing water-borne crud at the operating temperatures of pressurized-water loops. In addition, magnetite is ferromagnetic and has a curie temperature (585°C) well above the operating temperature of PWR primary systems. This suggests the possibility of designing a remotely operated disposable-renewable filter in which the filter bed is supported by a magnetic field, similar to the unit described by McNamee and Shappert.[7] The presence of a magnetic field might also improve the retention of magnetic crud.

Water samples from the loop which had been previously filtered through a 0.45-μ filter were contacted at room-temperature with finely divided natural magnetite (obtained from the Prince Manufacturing Co.) in batch equilibrations and in column experiments. In both cases a large portion of the activity was retained by the magnetite. In tests currently in progress, similar water samples have been placed in a bomb and heated to 250 to 260°C in contact with magnetite. Results obtained thus far show that virtually all the activity present in the water samples is removed, partly by the magnetite and partly by the walls of the stainless steel bomb. These tests will be continued.

---

[6]C. P. Paulson, Performance of Magnetite Bed Filters, Chem. Eng. Prog., 56(3): 64 (1960).

[7]R. J. McNamee and L. B. Shappert, An Engineering Evaluation of a Magnetic Filter As a Means of Remote Controlled Filtration, ORNL CF-58-5-32.

4. ADVANCED CORE DEVELOPMENT

Zircaloy Fuel-Element Container Studies

T. D. Anderson E. E. Gross
C. L. Whitmarsh

The stainless steel fuel-element containers in the NS SAVANNAH reactor account for about one-third of the total stainless steel in the active portion of the core. The fuel-element container assembly is shown in Fig. 4.1. Since it appeared probable that the replacement of the present stainless steel structure (fuel-element containers and spacer bars) by a similar structure of Zircaloy would result in an improvement in neutron economy, an evaluation of the substitution of Zircaloy for stainless steel was undertaken. This evaluation has included several areas of investigation, as shown in Fig. 4.2. The progress in each of these areas of investigation is summarized in the following sections.

Physics (E. E. Gross, B. W. Colston, M. L. Winton)

The heterogeneous nature of the NS SAVANNAH core I is illustrated by Fig. 4.3, which shows a portion of the core through a ferrule plane. A proper assessment of the influence of a material change in the fuel element containers (the so-called "egg crate") requires knowledge of detailed flux distributions, particularly in the neighborhood of the egg crate. In order to generate detailed flux information throughout the geometry of Fig. 4.3, a previously described[1] four-group model employing a combination of one-dimensional S_n transport theory and two-dimensional diffusion theory calculations was developed. The detail contained in this analytical model is displayed by Fig. 4.4, which gives the calculated average four-group fluxes in all the regions of Fig. 4.3 (with the exception of the control rod) at 508°F. In Fig. 4.4 all fluxes are normalized to unity in the UO_2. As may be seen, the egg-crate region is exposed to a relatively high thermal flux.

---

[1]Maritime Reactor Project Ann. Prog. Rep. Nov. 30, 1960, ORNL-3046, pp. 41–49.

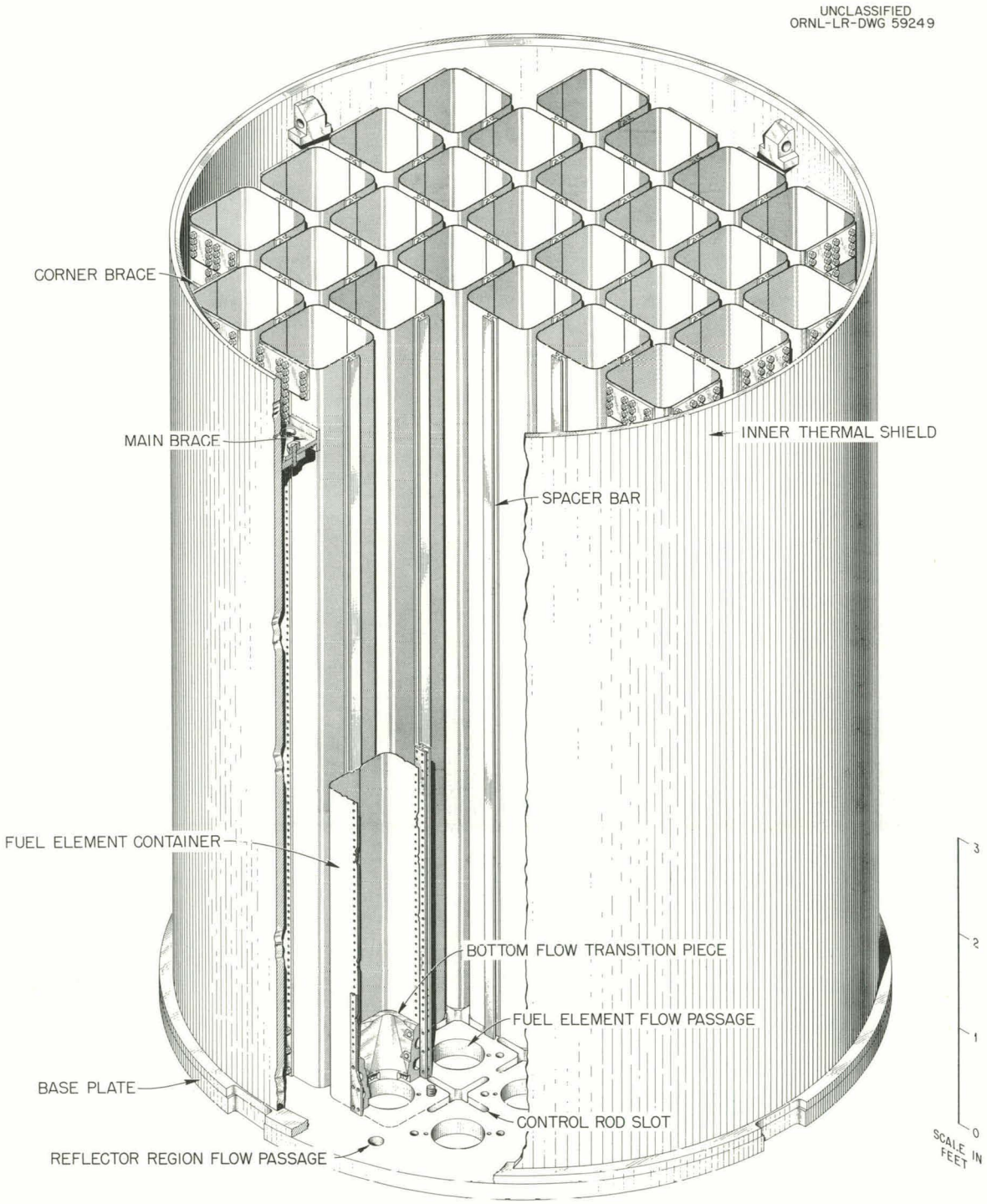

Fig. 4.1. NS SAVANNAH Fuel-Element Container Assembly.

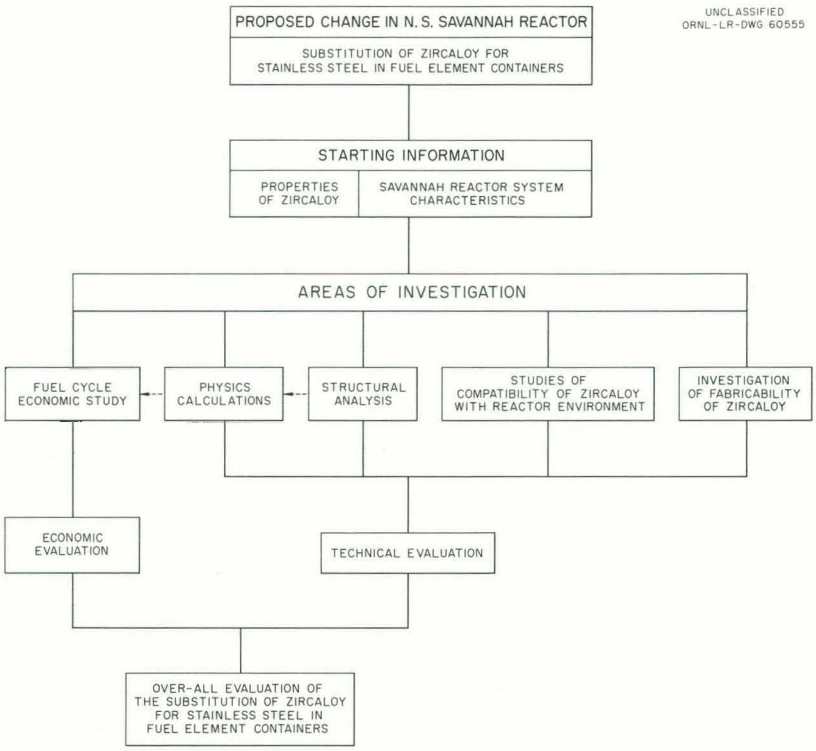

Fig. 4.2. Diagram Showing Scope of Zircaloy Evaluation.

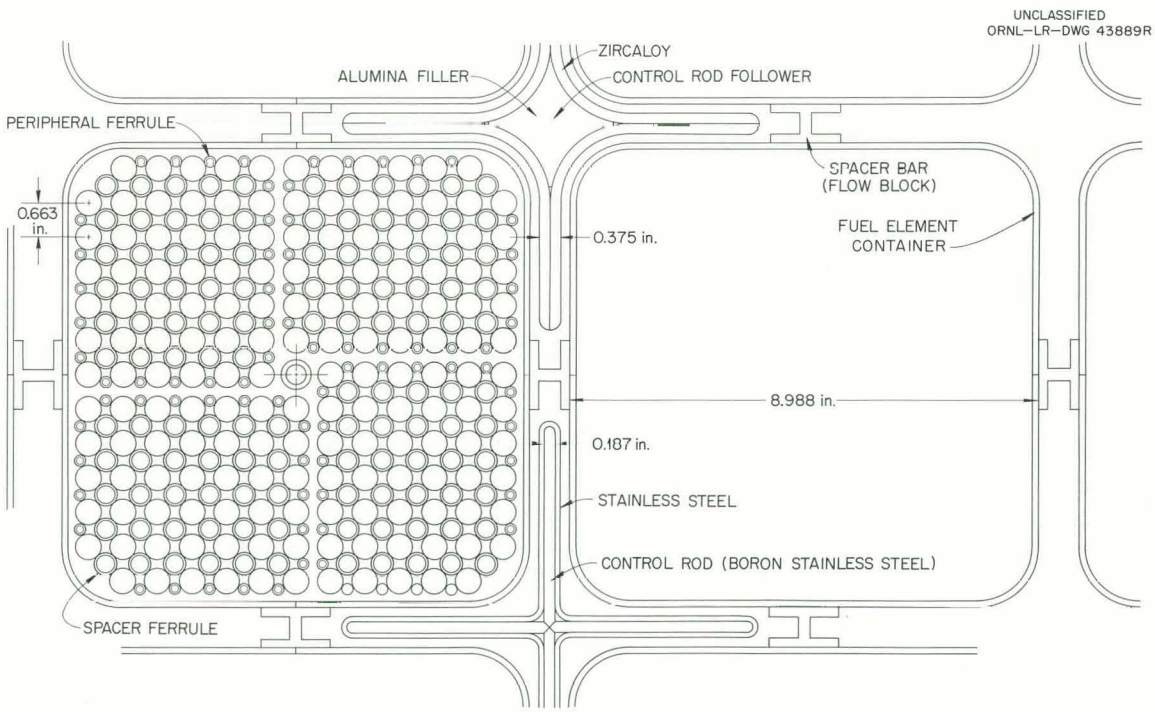

Fig. 4.3. Portion of NS SAVANNAH Core I at a Ferrule Plane.

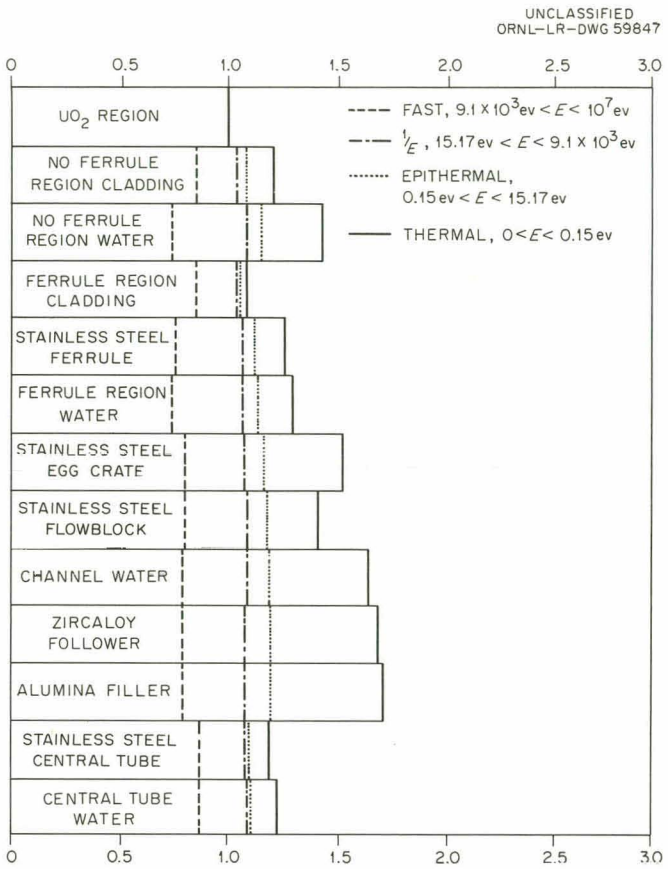

Fig. 4.4. Four-Group Fluxes in NS SAVANNAH Core I Components at 508°F.

Another important feature of the analytical model was the use of the S_n method to calculate four-group transport theory boundary conditions at the surface of a control rod.[2] The S-5 approximation to the S_n transport method[3] was used to solve for the four-group fluxes in an appropriate one-dimensional representation of a control rod cell. From these results, transport theory values for the ratio of the current to the flux at the control rod surface were obtained and then used as control rod boundary conditions in a two-dimensional diffusion theory calculation of the full NS SAVANNAH core in the geometry of Fig. 4.5.

---

[2]B. W. Colston, E. E. Gross, and M. L. Winton, Heterogeneous Control Rod Studies, in Proceedings of the ANPP Reactor Analysis Seminar, October 11–12, 1960, MND-C-2487, January 1961.

[3]B. G. Carlson and G. P. Bell, Solution of the Transport Equation of the S_n Method, Geneva Conference Paper 2386 (1958).

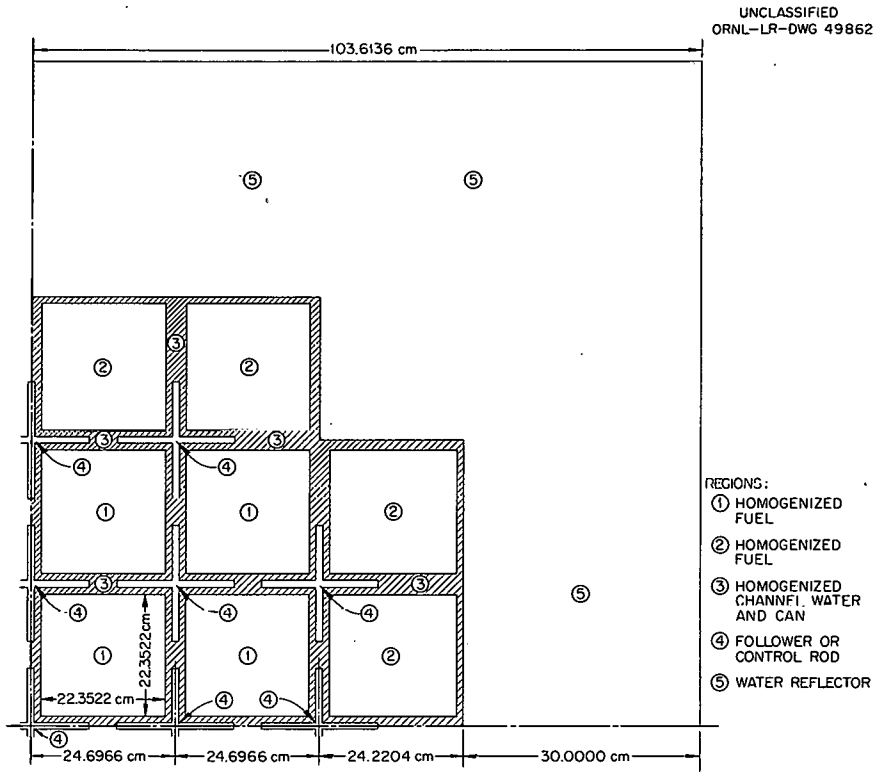

Fig. 4.5. Geometrical Model for One Quadrant of NS SAVANNAH Core I.

The adequacy of the S-5 approximation may be judged by the S-5 results for the Milne problem[4] shown in Figs. 4.6 and 4.7. The angular distribution of one-velocity neutrons at the boundary between a semi-infinite plane diffusing medium and a void is presented in Fig. 4.6. The S_n method solves for the neutron flux in discrete directions ($\mu = \cos\theta = \pm 0.1, \pm 0.5, \pm 1$ in the S-5 approximations used here) and assumes a linear variation in the flux between neighboring directions. The variation of the total (scaler) flux near the void boundary is shown in Fig. 4.7. In both Figs. 4.6 and 4.7, the exact and P-3 solutions to the Milne problem are also shown for comparison. The S-5 solution compares favorably with the exact solution.

Application of the four-group model to the geometry of Fig. 4.3 yielded the beginning of the life multiplication factor results shown in

[4]A. M. Weinberg and E. P. Wigner, The Physical Theory of Neutron Chain Reactions, pp. 253–266, University of Chicago Press, Chicago, 1958.

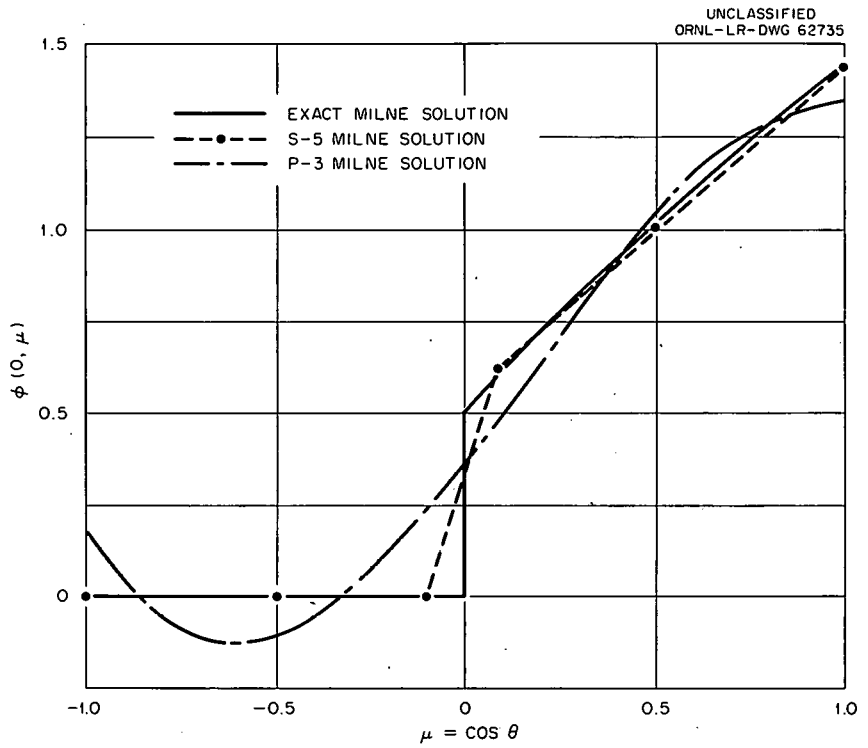

Fig. 4.6. Milne Problem Solutions for the Angular Flux at the Void Boundary Normalized so that $\int_{-1}^{+1} \phi(0,\mu)\, d\mu = 1$. Exact and P-3 solutions taken from ref. 4, p. 262.

Figs. 4.8 and 4.9. These results are for cores containing single-zone enrichment and serve to summarize results on the reactivity effects of a material change in the egg-crate structure. From Fig. 4.8 it is apparent that replacement of the stainless steel egg crate in the 4.2 wt % U^{235}-enriched core (the enrichment of the inner zone of NS SAVANNAH core I) by a Zircaloy egg crate could increase core reactivity by $\Delta k = 0.065$ for the case when followers are in the core at 68°F.

The worth of the control rods may be obtained from Fig. 4.8 by subtracting the multiplication factor of the core with rods from the multiplication factor of the core with followers. The rod worth obtained in this way appears to be independent of enrichment in the enrichment range of 3.0 to 4.2 wt % U^{235}. Although the 21 control rods appear to be worth 4% Δk more in the Zircaloy egg-crate core than in the stainless steel

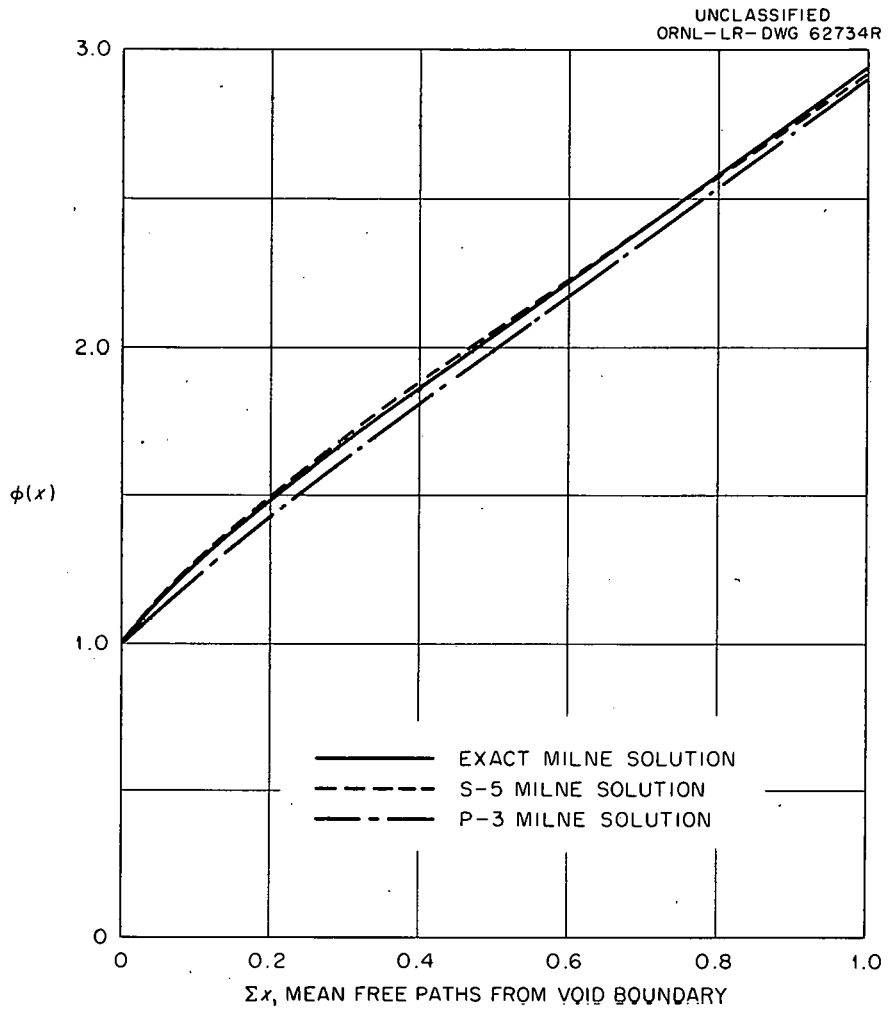

Fig. 4.7. Milne Problem Solutions for Total Flux Variation Near Void Boundary. Exact and P-3 solutions taken from ref. 4, p. 263.

egg-crate core, this rod worth is barely enough to control 4.2 wt % U^{235}-enriched core I fuel elements. To obtain the same shutdown margin as is now present in the stainless steel egg-crate core with the central rod stuck out of the core, the Zircaloy egg-crate core would require 3.86 wt % U^{235}-enriched fuel elements.

Calculated multiplication factors for full-power conditions at the beginning of core life are shown in Fig. 4.9. By comparing Fig. 4.9 with Fig. 4.8, an over-all temperature deficit (loss of reactivity in going from room temperature to full power) of 5.3% Δk is evident for the stainless steel egg-crate core and 5.7% Δk for the Zircaloy egg-crate core. Also from Fig. 4.9, it is evident that a fuel enrichment of 3.38 wt % U^{235}

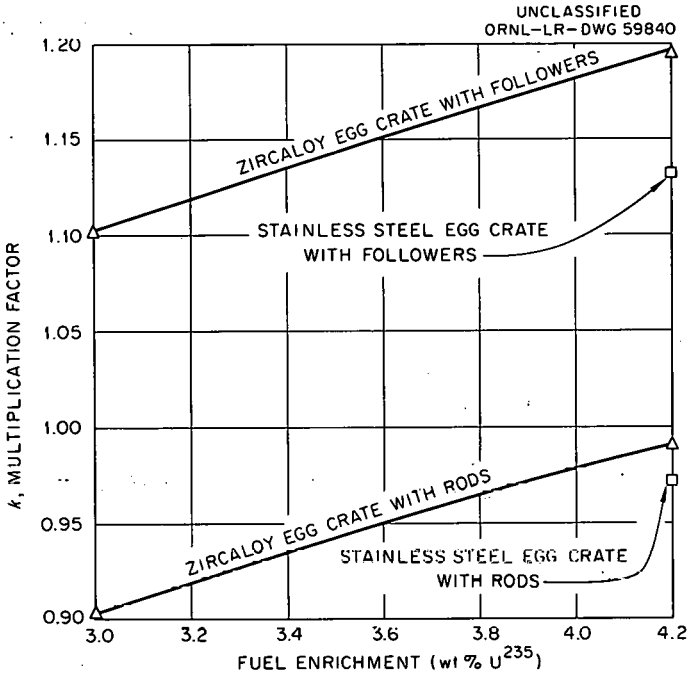

Fig. 4.8. Calculated Multiplication Factors for Core I-Type Fuel Elements at 68°F in Zircaloy and in Type 304 Stainless Steel Egg Crates at Beginning of Life.

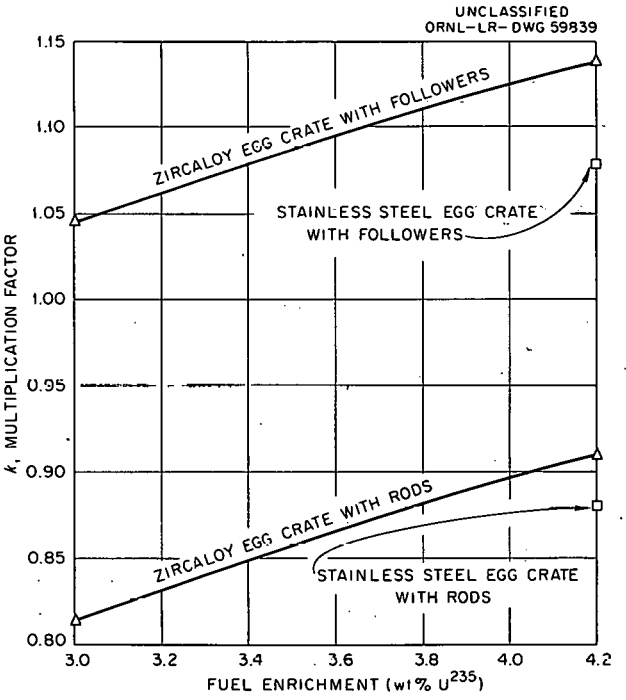

Fig. 4.9. Calculated Multiplication Factors for Core I-Type Fuel Elements at 508°F in Zircaloy and Type 304 Stainless Steel Egg Crates at Beginning of Life (Full Power and No Xenon).

in Zircaloy egg crates would provide the same initial hot reactivity (and therefore about the same reactivity lifetime) as 4.2 wt % U^{235} fuel in stainless steel egg crates. A fuel enrichment of 3.86 wt % U^{235} in Zircaloy egg crates (this enrichment gives the same one-stuck-rod shutdown margin) would have 4% Δk more hot reactivity available for burnup than is present in 4.2 wt % U^{235} fuel in stainless steel egg crates.

In order to complete the evaluation of a Zircaloy egg crate, lifetime calculations were made to compare the reactivity lifetime of Zircaloy and stainless steel egg-crate cores. The comparison was based on a one-dimensional radial burnup calculation using the CANDLE code.[5] Four-group flux-averaged cross sections for CANDLE were obtained by homogenizing the two-dimensional PDQ calculations of the full core containing followers. The burnup was computed for a power level of 63 Mw, and the reactor was assumed to be controlled by a uniformly distributed poison.

The full-power multiplication factor as a function of time, calculated with CANDLE (with the above assumptions), is shown in Fig. 4.10. After equilibrium xenon and samarium have built up (~0.3 yr), the multiplication factor as a function of time appears to be remarkably linear,

[5] O. J. Marlowe et al., CANDLE — A One-Dimensional Depletion Code for the IBM-704, WAPD-TM-53.

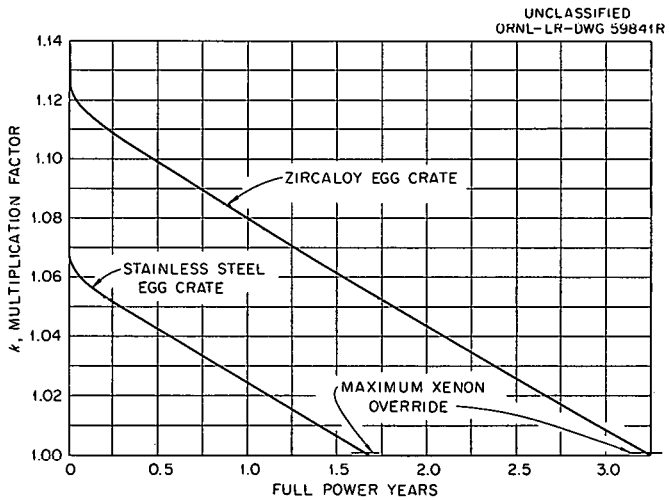

Fig. 4.10. Calculated Reactivity Lifetime of 4.2 wt % U^{235}-Enriched Core I Fuel in Zircaloy and in Type 304 Stainless Steel Egg Crates at a Power Level of 63 Mw.

with the same slope (0.036 $\Delta k/yr$) for both Zircaloy and stainless steel egg-crate cores. The xenon peak occurs about 4 hr after shutdown and reduces the multiplication factor of the equilibrium xenon core by only $\Delta k = 0.0008$.

According to the CANDLE calculations, 4.2 wt % U^{235}-enriched core I fuel should last about twice as long in a Zircaloy egg crate as in a stainless steel egg crate; however, to maintain the same shutdown margin with the central rod stuck out of the core as is now present in the stainless steel egg-crate core would require reducing the fuel enrichment to about 3.86 wt % U^{235} in a Zircaloy egg-crate core. Using the results of Fig. 4.9 to estimate the initial hot reactivity for this enrichment and using the slope of the burnup curve (Fig. 4.10), such a core is estimated to have a reactivity lifetime about 0.9 full-power years longer than that of the 4.2 wt % U^{235}-enriched fuel in a stainless steel egg-crate core.

Structural Analysis of Containers (T. D. Anderson, L. R. Shobe)

Stress analyses have been made of the present stainless steel container assembly both with core I fuel elements[6,7] and core II fuel elements[8] installed. An additional stress analysis was performed to determine the Zircaloy fuel-element container wall thickness required to maintain structural integrity and to limit deflections of the container walls so as not to interfere with control rod motion or coolant flow around the fuel elements. Since the fuel container assembly is a permanent part of the reactor system, consideration was given to container requirements which may be imposed by future reactor fuel elements. It was, of course, impossible to guess the form of future fuel elements; however, it appeared that the two types of fuel elements already in existence (core I and core II)

---

[6]T. A. Hughes and D. L. Mayer, The Stress and Deflection Characteristics of N. S. SAVANNAH Fuel Element Containers Due to Internal-to-External Pressure Differentials, Trans. Am. Nuc. Soc., 4(1): 15 (1961).

[7]Structural Analysis of Fuel Container Assembly — First Core, Ebasco Report No. ESI-3(a)(b)-1, April 1960.

[8]Structural Analysis of Fuel Container Assembly — Second Core, Ebasco Report No. ESI-3(a)(b)-2, May 1960.

were sufficiently different to be representative of possible future designs.

For purposes of this analysis, it was assumed that the reactor would operate at the design power of 69 Mw (thermal) for 20 years and at 130% of design power for short periods. Operation with either two or four coolant pumps was considered, although the former condition was assumed to occur infrequently.

Coolant flow through the reactor gives rise to pressure differentials between the inside of the fuel-element containers and the control rod channels. The diagram of Fig. 4.11 shows the flow paths through the reactor. Pressure and flow data for the reactor have been reported[9] by Babcock & Wilcox. These data were obtained from tests on a scale model of the reactor vessel and tests on a full-sized element. This pressure-drop information,

[9]Don M. Bylund, Nuclear Merchant Ship Reactor Project, Survey of the Reactor and Control Drive System Research and Development Program, BAW-1153-1, August 1959.

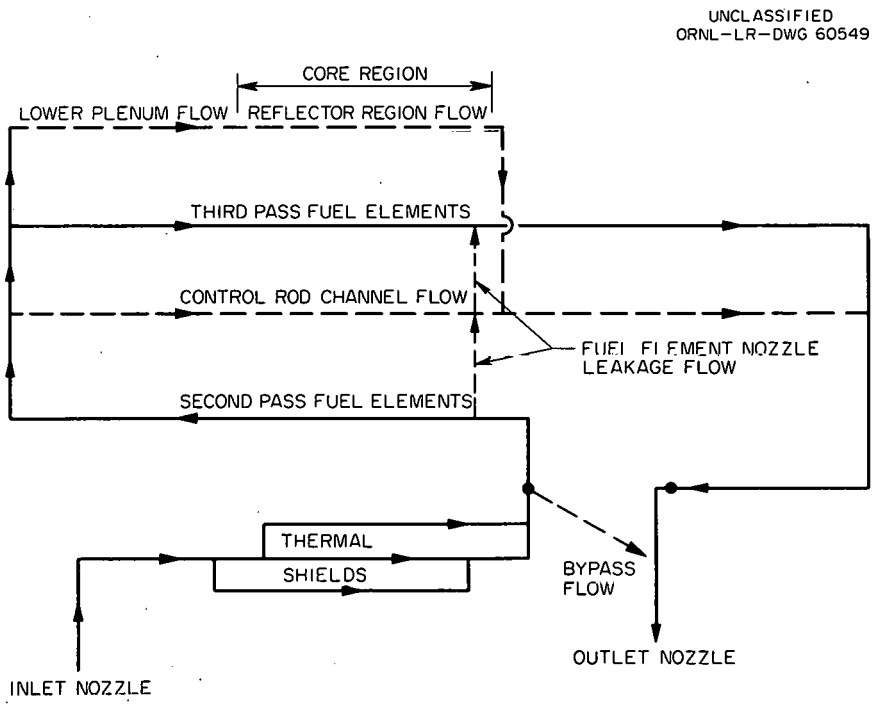

Fig. 4.11. Diagram of NS SAVANNAH Reactor Flow Paths.

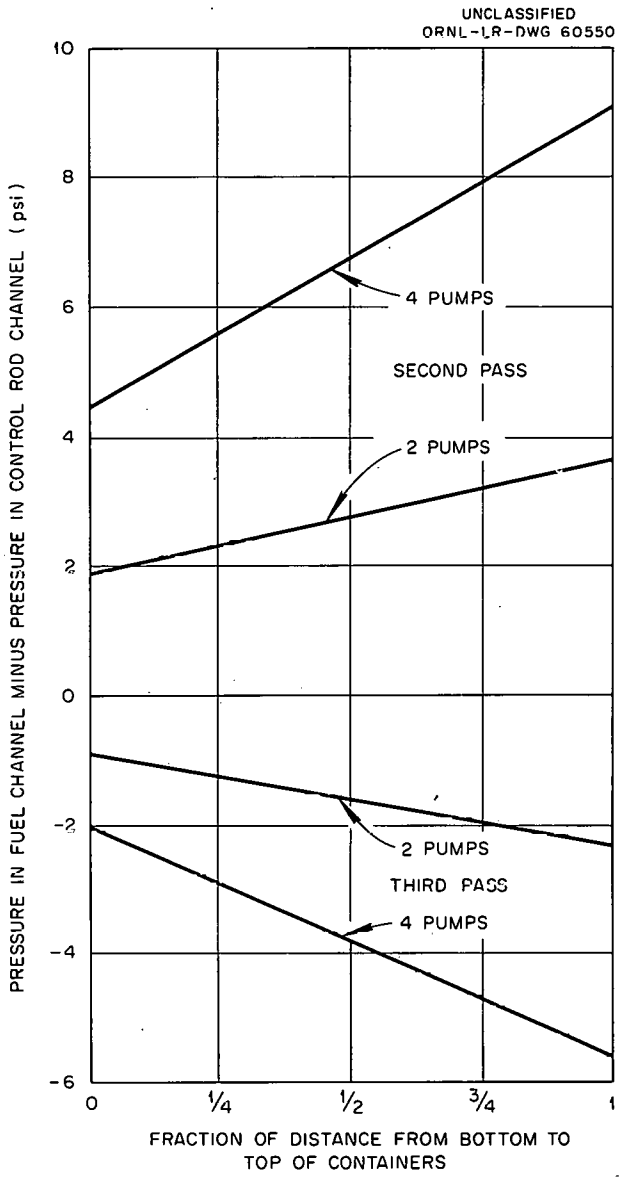

Fig. 4.12. Maximum Pressure Differential Across Container Walls with No Core Bypass Flow.

which was given for the original design flow rate of 8 million pounds per hour, was scaled-up by the square of the flow rate to correspond to a reactor flow rate of 9.2 million pounds per hour. The latter figure is the maximum flow-rate with no by pass holes in the upper grid plate. The adjusted pressure differential curves are shown in Fig. 4.12, both for two- and four-pump operation.

The various ship motions which were considered for normal operation of the NS SAVANNAH are the following:

1. 30-deg roll with a 14-sec period,
2. 7-deg pitch with a 7-sec period,
3. fore and aft acceleration of 0.25 g,
4. lateral heave of 0.7 g,
5. vertical heave of 0.3 g.

It was considered that any or all these motions could occur simultaneously; thus, in combining stress or deflections, no credit was taken for forces acting in opposite directions. In addition to the normal conditions outlined above, the unusual circumstance of the ship lying on its side with a vertical heave of 2 g was considered.

It was obvious that the 30-deg roll with simultaneous 0.7-g lateral heave (assumed to be normal to the ship's longitudinal vertical plane of

symmetry) and 0.3-g vertical heave would constitute the most severe normal operating condition. Consequently, this was the only normal operating condition examined. Further, in considering the loading of the fuel elements, it appeared that the more flexible core II fuel element would present the worst loading condition at the core mid-plane. However, there is a larger pressure loading at the top of the fuel-element containers that may make this a more critical area when the core I fuel elements are considered. This is being investigated. The loadings at the core mid-plane on a container with core II fuel elements are the following:

Ship Motion	Load (lb)
30-deg roll, 0.7-g lateral heave, 0.3-g vertical heave	513
Ship on side, 2-g vertical heave	1140

It was felt that the temperature differentials in the assembly would induce bowing and stresses of significant magnitude in the spacer bars. A theoretical analysis treating the spacer bars as beams on elastic foundations showed, however, that the maximum stress was less than 500 psi and that the maximum deflection was extremely small. Therefore temperature induced stresses and deflections were ignored.

Three different models were considered in determining the stresses and deflections from beam action of the fuel-element containers. First, the entire assembly of 32 containers (with the weight but not the strengthening effect of the separator bars considered) was treated as a simply supported, builtup beam. Second, a single fuel-element container was considered as a propped cantilever beam. The third model was that of a single fuel-element container acting as a simply supported beam. Since the latter model was the most conservative, the single container treated as a simple beam was chosen for dealing with deflections and stresses from beam action. With the ship on its side and subjected to a vertical heave of 2 g, the following quantities were calculated for 91-mil-thick containers:

Axial bending stress, psi	3000
Maximum deflection, in.	0.033
Shear stress, psi	463

As may be seen, beam action is not an important consideration in the fuel-element container design.

For determining the stresses and deflections from plate action in the sides of the containers, two columns of containers were considered. These two columns along with the assumed attitude of the ship are shown in Fig. 4.13. Column 1 consists of second-pass containers only, and column 2 consists of four third-pass containers with second-pass containers at top and bottom. The second-pass containers are all subjected to an internal pressure (at mid-height) of 7 psig (see Fig. 4.12), and their left faces receive no support from an adjacent container. Simple supports at the upper corners were, therefore, assumed for column 1 in order to allow

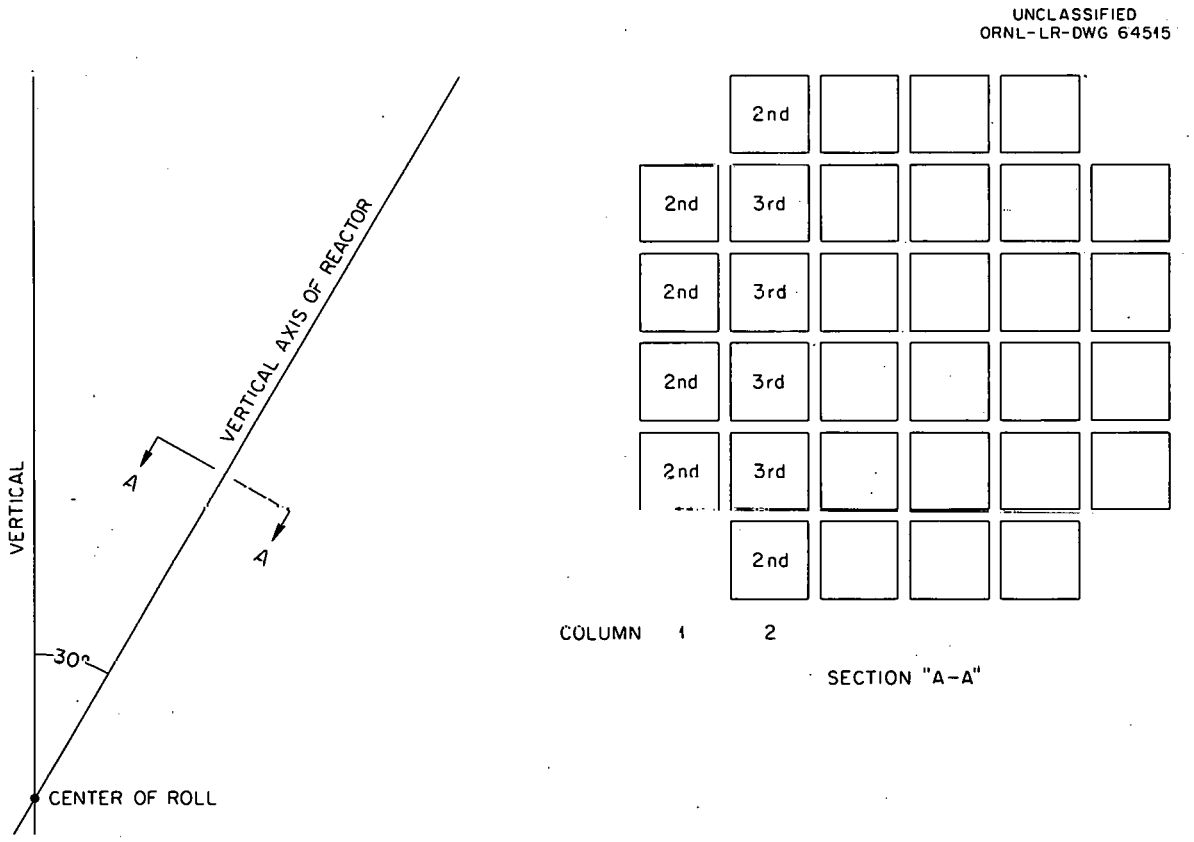

Fig. 4.13. Orientation of NS SAVANNAH Fuel-Element Containers Used in Analyzing Stresses Arising from Plate Action.

the sides of the containers to deflect freely. The third-pass containers are subjected to an internal pressure (at mid-height) of 4 psig and each is supported by an adjacent container on every side. Furthermore, the supports are such that there should be little, if any, rotation at the supports; thus, fixed supports were assumed on the third-pass containers. The right supports of the second-pass containers at the top and bottom of column 2 are likewise greatly fixed against rotation by adjacent cans, while the left sides are free. The second-pass containers in column 2 were assumed to be simply supported at the midpoints of their sides. All intermediate containers or frames in a given column were assumed to be identical in loading, stresses, and deflections. Based on the above considerations, the two models shown in Fig. 4.14 were chosen for the rigid-frame analysis.

Examination of the stresses in the models shown in Fig. 4.14 required analyses of three basic rigid frames. These three basic frames are shown in Fig. 4.15. The frames were analyzed by the slope-deflection method. The results indicated that the most severe stress condition for interior walls existed in the bottom side of the top fuel-element container in the column-2 model (see Fig. 4.14). Using a design stress for 20% cold-worked Zircaloy of 17 000 psi (~1/3 of the ultimate tensile strength), the required container-wall thickness was found to be 0.140 in. With this thickness the maximum deflection of an interior wall would be about 0.080 in. These quantities were computed for the previously defined worst normal operating condition. For the unusual ship-on-its-side condition, the maximum stress and deflection for an interior wall would be 22 000 psi and 0.101 in., respectively; these values are applicable at the core midplane with core II-type fuel elements.

Since the fuel-element containers will be subjected to an alternating stress arising from ship motion, a fatigue analysis was performed. The results for containers with 140-mil walls indicated that fatigue failures would not occur in the interior walls even with continuous 30-deg rolling of the ship for 20 years.

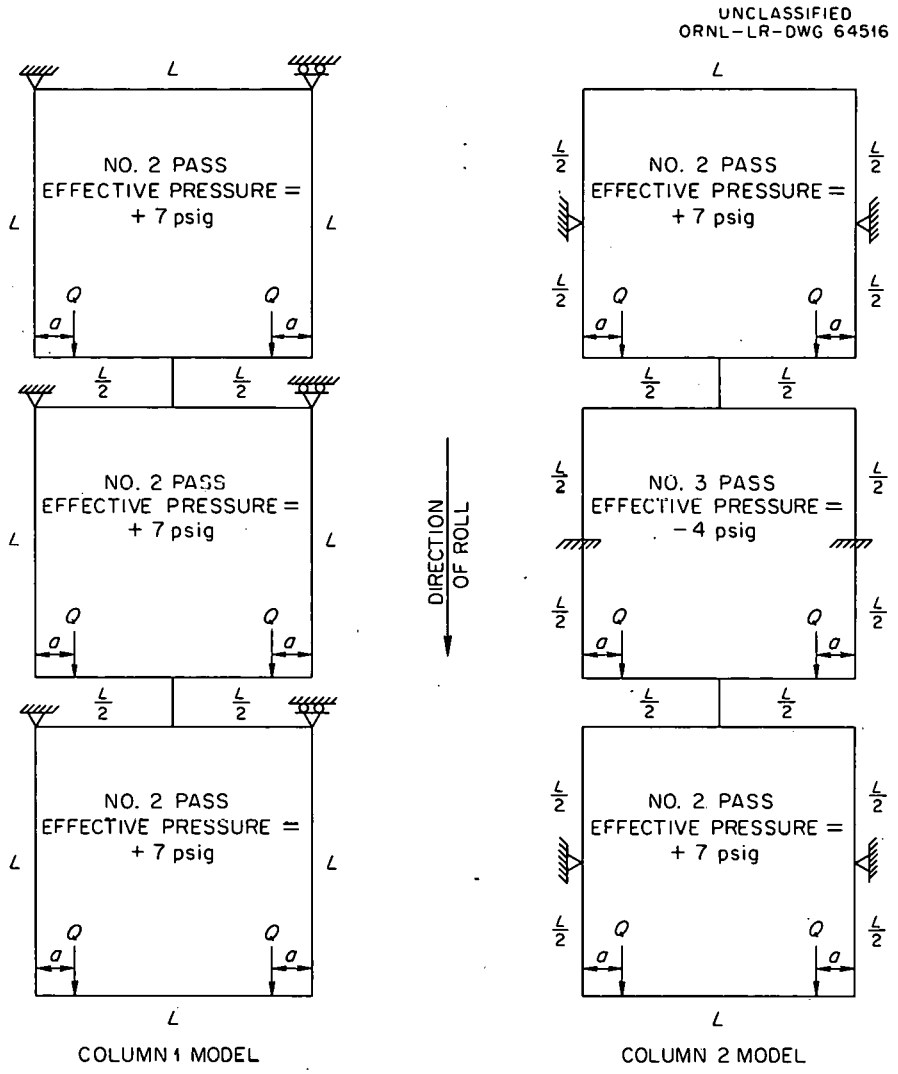

Fig. 4.14. Container Assembly Models Used in Analyzing Stresses from Plate Action of NS SAVANNAH Fuel-Element Containers.

The investigation is not complete, but it is known that the exterior walls of the peripheral fuel-element containers require additional support if the stress in the walls and the wall thickness are to be held to 17 000 psi and 0.140 in., respectively. In addition, it appears that some design changes of the upper flow nozzles and of the main braces near the top of the core may be required in order to provide the positive support consistent with the simply-supported-beam assumption and to hold shearing stresses in the fuel containers to an acceptable level.

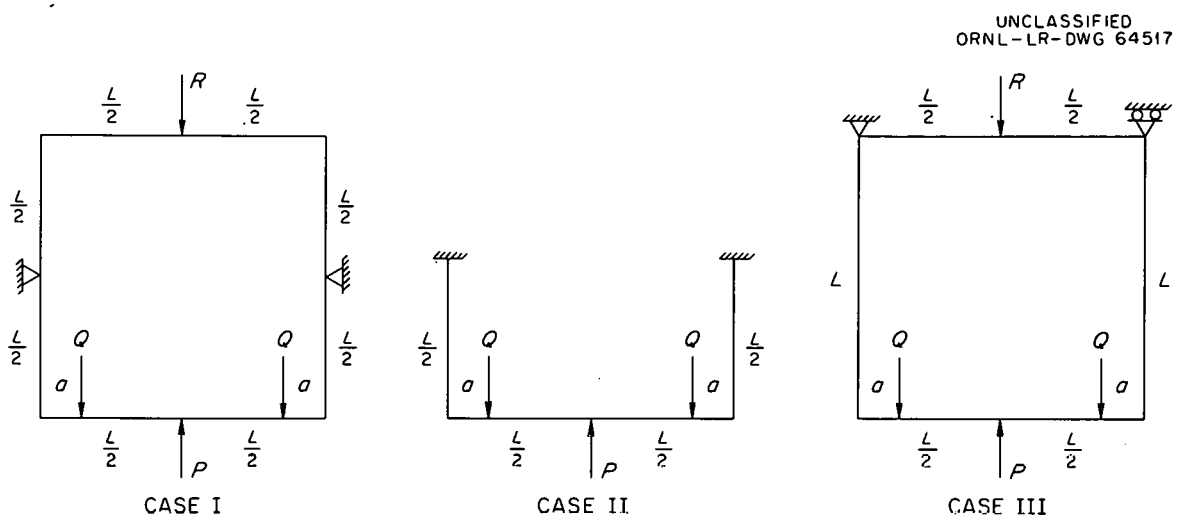

Fig. 4.15. Basic Rigid-Frame Models Used in Stress Analysis of NS SAVANNAH Fuel-Element Containers.

Compatibility (C. L. Whitmarsh, T. D. Anderson)

It is desired that the fuel-element container assembly, like other permanent parts of the reactor system, have a useful life of about 20 years. Both Zircaloy-2 and -4 were therefore evaluated for long-term service in the core of the NS SAVANNAH on the basis of a literature survey of basic properties of the materials, an evaluation of the water chemistry,[10] and operating experience of existing pressurized-water reactors.

Corrosion. Corrosion rates applicable to exposure conditions in the core of the NS SAVANNAH are listed in Table 4.1. Since the corrosion film is adherent, specimen weight gain is considered indicative of corrosion rate. Since the NS SAVANNAH core inlet and outlet water temperatures are 495 and 520°F, respectively, corrosion calculations were based on a bulk water temperature of 550°F for conservative design purposes. Other conditions such as flow rate and water chemistry are not expected to significantly affect the corrosion rate. Experimental data indicate that exposure to fast neutrons will increase corrosion, but the magnitude of the effect is uncertain; increases up to a factor of 5 have been obtained with two or three being a more probable value.

[10]C. L. Whitmarsh, Water Chemistry in the N. S. SAVANNAH Reactor — Effect of a Core Component Change from 304 Stainless Steel to Zircaloy-4, ORNL-CF-61-1-109, January 20, 1961.

Table 4.1. Corrosion Rate of Zircaloy-2 in Static, Neutral Water at 550°F

Source	Weight Gain (mg/dm^2 per day)	Comments
Lustman and Kerze[a]	$0.95\ t^{-0.70}$ (t in days)	Pretransition rate; tests up to 1000 days did not show transition
KAPL[b]	<0.02	Tests at 600°F showed rate of 0.02; lower temperature tests not reported
Chalk River[c]	<0.03	Tests at 572°F showed rate of 0.03, lower temperature tests not reported
Zircaloy properties literature survey	0.015	Extrapolation of averaged data from several sources correlated in a 1/T plot

[a]B. Lustman and F. Kerze, The Metallurgy of Zirconium, p. 622, McGraw-Hill Book Co., New York, 1955.

[b]A. B. Riedinger, Corrosion Behavior of Zircaloy, Thesis, Union College (May 1958).

[c]E. C. W. Perryman, A Review of Zircaloy-2 and Zircaloy-4 Properties Relating to the Design Stress of CANDU Pressure Tubes, CRMet-937 (June 1960).

Predictions of long-term corrosion show a considerable spread of data when the rates from Table 4.1 are plotted (Fig. 4.16). However, the highest rate indicated would result in a weight gain of only 220 mg/dm^2 in 20 years, or a metal penetration of 0.4 mils on each exposed surface. If a factor of 5 were applied to this to account for radiation effects, the maximum total corrosion would be 1200 mg/dm^2 or 2 mils per surface. These figures indicate satisfactory corrosion resistance.

These predictions of corrosion behavior are based on no external effects, for example, fretting or wear or both. Each time the protective oxide film is mechanically removed or broken (result of fretting or wear), it is replenished by reaction between the water and the exposed surface of Zircaloy, thereby causing an accelerated corrosion rate. Resistance of Zircaloy to fretting and wear is uncertain; experimental data from different sources and reactor operating experience give conflicting results.

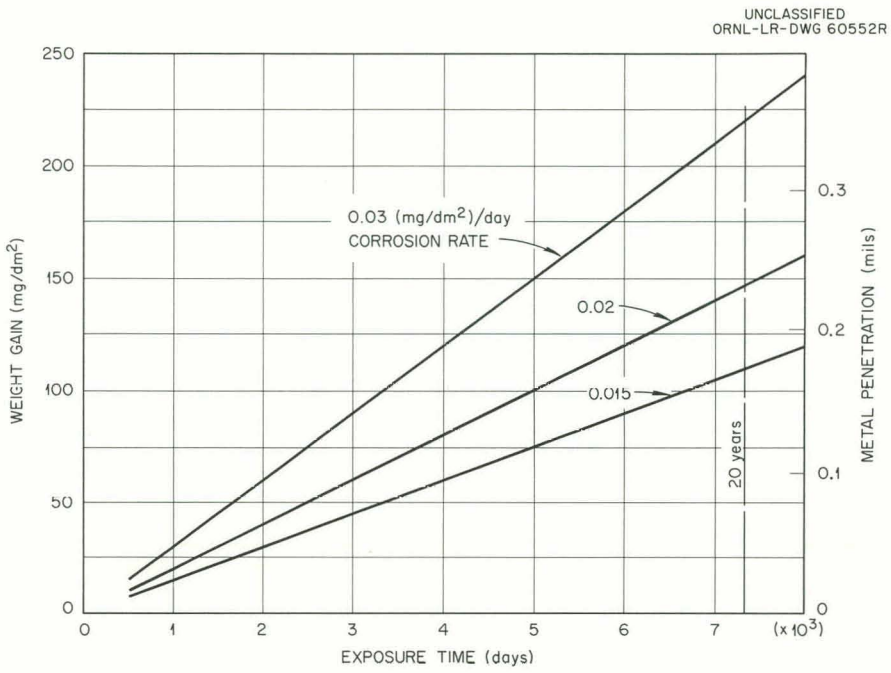

Fig. 4.16. Long-Term Corrosion Behavior of Zircaloy-2 in Water at 550°F.

Zirconium is known to have poor resistance to fretting corrosion, and experiments have indicated that the corrosion rate of Zircaloy-2 in water will be increased if fretting occurs. However, in-reactor service experience with Zircaloy-2 has indicated that accelerated corrosion rates resulting from fretting are short-lived and the effect on over-all corrosion behavior is minor.[11]

Continued use of Zircaloy in reactors and the absence of any corrosion problems attributed to fretting or wear during in-reactor service would lead one to believe that this is not a serious problem. However, the possibility of accelerated corrosion from fretting and wear must be recognized, since conclusive evidence is not available.

Hydrogen Absorption. Hydrogen absorption will probably be the limiting service condition for Zircaloy in the NS SAVANNAH. Long-term accumulation of hydrogen in Zircaloy plates exposed to NS SAVANNAH core conditions was calculated, and the results are presented in Fig. 4.17. The

[11]E. C. W. Perryman, A Review of Zircaloy-2 and Zircaloy-4 Properties Relating to the Design Stress of CANDU Pressure Tubes, CRMet-937, June 1960.

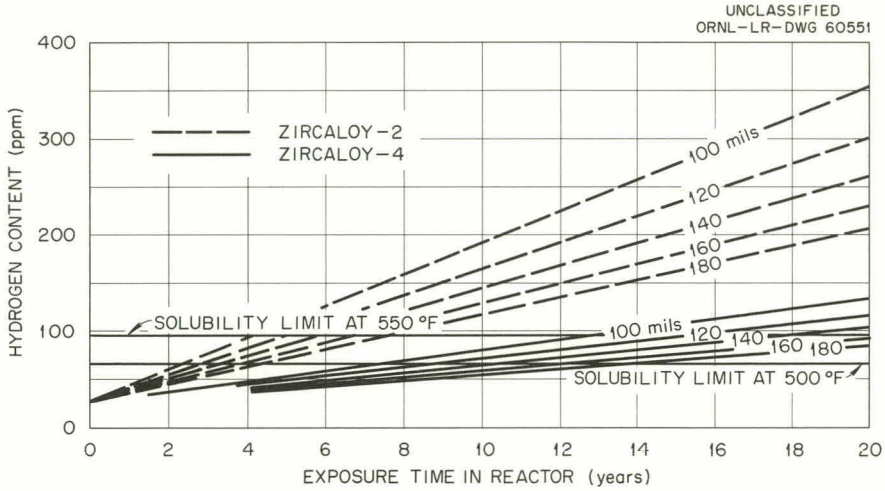

Fig. 4.17. Predicted Hydrogen Pickup of Zircaloy Plates of Several Thicknesses in the NS SAVANNAH Reactor Core.

assumptions and conditions on which the calculations were based were the following:

1. The average temperature of the Zircaloy during reactor operation would be in the range 500 to 550°F.

2. The initial hydrogen concentration in the Zircaloy would be 25 ppm.

3. All the Zircaloy would be corrosion tested prior to use and would have a corrosion weight gain of 10 mg/dm^2.

4. Hydrogen pickup of Zircaloy-2 would be 30% of theoretical during corrosion testing and 100% during reactor service.[11]

5. Hydrogen pickup of Zircaloy-4 would be one-third that of Zircaloy-2.[11]

6. The average corrosion rate would be 0.03 mg/dm^2 per day during reactor service and would occur on both surfaces of the plates.

7. The effect of dissolved hydrogen in the water would be negligible.

8. Redistribution effects of thermal and stress gradients would be negligible.

The data in Fig. 4.17 indicate that the solubility limit for hydrogen in Zircaloy at 550°F in the NS SAVANNAH will be exceeded in 20 years for Zircaloy-4 plates less than 160 mils thick. Thus, if the conservative

approach of using solubility limit as the maximum permissible concentration is taken, only plates of Zircaloy-4 which are greater than 160 mils thick would be acceptable for 20-year service. For both Zircaloy-2 and -4 at 500°F none of the thicknesses considered would be adequate; however, it should be noted that these calculations were conservative from the standpoint of corrosion rate, maximum initial hydrogen content, and hydrogen-absorption rate. If only one of these factors, for example, corrosion rate, were assumed to have a more realistic value (0.015 mg/dm^2 per day), the Zircaloy-4 plate thickness could be reduced to 100 mils and still be well below the solubility limit at 550°F for 20-year service; and plates greater than 140 mils thick would be below the 500°F solubility limit. It is doubtful that the use of Zircaloy-2 for 20-year service could be justified with respect to the solubility limit acceptance criterion within the range of conditions and plate thicknesses studied.

When evaluating this information, the high degree of uncertainty involved in the calculations must be considered. Investigators still do not have a fundamental understanding of the mechanism of hydrogen pickup; and, in addition, available data are by necessity obtained from relatively short-term tests. Long-term experience in operation of pressurized-water reactors is, of course, nonexistent. Another uncertainty lies in establishing a maximum permissible level for hydrogen concentration. The solubility limit is probably a lower limit for an acceptance criterion, since effects of hydrogen on mechanical properties of Zircaloy are apparently not prohibitive at concentrations less than 500 ppm. Based on the available information, it seems likely that, relative to hydrogen absorption, Zircaloy-4 fuel-element containers would be suitable for long-term service in the NS SAVANNAH reactor.

Corrosion-Product Activity. In any pressurized-water reactor an accumulation of corrosion products (crud) occurs in the primary system. Deposition of this crud in low-velocity regions creates problems of low heat transfer and high radiation levels. The crud problem is dependent on the formation of corrosion products, transport of these corrosion products, and activation of certain isotopes. Experience with existing reactors has shown that most of the long-lived activity in crud can be attributed to

Co^{58} and Co^{60}, which are produced by the reactions $Ni^{58}(n,p)Co^{58}$ and $Co^{59}(n,\gamma)Co^{60}$, respectively.

Radiochemical analyses of crud samples from two pressurized-water reactors are listed in Table 4.2 (see also chap. 3, this report, for data on crud activity of the ORR Pressurized-Water Loop). Even though the PWR contains Zircaloy-clad fuel elements, greater than 56% of its activity is from cobalt isotopes. Compared with stainless steel, Zircaloy is not a significant source of Co^{58} or Co^{60}. Reactor-grade type 304 stainless steel contains 8 to 12% nickel and 50 to 100 ppm cobalt. Chemical analyses of crud samples show the major component (80 to 95%) to be iron as Fe_3O_4.

Table 4.2. Relative Crud Activities in Pressurized-Water Reactors

Nuclide	Long-Lived Activity (% of total activity after 1400 effective full-power hours)	
	SM-1	PWR
Co^{60}	10.8	39.2
Co^{58}	58.0	16.9
Cr^{51}	13.5	14.8
Zr^{95}		6.5
Fe^{59}	13.8	12.1
$Hf^{181(175)}$		5.1
Mn^{54}	3.9	5.4
Total	100.0	100.0

On the basis of this information, it appears that increasing the amount of Zircaloy exposed to the primary coolant (with consequent reduction of stainless steel) would tend to decrease the primary system activity resulting from crud. However, since the fuel-element containers do not constitute the major portion of the primary system surface area, changing this component to Zircaloy is not likely to have a pronounced effect on crud activity.

Fabrication (T. D. Anderson, E. A. Wick)

In performing other studies on Zircaloy fuel-element containers, it was tacitly assumed that the design of the Zircaloy containers would be substantially the same as that of the present stainless steel containers; that is, the change to Zircaloy could be accomplished by a simple substitution of Zircaloy for stainless steel with, perhaps, some increase in metal volume. The validity of this assumption depended on whether or not a Zircaloy fuel-element container assembly could be fabricated using the stainless steel design. In order to resolve this question, the fabricability of Zircaloy was studied. The intent of this study was not to detail a step-by-step fabrication procedure; rather, the purpose was to determine whether the fabrication of the container assembly would involve anything new in Zircaloy technology. It was concluded that, using present Zircaloy technology, there would be no outstanding difficulties in fabricating the Zircaloy containers.

Economics (C. L. Whitmarsh, T. D. Anderson)

Since the incentive for considering the use of Zircaloy fuel-element containers was improved economics, a fuel-cycle cost analysis was performed. In order to evaluate the cost savings resulting from the Zircaloy substitution, it was first necessary to establish a steady-state fuel-cycle cost for a reference core. The reference core, designated as Case S-420, consisted of core I-type fuel elements (one-zone U^{235} enrichment of 4.2 wt %) in stainless steel fuel-element containers.

The total fuel-cycle cost is composed of the sum of various cost components. These cost components are diagrammed in Fig. 4.18. The estimated fuel-cycle costs for the reference core are given in Table 4.3.

Zircaloy fuel-element containers can be utilized to reduce fuel-cycle costs by either increasing core lifetime or decreasing enrichment (keeping lifetime constant). In order to examine the relative merits of these two approaches, a cost analysis of three different Zircaloy-container-core cases was made. A summary of the estimated cost reduction for the Zircaloy fuel-element container cases is given in Table 4.4.

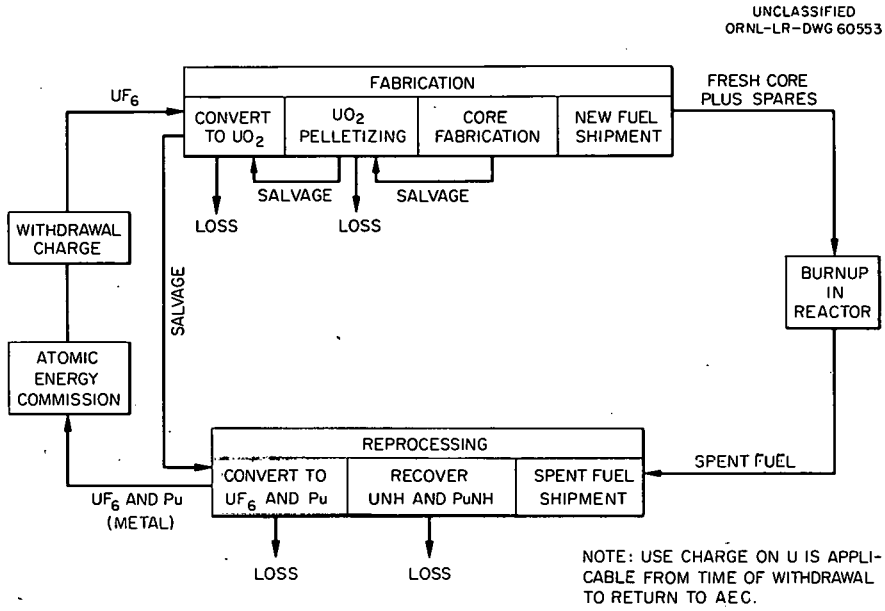

Fig. 4.18. Fuel Cycle Flow Chart.

Table 4.3. Reference Core Estimated Fuel-Cycle Costs

	Costs		
	$/core	$/year[a]	mills/shp-hr
Fabrication	958,900	458,800	3.9
Net fuel burnup	309,000	147,800	1.3
Reprocessing	582,800	278,900	2.4
Uranium use charge	320,400	153,300	1.3
Working capital interest	161,000	77,030	0.6
Total	2,332,100	1,115,830	9.5

[a]Core lifetime is 1.4 full-power years; assumed load factor is 0.67.

The cost saving for Case Z-420 shows the effects of the direct substitution of Zircaloy for stainless steel. The results indicate that a reduction in total fuel-cycle cost of about 37% could be realized for this case. However, Case Z-420 is somewhat marginal with respect to shutdown safety. Thus it appears that different control rods or a burnable poison would be necessary before the indicated cost savings could be achieved in practice.

Table 4.4. Cost Reductions Resulting from Substituting Zircaloy for Stainless Steel in Fuel Element Containers

Cost Component	Cost Reduction Based on Reference Case S-420[a] (%)		
	Case Z-420[b]	Case Z-386[c]	Case Z-338[d]
Fabrication	53	41	9
Net fuel burnup	2	2	2
Reprocessing	53	41	7
Uranium use charge	7	15	26
Working capital interest	2	5	9
Total fuel cycle	37	30	10

[a]Case S-420: reference case, core I-type fuel elements (uniform U^{235} enrichment of 4.2 wt %) in stainless steel containers.

[b]Case Z-420: same as reference case except Zircaloy containers; lifetime, 3.0 full-power years.

[c]Case Z-386: core I-type fuel elements (uniform U^{235} enrichment of 3.86 wt %) in Zircaloy containers; enrichment adjusted to give same shutdown margin with central rod out as reference case; lifetime, 2.3 full-power years.

[d]Case Z-338: core I-type fuel elements (uniform U^{235} enrichment of 3.38 wt %) in Zircaloy containers; enrichment adjusted to give same lifetime as reference case (1.4 full-power years).

Case Z-386 could be controlled with the present control rods and without the use of burnable poisons. The estimated fuel-cycle cost reduction for this case is 30%. This cost reduction is brought about by both an increase in lifetime and a reduction in enrichment relative to the reference core. Extension of lifetime is, however, the more important effect.

The economic effect of utilizing Zircaloy containers to reduce enrichment (keeping lifetime constant) is well illustrated by Case Z-338. Decreasing the enrichment from 4.2 to 3.38 wt % U^{235} results in a fuel-cycle cost savings of 10%. Although substantial, this cost reduction does not compare favorably with savings for the other cases. This demonstrates that increasing lifetime is the more profitable approach to reducing fuel-cycle costs for the NS SAVANNAH.

Unfortunately, fuel-cycle cost studies are somewhat unreliable because of the large number of uncertainties in the various cost components. In this analysis, core fabrication cost data were based on average costs from AEC sources, suppliers, and manufacturers; this approach was necessary because no information was available on fabrication costs for NS SAVANNAH fuel elements. Reprocessing costs have been published by the AEC, but they are based on a hypothetical plant; there is some uncertainty as to whether these costs are realistic. The estimated fuel burnup cost depends on burnup calculations that are not completely reliable. In addition, the estimated load factor (0.67) is obviously a guess, since experience with nuclear-powered merchant vessels does not exist. As may be seen, the absolute cost figures given in Table 4.3 are subject to question. It is felt, however, that the relative cost savings shown in Table 4.4 are reasonably valid; this is supported by Fig. 4.19, which shows that

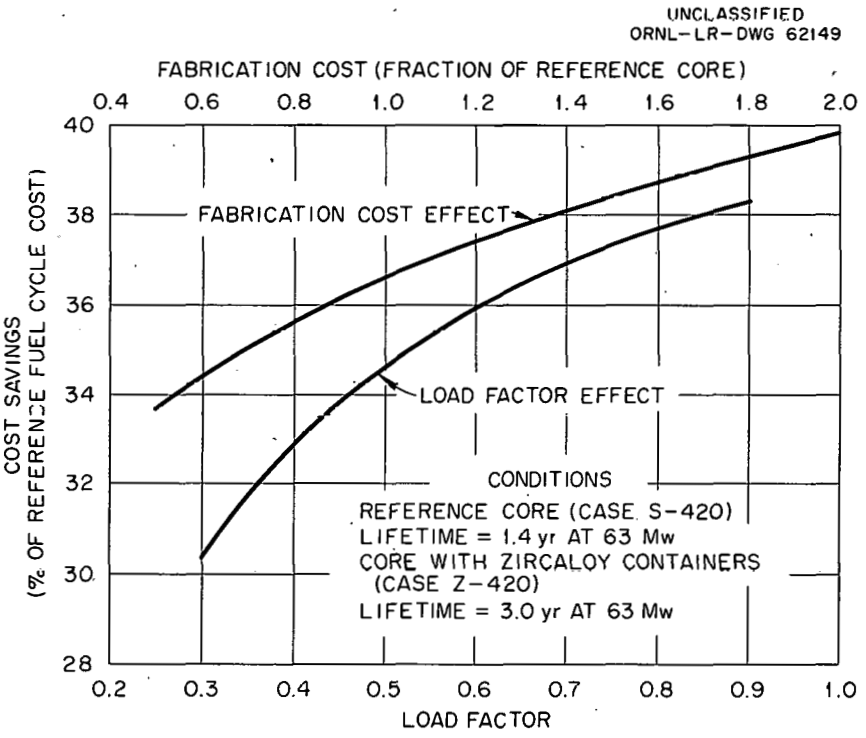

Fig. 4.19. Effects of Load Factor and Fabrication Cost Estimate on Fuel-Cycle Cost Savings Resulting from Use of Zircaloy Fuel-Element Containers in the NS SAVANNAH Reactor.

the relative cost savings are rather insensitive to changes in core fabrication cost or load factor.

Core I Lifetime Studies

E. E. Gross B. W. Colston
M. L. Winton

Additional lifetime studies were undertaken using the CANDLE code to investigate the effects of various fuel-management schemes on the burnup of an initial two-zone core I (4.2 wt % U^{235} inner zone, 4.6 wt % U^{235} outer zone). The schemes examined were (1) switching inner and outer fuel zones at the end of core I burnup, (2) removing the burned inner zone, replacing it with the burned outer zone, and inserting a fresh outer zone, and (3) leaving the burned core I fuel in place but replacing the stainless steel egg crate with a Zircaloy egg crate. Movement of burned fuel is accompanied by the movement of the associated fission products, including equilibrium xenon and samarium.

Calculated reactivity lifetimes for these schemes are shown in Fig. 4.20. Of the three fuel-management schemes studied, replacement of the

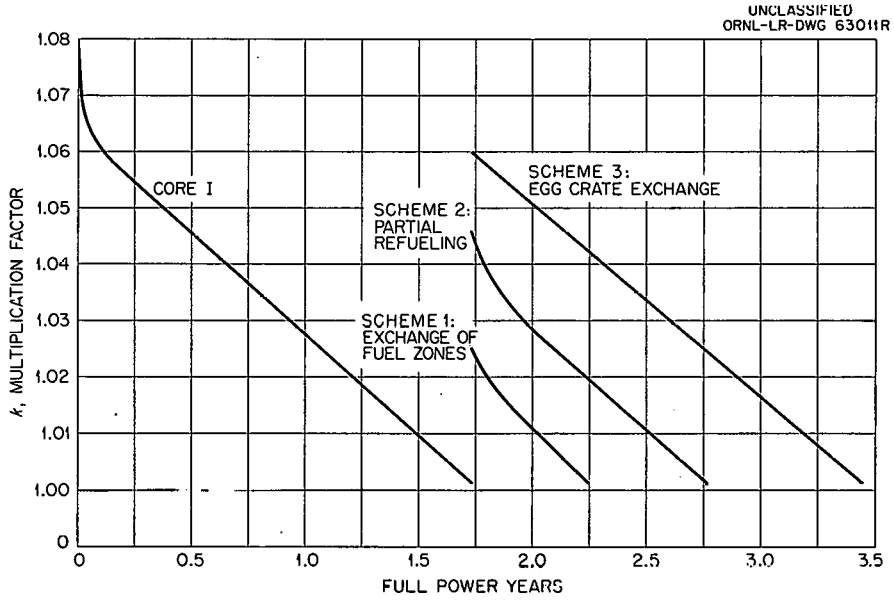

Fig. 4.20. Lifetime Studies of NS SAVANNAH Core I.

stainless steel egg crate by a Zircaloy egg crate (scheme 3) in a burned core I is the most attractive from the point of view of increased reactivity lifetime. The behavior of the scheme 3 reactivity lifetime curve is consistent with the burnup curve obtained for one-zone 4.2 wt % U^{235}-enriched fuel in a Zircaloy egg crate (Fig. 4.10).

Simple switching of the burned zones (scheme 1) provides only an additional seven months of core life and appears to be the least attractive of the fuel-management schemes. The initial curvature in the reactivity lifetime curve for scheme 1 is the result of the difference between the equilibrium xenon and samarium concentrations before and after the switch is made.

Addition of half a fresh core (4.6 wt % U^{235}) to the outer zone (scheme 2) is calculated to extend core life an additional 1.2 years. It is estimated that an enrichment of 5.65 wt % U^{235} in the fresh outer zone would be required to obtain a core life equal to that obtainable from an exchange of egg-crate materials (scheme 3).

In all the burnup calculations reported above, the fission products were characterized by a single element with an absorption resonance integral of 214 barns and a thermal absorption cross section of 43 barns at 2200 meters/sec.[12] It has been customary to neglect nonthermal absorptions in fission-product poisons, mainly because of the scarcity of experimental information on these nuclei. In order to test the effect of nonthermal absorptions in fission products on the calculated lifetime of the NS SAVANNAH core I, another burnup calculation was performed using a zero resonance absorption integral for the fission products. The calculated reactivity lifetimes for the two assumed values of the resonance absorption integral for fission products are compared in Fig. 4.21. It is apparent from Fig. 4.21 that NS SAVANNAH-type cores are sensitive to resonance absorptions in fission products.

---

[12]E. A. Nephew, Thermal and Resonance Absorption Cross Sections of the U^{233}, U^{235}, and Pu^{239} Fission Products, ORNL-2869, January 18, 1960.

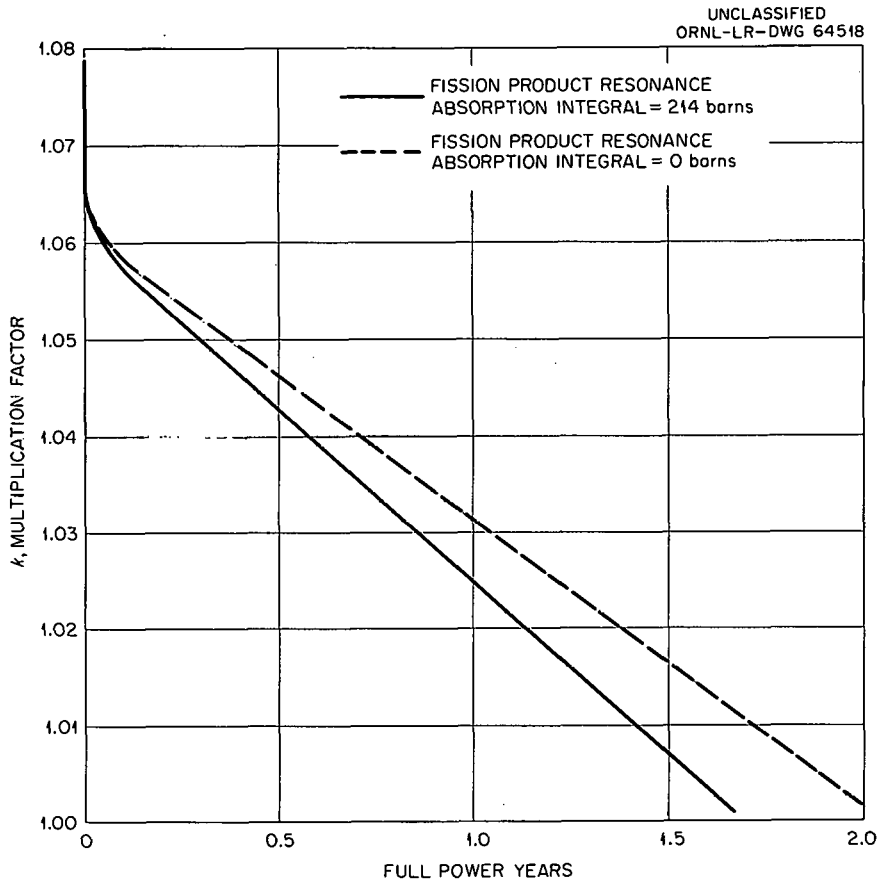

Fig. 4.21. Dependence of Calculated Reactivity Lifetime of NS SAVANNAH Core I on Resonance Absorption Integral of Fission-Product Poisons.

Fuel Development

W. C. Thurber

Fuel-Rod Swaging Studies (J. T. Lamartine)

Efforts are being made to produce high-density UO_2 fuel rods by swaging oxides not normally considered suitable for this type of compaction and subjecting these rods to postswaging sintering treatments, since it has been reported[13,14] that UO_2 can be sintered to a high density at a relatively low temperature if the initial oxygen-to-uranium ratio is on

[13]Scott and Williams, Trans. Brit. Ceram. Soc., 57: 199 (1958).

[14]Olin-Matheison Company, Fuel Cycle Development Program First Quar. Rep. Sept. 30, 1959, NYO-2684.

the order of 2.2 to 2.3. In order to test this concept, two oxides which had previously been swaged to low densities[15] were roasted in air at 120°C for 8 hr to increase the oxygen-to-uranium ratios to the values given in Table 4.5. The oxides were then swaged in the conventional manner to 55% reduction in area. Finally, portions of the rods with exposed ends were sintered in flowing tank nitrogen for 20 hr at 1200°C. As indicated in Table 4.5, major increases in density occurred during sintering. These changes were coupled with reductions in the oxygen-to-uranium ratio to nearly stoichiometric proportions and large decreases in surface area. As might be expected, diametral shrinkage of the UO_2 in the range 0.040 to 0.070 in. was measured. This large diametral shrinkage suggests that an additional swaging operation would be desirable to reduce the gap between fuel and cladding.

Table 4.5. Property Changes Resulting from Sintering of Swaged UO_2

Oxide Identification	Initial Oxygen-to-Uranium Ratio	Swaged Density (% of theoretical)	Sintered[a] Density (% of theoretical)	Sintered Oxygen-to-Uranium Ratio	Sintered Surface Area (m^2/g)
Ceramic No. 21	2.225	55.4	90.2	2.002	0.073
High fired SR-772	2.324	71.4	87.8	2.002	0.034

[a]Sintered 20 hr in N_2 at 1200°C.

Defective Fuel Rod Testing (J. C. Griess, W. C. Thurber)

Before unsintered UO_2 fuel can be recommended for use in the NS SAVANNAH it will be necessary to know the behavior of this material in fuel rods containing unintentional defects. Although it has been demonstrated that pressed and sintered UO_2 pellets are relatively stable in

[15]J. T. Lamartine and W. C. Thurber, Development of Swaged Stainless Steel Fuel Rods Containing UO_2, ORNL CF-59-10-8, Oct. 12, 1959.

high-temperature water,[16,17] it could be postulated that corrosion-erosion losses through defective cladding would be significantly increased in vibratory-compacted or swaged fuel. A series of out-of-pile tests are therefore in progress in a circulating-water loop where the comparative losses of swaged, vibratory-compacted, and pelletized UO_2 from fuel rods will be determined. Screening tests have been completed on all but the vibratory-compacted fuel.

The loop water conditions for the tests are the following: temperature, 275°C; pressure, 1750 psi; velocity, 10 fps; pH, neutral; oxygen content, 3 to 6 ppm. The 30-in. fuel rods are clad with 0.500-in.-o.d., 0.035-in.-wall, type 304 stainless steel. During each test a defective sample with a 0.013-in.-diam hole and a defect-free control sample are simultaneously exposed. The loop is periodically subjected to either isothermal pressure cycles (1000 to 1750 psi) or simultaneous pressure-temperature cycles (50 to 1750 psi and 100 to 275°C) and the uranium content of the loop water is monitored.

The results of the tests completed thus far are summarized in Table 4.6. It may be observed that the weight changes in both the defective

[16]J. D. Eichenberg et al., Effects of Irradiation on Bulk UO_2, WAPD-183, pp. 76–94, Oct. 1957.

[17]J. Belle and B. Lustman, Fuel Elements Conference, Paris, November 18–23, 1957, TID-7546, Book 2, p. 500, March 1958.

Table 4.6. Summary of Results of Corrosion-Erosion Tests on Defective UO_2 Fuel Rods

Identification			Number of Pressure Cycles	Number of Pressure-Temperature Cycles	Test Duration (hr)	As-Tested Weight Gain (g)	Vacuum-Dried Weight Gain (g)
Run No.	Fuel	Type of Sample					
1	UO_2 pellets	Defective	8	2	133	5.680	0.030
		Control	8	2	133		0.024
2A	Swaged UO_2	Defective		10	344	2.842	2.758
		Control		10	344		0
2B[a]	Swaged UO_2	Defective		10	313	2.768	2.758
		Control		10	313		−0.010
3	Swaged UO_2	Defective		10	356	5.940	5.928
		Control		10	356		0.006

[a]Test 2B was a continuation of test 2A after intermediate evaluation.

and the control samples containing UO_2 pellets were essentially negligible. For the swaged rods, on the other hand, relatively large weight increases were noted. The fact that the weight changed little after vacuum drying suggests that the observed changes were a result of oxidation of the UO_2 to a higher oxide rather than moisture pickup. Metallographic examinations of the defective areas after the tests revealed the presence of small quantities of material other than UO_2. It was impossible to identify the material by x-ray diffraction. No changes in the uranium content of the loop water were detected in samples taken before and after cycling of the fuel rods.

Thermal Expansion Behavior of Swaged Fuel Rods Containing UO_2

(F. L. Carlsen, Jr.)

The coefficient of thermal expansion of nine samples of UO_2 swaged in type 304 stainless steel was determined. The difference between the coefficients of the UO_2 and the stainless steel was determined by measuring coefficients with the push rod of the dilatometer directly on the UO_2 and then with the push rod on the stainless steel. The results of these determinations are presented in Table 4.7.

As indicated, the measurements of samples F through I were made in vacuum rather than in helium. This change was made because there was some oxidation of the UO_2 in samples D and E. For the other samples measured in helium, a slight weight loss, indicative of a satisfactory atmosphere, was observed after the determination.

The effect of the UO_2 on the coefficient for the stainless steel may be seen by comparing the coefficient measured for sample B with the push rod on the stainless steel and the UO_2 in place with that measured with the UO_2 removed. For comparison, a coefficient of thermal expansion of 1.0×10^{-5} in./in.·°C (0 to 1000°C) has been reported[18] for solid UO_2 (95% theoretical density). These results suggest that some interaction between the fuel and cladding occurs under isothermal conditions, since

[18] S. D. Fulkerson, Apparatus for Determining Linear Thermal Expansion of Materials in Vacuum or Controlled Atmosphere, p. 35, ORNL-2856, Dec. 21, 1959.

PP 83-6

NSIC 102

Table 4.7. Results of Measurements of the Coefficients of Thermal Expansion of Samples of UO_2 Swaged in Type 304 Stainless Steel

Sample No.	UO_2 Type[a]	Push-Rod Position	Atmosphere	Coefficient of Thermal Expansion (in./in.·°C) in the Range 0 to 1000°C
				$\times 10^{-5}$
A	1	UO_2	Helium	1.40
		Steel	Helium	1.60
B	1	UO_2	Helium	1.56
		Steel	Helium	1.61
C	1	UO_2	Helium	1.58
D	2	UO_2	Helium	(b)
E	2	Steel	Helium	(b)
F	2	Steel	Vacuum	1.61
G	3	UO_2	Vacuum	1.51
		Steel	Vacuum	1.74
H	3	UO_2	Vacuum	1.48
		Steel	Vacuum	1.68
I	3	UO_2	Vacuum	1.49
		Steel	Vacuum	1.68
B	UO_2 removed	Steel	Helium	1.86

[a] 1 = Spencer fused and ground.
2 = Y-12 high fired.
3 = Mallinckrodt special dense oxide.

[b] UO_2 oxidized.

the expansion coefficients are intermediate between those of the individual materials.

Fission-Gas Release from Fused-and-Ground UO_2 (D. F. Toner, J. L. Scott)

A significant problem in the design of high-temperature nuclear reactors is the rate of release of the fission gases generated in the fuel. Especially in clad fuel elements, excessive release of these gases may not only stress the cladding but also reduce the thermal conductivity at the

fuel-to-cladding interface. This could cause higher operating temperatures, attendant increases in gas release, and swelling of the fuel material. The ability to retain fission gases within the atomic lattice is therefore a significant factor in evaluating fuel materials.

Fission-gas release from nuclear fuels is commonly investigated by using the neutron-activation technique. A specimen of the fuel material is briefly irradiated to produce trace quantities of the fission gases. The sample is then subjected to an out-of-pile annealing operation in which the Xe^{133} diffuses out of the specimen and is collected in a charcoal trap cooled with liquid nitrogen. The radioactivity of the collected fission gas is continuously monitored, and the amount of Xe^{133} released can be calculated. The total amount of Xe^{133} contained in the specimen can be determined from the irradiation exposure measured with a cobalt flux monitor. By appropriate correction for decay of Xe^{133}, the fractional release of the gas can be computed as a function of annealing time and temperature. The technique and equipment used have been previously described in detail.[19]

If diffusion is the principal mechanism controlling fission-gas release from the fuel material, the fractional release is proportional to the square root of the annealing time, and fission-gas-release data are best described in terms of a release rate parameter, D', which may be calculated from the following equation:

$$D' = \frac{\pi f^2}{36t} \quad , \tag{1}$$

where

D' = release rate parameter (sec^{-1}),

f = fraction of Xe^{133} released by diffusion,

t = time of the diffusion-controlled release (sec).

---

[19]D. F. Toner and J. L. Scott, Study of the Factors Controlling the Release of Xe^{133} from Bulk UO_2, paper presented at the Symposium on Radiation Effects on Refractory Fuel Compounds, 64th Annual Meeting of the American Society for Testing Materials, Atlantic City, N. J., June 25–30, 1961.

The release rate parameter, D', is related to the diffusion coefficient of xenon in the sample (UO_2) by the equation:

$$D' = \frac{D}{a^2} \quad , \tag{2}$$

where

D = the diffusion coefficient (cm^2/sec),

a = radius of the uniform sphere (cm).

The uniform sphere model, which has also been described,[18] suggests that a fuel body could be assumed to consist of spheres of theoretical density with the same surface area per unit weight as the body. For UO_2 with a surface area, S, the equivalent sphere radius, a, is

$$a = \frac{3}{\rho_0 S} \quad ,$$

where ρ_0 is the theoretical density of UO_2.

In order to determine D' for fused-and-ground UO_2 powder, a possible fuel for use in core III of the NS SAVANNAH reactor, two neutron-activation tests were run on powder supplied to ORNL by the Spencer Chemical Company. The powder is described below:

Particle size	-20 +35 mesh
Enrichment in U^{235}	2.05%
Oxygen-to-uranium ratio	2.023
BET surface area	200 cm^2/g

Impurities	Concentration (wt %)
Al	3.0×10^{-3}
B	$<3.3 \times 10^{-5}$
Cd	$<1.3 \times 10^{-3}$
Cr	2.4×10^{-4}
Fe	2.5×10^{-3}
Mn	$<3.3 \times 10^{-5}$
Ni	1.8×10^{-4}
Si	$<1.6 \times 10^{-4}$
C	1.7×10^{-4}

The results of xenon fission-gas-release measurements at 1400 and 1600°C are presented in Table 4.8. It may be noted that $D'_{1400°C}$ for the fused-and-ground oxide is of the same order of magnitude (10^{-11} sec^{-1}) as reported earlier[20] for the 92%-dense pressed-and-sintered UO_2 fuel bodies used in core I. At 1600°C, D′ for the fused-and-ground UO_2 is comparable with values representative of other[19] pressed-and-sintered UO_2 samples tested at 1600°C.

Table 4.8. Values of the Release Rate Parameter, D′, for Neutron-Activated Fused-and-Ground UO_2 Powder

Annealing Temperature (°C)	Accumulated Annealing Time (hr)	Accumulated Fraction of Gas Released	Release-Rate Parameter, D′ (sec^{-1})
		$\times 10^{-3}$	
1400	1.5	3.51	
	17.5	5.71	
	19.5	5.79	
	22.5	5.91	1.1×10^{-11}
1600	2.0	5.01	
	3.5	6.40	
	19.5	15.0	
	29.5	16.7	2.7×10^{-10}

Preparation of Irradiation Test Specimens for ORR Loop (J. T. Lamartine, W. S. Ernst, Jr.)

As a continuation of the fuel-rod irradiation program in the ORR pressurized-water loop, additional experimental assemblies 4, 5, and 6 have been fabricated.[21] Each assembly consists of three rods brazed to electroless-nickel-plated ferrule spacers, as shown in Fig. 4.22. Assemblies 4 and 5 each include one rod with swaged UO_2 and two rods with

[20]Maritime Reactor Project Ann. Prog. Rep. Nov. 30, 1960, ORNL-3046, p. 16.

[21]J. T. Lamartine, Maritime Pressurized-Water Loop Irradiation Experiments 4, 5, and 6: Specimen Manufacturing Procedures, ORNL-CF-61-10-29, October 13, 1961.

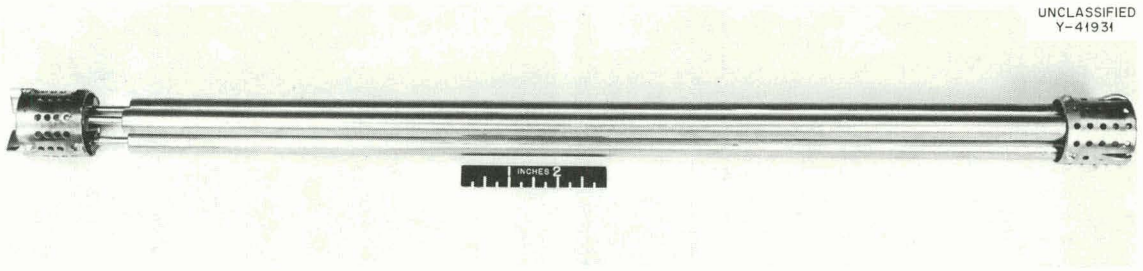

Fig. 4.22. Fuel Rod Cluster of the Type Used in ORR Pressurized-Water Loop Experiments 4, 5, and 6.

vibratory-compacted UO_2, whereas assembly 6 has only rods with vibratory-compacted fuel. The rods are 19 in. long and are fabricated of 0.500-in.-o.d., 0.035-in.-wall, type 304 stainless steel.

Although no difficulty was experienced in fabricating swaged UO_2 to 90% theoretical density, problems were encountered in vibratory compacting UO_2 to the specified density of 87% of theoretical. In the first rod, designated 4-0-1 (2A), the UO_2 was initially compacted to 85% of theoretical density, which is 2% less than the specified minimum. A screen analysis of the vibrated UO_2 in this rod revealed extensive breakup of the material, which greatly changed the starting distribution. The coarse fraction was reduced from 60 wt % of the total to only about 50 wt %. The rod was then reloaded with the starting distribution (60 wt % -10 +mesh, 15 wt % -50 +100 mesh, and 25 wt % -200 mesh) utilizing as much previbrated UO_2 as could be obtained for each particle-size fraction. The part of a given size fraction that could not be filled with previbrated UO_2 was filled with unvibrated UO_2. After compacting this mixture for an additional 15 min, an acceptable density of 87.2% of theoretical was obtained. This procedure was employed for preparing all the vibratory-compacted specimens used in experiments 4 and 5.

For those rods scheduled for experiment 6, the procedure outlined above did not yield densities in excess of 87% of theoretical. However, attainment of densities in excess of the specified minimum could be achieved by using in each size fraction only material which had survived a 15-min preliminary vibration under conditions similar to those used in the final loading. In the final vibration operation, the UO_2 in the first

two rods (Table 4.9) was compacted on a NAVCO BH 1 5/8-in. pneumatic vibrator with 90-psi air pressure, and the UO_2 in the remaining rods was compacted on a NAVCO BH 2-in. vibrator with 95-psi air pressure, which yielded slightly higher densities. Each rod was vibrated 5 min with no load followed by 10 min with a 176-g load. Data on all the vibratory-compacted material are summarized in Table 4.9.

Table 4.9. Bulk Densities of Vibratory-Compacted UO_2 in Fuel Rods for Experiments 4, 5, and 6

Rod No.	Fuel Enrichment (% U^{235})	Weight of UO_2 in Rod[a] (g)	Vibrated Bulk Density	
			(g/cm^3)	(% of theoretical)
4-O-1 (2A)	1.87	373.2	9.57	87.2
4-O-1 (17A)	1.87	373.2	9.57	87.2
4-P-1 (22)	1.12	375.0	9.66	88.1
4-P-1 (23)	1.12	374.1	9.65	88.1
5-A-1 (4)	3.78	374.9	9.67	88.2
5-A-1 (24)	3.78	375.2	9.65	88.1
5-B-1 (3)	4.22	375.1	9.64	88.0
5-B-1 (29)	4.22	374.1	9.64	88.0
6-P-1 (12)	2.85	375.9	9.60	87.5
6-P-1 (33)	2.85	375.9	9.64	88.0
6-N-1 (16)	2.85	375.2	9.64	88.0
6-N-1 (30)	2.85	376.3	9.66	88.1

[a]Particle size distribution is 60 wt % -10 +16 mesh, 15 wt % -50 +100 mesh, and 25 wt % -200 mesh for all rods except No. 5-A-1 (24), which has a distribution of 53.4 wt % -10 +16 mesh, 6.6 wt % -16 +50 mesh, 15 wt % -50 +100 mesh, and 25 wt % -200 mesh.

No problems were encountered in brazing the three clusters required for these experiments. Since there was some indication from experiment 3 that electroless-nickel deposits on the rods minimized crud buildup, a 2-in.-long band of this material was plated at midlength on one of the rods in experimental assembly No. 6. The plating was then fused during the brazing operation. This area will be carefully examined after irradiation to test the validity of the observation in experiment 3.

Fabrication Studies on Vibratory Compaction of Fuel (W. S. Ernst, Jr.)

A study was made to determine the particle-size distributions that would yield high bulk densities when vibratory compacted. In this work a thorium oxide–3.4 wt % uranium oxide mixture was used because this material was readily available in the form desired. The mixture is believed to be quite similar to UO_2 in its compaction behavior. Three-particle-size fractions (-10 +16 mesh, -70, +100 mesh, and -200 mesh) were chosen because these fractions had been used in previous work and some knowledge of their compacting behavior was available. The vibrated bulk densities obtained ranged from 67 to 89% of theoretical as shown in Table 4.10. The mixtures listed are also plotted on a ternary diagram in Fig. 4.23. Most of the mixtures tested were in the portion of the diagram representing greater than 50% coarse material, because previous experience had shown that use of these mixtures would lead to high densities.

Although three-fraction mixtures give higher densities than two-fraction systems, they have the disadvantage of requiring a medium-sized

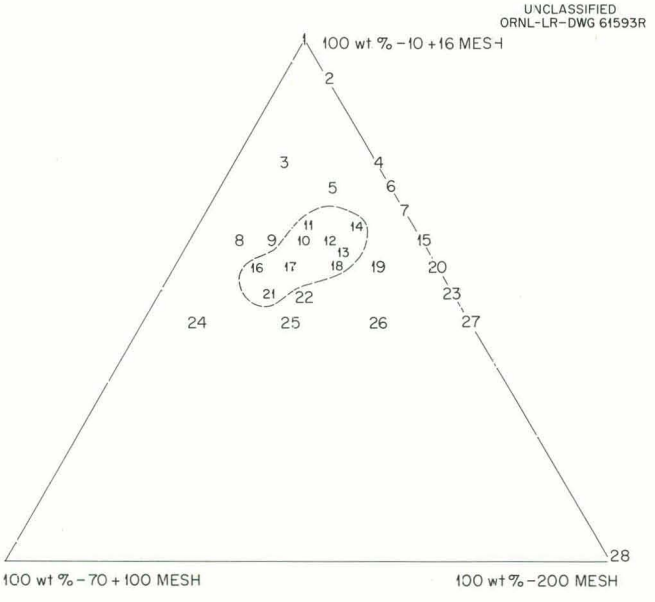

Fig. 23. Diagram Showing Effect of Particle-Size Distribution on Vibrated Density of Three-Particle-Size Mixtures of ThO_2-3.4 wt % UO_2. Broken line encloses approximate area where density exceeds 88% of the theoretical density. The numbers indicate individual experiments (see Table 4.10 for density values).

Table 4.10. Bulk Densities Obtained by Vibratory Compacting ThO_2–3.4 wt % UO_2 Mixtures of Various Particle-Size Distributions[a]

Mixture No.	Particle-Size Distribution (wt % of indicated particle-size fraction)			Vibrated Bulk Densities (g/cm^3)
	-10 +16 mesh	-70 +100 mesh	-200 mesh	
1	100			6.77
2	90		10	7.42
3	75	15	10	8.32
4	75		25	8.59[b]
5	70	10	20	8.66
6	70		30	8.74[c]
7	65		35	8.68[c]
8	60	30	10	8.64
9	60	25	15	8.69
10	60	20	20	8.90
11	62.5	17.5	20	8.88
12	60	15	25	8.85
13	58	15	27	8.84
14	62.5	10	27.5	8.22
15	60		40	8.62[c]
16	55	30	15	8.89
17	55	25	20	8.94
18	55	17.5	27.5	8.89
19	55	10	35	8.58
20	55		45	8.55
21	50	30	20	8.84
22	50	25	25	8.73
23	50		50	8.22
24	45	45	10	8.32
25	45	30	25	8.74
26	45	15	40	8.44
27	45		55	8.19
28			100	6.72

[a]All mixtures were vibrated in NAVCO BH 1 1/4-in. pneumatic vibrator with an air pressure of ~90 psi; length of vibration run was 10 min; material vibrated was fused ThO_2–3.4 wt % UO_2; the rod was type 304 stainless steel, 19 in. long, 0.5 in. o.d., 0.035 in. wall.

[b]Average of three vibration runs.

[c]Average of two vibration runs.

fraction that is difficult and expensive to obtain. In view of this consideration, the maximum bulk density that could be obtained using the two-particle-size fractions (-10 +16 mesh and -200 mesh) was determined. Densities achieved with these mixtures are listed also in Table 4.10. A plot of these data clearly illustrates (Fig. 4.24) the relationship between density and particle-size distribution for the two-fraction system. A maximum density of about 87.5% of theoretical was obtained using a mixture of 70 wt % -10 +16 mesh and 30 wt % -200 mesh material. This work is being continued, and the effect of the thrust to the rod on compaction efficiency is being studied. Preliminary results show that a small increase in density can be obtained by increasing the thrust.

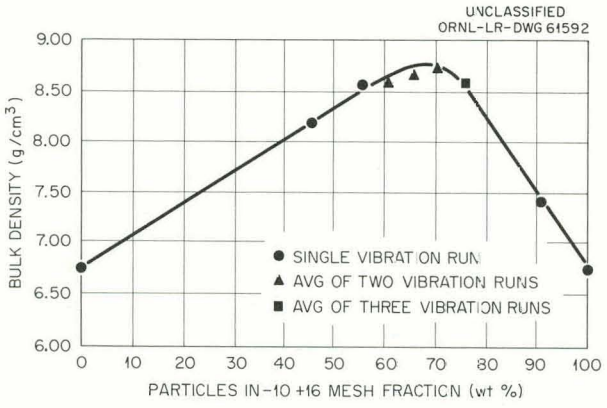

Fig. 4.24. Effect of Particle-Size Distribution on the Vibratory-Compacted Density of Two-Particle Size (-10 +16 and -200 Mesh) ThO_2–3.4 wt % UO_2 Material.

Particle-size distributions containing 4-, 5-, and 7-size fractions, which have been reported by other laboratories[22-24] to yield densities in excess of 90% of theoretical, were compared under conditions similar to those employed in the studies described above. Comparable bulk densities of 87 to 88% of theoretical were obtained in all cases. These values were

---

[22]J. J. Hauth, Vibrationally-Compacted Ceramic Fuels, HW-67777.

[23]Heavy-Water Moderated Power Reactor Prog. Rep. Oct. 1960, DP-555, pp. 16–17.

[24]Summary Report for Period Ending May 31, 1960 – Development and Testing of the UO_2 Fuel Element System, CEND-88, June 1, 1960.

about 1% lower than the maximum obtained in the ternary system studied at ORNL.

Test Bundles for Irradiation in the Vallecitos Boiling-Water Reactor (VBWR)
(W. S. Ernst, Jr., J. T. Lamartine, J. W. Tackett)

Present plans call for irradiating two 16-rod fuel bundles in the VBWR. Each bundle will contain 40-in.-long rods of 0.500-in.-o.d., 0.035-in.-wall, type 304 stainless steel fueled with fused-and-ground UO_2. The fuel in the rods for one bundle will be fabricated by rotary swaging, while the fuel in the second bundle of rods will be vibratory compacted.

Preliminary swaging studies with rods of this geometry indicated that no problems would be expected in fabricating the 40-in.-long rods and that a fuel density of 90% of theoretical should be readily attainable. The density variation along a rod was found to be ±0.5% of theoretical or less. On the basis of similar work on vibratory-compacted material, densities of approximately 87% of theoretical are expected with this method of fabrication.

Fused-and-ground UO_2 enriched 5% in U^{235} was procured for the two bundles, but the material to be used in the vibratory-compacted bundle was found to be unsatisfactory. Significant degradation of the coarse-size fraction occurred during vibration, and the maximum attainable density was only 84% of theoretical. The maximum density of individual particles, as measured with a mercury pycnometer, was found to be only 96% and explained, in part, why the bulk compacted densities were lower than expected. The material must be returned to the vendor for reprocessing. The oxide procured for the swaged bundle has not yet been evaluated.

Procedures have been developed for brazing these fuel bundles. A full-size prototype bundle containing dummy fuel was assembled and electroless-nickel brazed[25] in a specially designed fixture. The prototype bundle consisted of 16 tubes (with iron slugs inside), 54 electroless-nickel-plated internal spacer ferrules, and 72 electroless-nickel-plated peripheral ferrules. The partially assembled unit is shown in Fig. 4.25a,

[25]P. Patriarca et al., Electroless-Plated Brazing Alloys, ORNL-2243, March 1957.

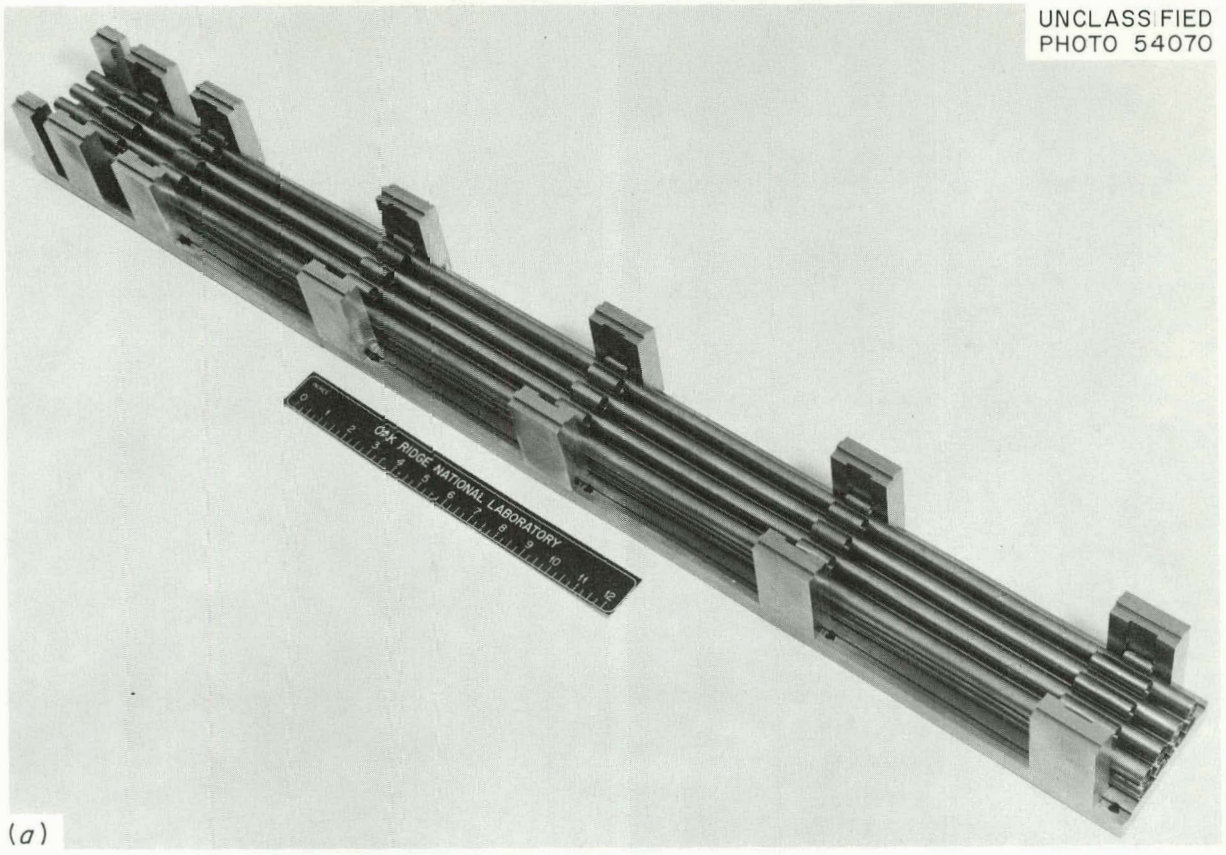

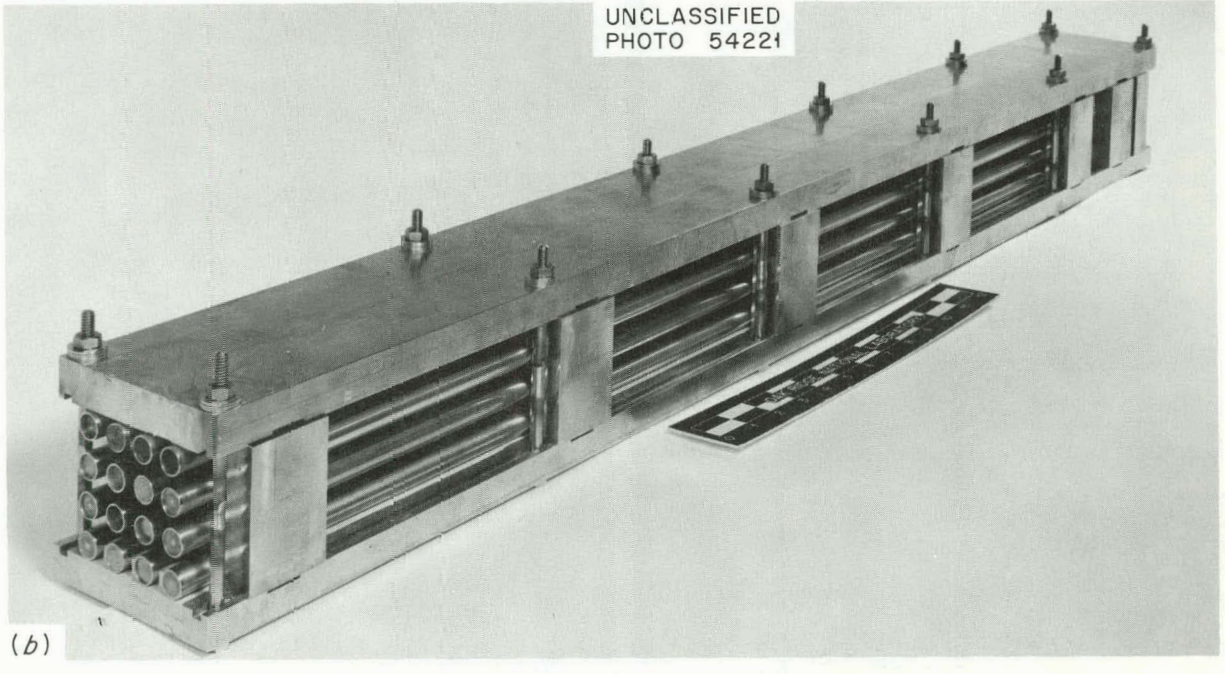

Fig. 4.25. (a) Partially Assembled Prototype Fuel Bundle for Irradiation in VBWR. (b) Prototype Bundle Assembled in the Fixture and Ready for Brazing.

and the prototype bundle assembled in the fixture and ready for brazing is shown in Fig. 4.25b.

After furnace brazing in dry hydrogen at 1000°C, the completed unit, shown in Fig. 4.26, was completely measured. Twenty-four measurements of the spacings between adjacent fuel rods were obtained at each of seven axial locations along the length of the fuel bundle. These measurements are summarized below:

Total number of measurements made	168
High measurement, in.	0.222
Low measurement, in.	0.203
Per cent within 0.212 ± 0.005 in.	88
Per cent within 0.212 ± 0.010 in.	100
Design requirement, in.	0.212 ± 0.020

Similarly, eight over-all width measurements were obtained at each of the seven axial locations along the length of the fuel bundle. These measurements are summarized below:

Total number of measurements made	56
High measurement, in.	2.651
Low measurement, in.	2.625
Per cent within 2.636 ± 0.005 in.	73
Per cent within 2.636 $^{+C.015}_{-C.011}$ in.	100
Design requirement, in.	2.636 ± 0.050 in.

It may be seen that the assembly appeared to be well within the required dimensional tolerances. Also, there was no evidence of sagging in the unsupported fuel-rod segments between spacer ferrules. Therefore, the same assembly and brazing procedures will be utilized in fabricating the actual fuel bundles containing swaged or vibratory-compacted UO_2.

Compartmented Fuel Plate Fabrication Development (R. G. Gilliland)

The advantages of greater heat-transfer area, lower central fuel temperature, the possibility of operating at higher specific power without central melting, less self-shielding of fuel, and less fission-product release from a single cladding defect in a compartmented fuel element, as

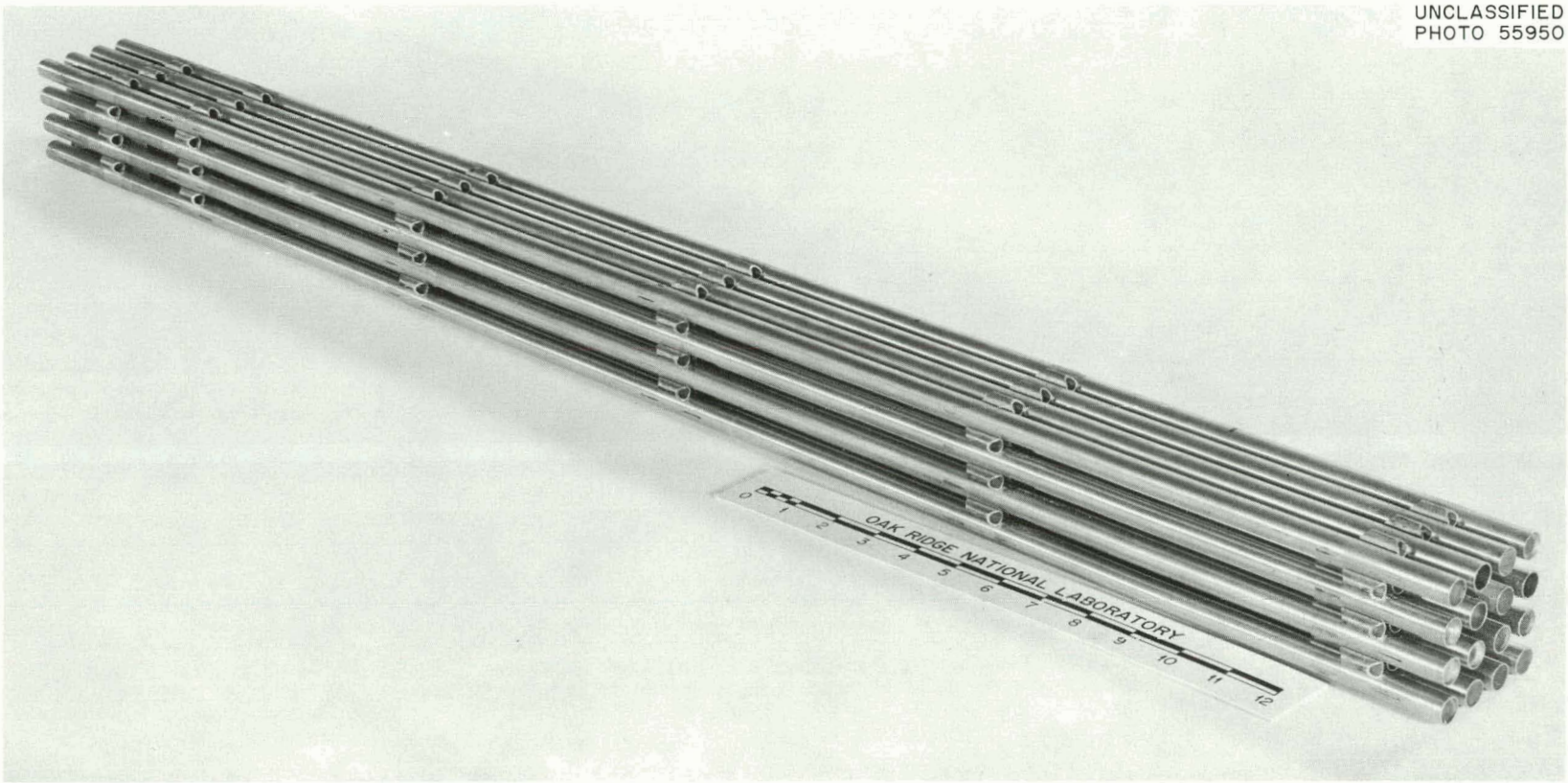

Fig. 4.26. As-Brazed Prototype Fuel Bundle for Irradiation in VBWR.

compared with the more conventional rod-type fuel element employed in most pressurized-water reactors,[26] suggested further study of compartmented fuel plates. Such a compartmented element in which platelets of a ceramic fuel, such as UO_2, are enclosed within a lattice-like frame between cover sheets is illustrated schematically in Fig. 4.27.

A feasibility investigation of resistance welding as a means for bonding cover sheets to the grid structure has been performed on a subcontract at Sciaky Brothers, Inc., Chicago, Illinois. The studies have

[26]W. C. Thurber, Some Design Considerations in Compartmented Plate-Type Fuel Elements Containing UO_2, ORNL CF-58-7-105, July 28, 1958.

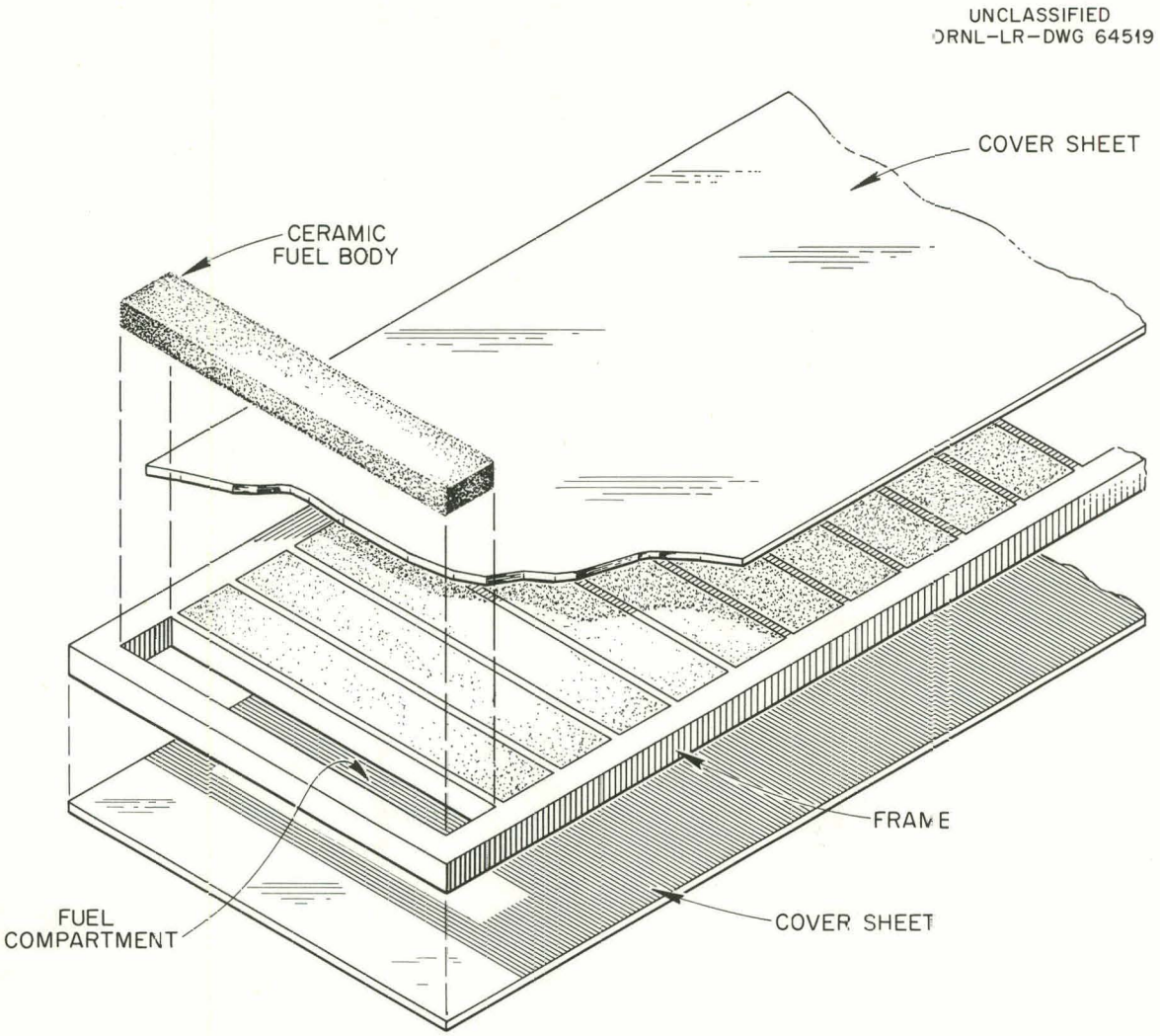

Fig. 4.27. Sketch of a Compartmented Fuel Plate.

indicated that this process is not readily applicable to the production of leaktight compartmented fuel plates. The joint configuration is not one that is suitable for resistance welding, and considerable equipment and process development would be required to demonstrate feasibility on a production scale.

The ORNL investigation of methods for fabricating compartmented fuel elements has involved brazing. Both spark-discharge and conventional machining have been evaluated[27] as techniques for grid structure preparation. Type 304L stainless steel was used throughout, and the mating parts were preplated with electroless-nickel brazing alloy.

Using a grid that had been machined by the spark-discharge process, a mockup element containing several compartments was constructed. The specimen was completely sealed along the outer edges by using the tungsten-arc-welding process, except for an evacuation tube. This tube was subsequently closed under vacuum by using the electron-beam process. Although it was thought that the internal vacuum would impart good fitup at the cover plate-to-grid joints without the need for platens, the technique was not completely successful in practice. Complete evacuation of some compartments was difficult to achieve, and some pillowing or bulging of the cover sheets was observed during the high-temperature brazing cycle. By using platens during brazing, however, full-size prototype fuel plates approximately 13 in. long, 4 in. wide, and 0.210 in. thick were successfully constructed. Grids fabricated by both machining techniques were preplated with brazing alloy and then brazed in a dry-hydrogen atmosphere. Hastelloy B platens were used because they have a thermal expansion coefficient lower than that of stainless steel and, consequently, assisted in the attainment of good fitup during brazing.

Each individual compartment in the plate with the conventionally machined grid was subsequently helium-leak checked with a mass spectrometer detector. Thirty-six of the thirty-eight compartments were completely leaktight, while two had very small intercompartmental leaks. The assembly is shown in Fig. 4.28, with leak-checking holes in each compartment, and

---

[27]Maritime Reactor Project Ann. Prog. Rep. Nov. 30, 1960, ORNL-3046, pp. 54–58.

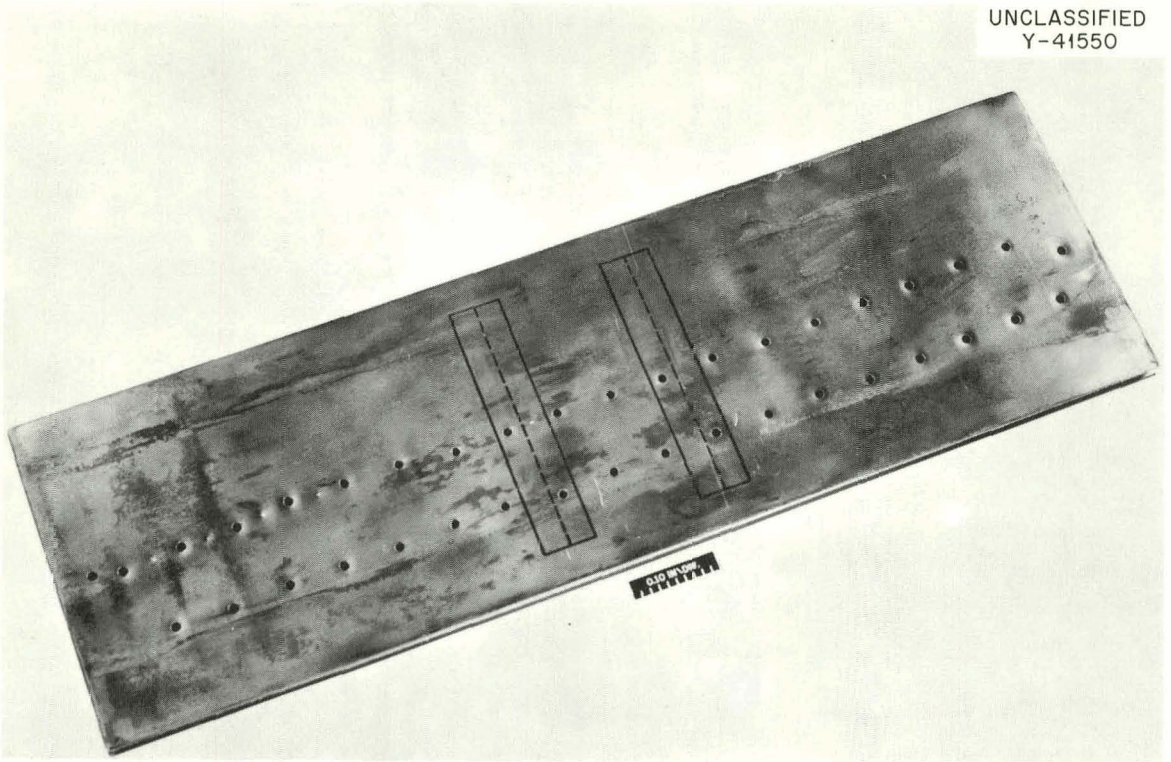

Fig. 4.28. Hydrogen-Brazed Compartmented Fuel Element Showing Location of Compartments Containing Leaks.

the locations of failures are marked. Metallographic evaluations are being conducted to determine the reason for the leakage. The plate with the spark-discharge machined grid has not yet been evaluated.

Gas Evolution from Fused-and-Ground UO_2 (J. T. Lamartine)

During the preparation of swaged fuel-rod clusters containing fused-and-ground UO_2 for irradiation in the ORR pressurized-water loop, it was observed that several of the rods had swelled markedly in the brazing operation, which is performed in hydrogen at 1010°C. Rupture was noted in one rod. Since four similar clusters had previously been fabricated without difficulty,[28] an investigation was initiated to determine the source and nature of gas which could produce sufficient pressure in the fuel rods to cause deformation of the 0.035-in.-thick stainless steel cladding at the brazing temperature.

[28]Ibid., p. 52.

In this investigation, 16 samples of fused UO_2 were outgassed in vacuum to 1010°C. The quantities of gas released in four temperature increments between 0 and 1010°C were measured, and samples collected from each increment were spectrographically analyzed for the major species. The results of these analyses, summarized in Table 4.11, indicate that quantities of gas ranging from 0.025 to 0.400 cm^3/g of UO_2 at standard temperature and pressure were released from fused-and-ground UO_2 at the brazing temperature. In most instances, the major fraction of the released gas was nitrogen. Substantial quantities of CO_2, H_2O, and H_2 were detected also. It is noteworthy that temperatures in excess of 500°C were generally required to remove a major fraction of the gas (see Table 4.11).

It was further learned that the evolved gases were probably present in the UO_2 as adsorbed gas or organically combined nitrogen, since no correlation was observed between the gas-release values and the preoutgassing inorganic nitrogen content of the oxides as determined by Kjeldahl analysis. As a conclusion to the investigation, it was found that the gas content

Table 4.11. Gases Evolved on Heating Fused-and-Ground UO_2

Oxide Lot	Gas Release (cm^3/g) in Indicated Temperature Range					Major Constituents Found by Spectrographic Analysis (%)			
	0–300°C	300–500°C	500–750°C	750–1010°C	Total	N_2 + CO	CO_2	H_2O	H_2
131-117-1	0.002	0.010	0.025	0.035	0.072	23	49	26	
129-19-1	0.011	0.006	0.005	0.005	0.027				91
131-117-2	0.001	0.005	0.007	0.012	0.025	24	38	36	
156-58	0.013	0.040	0.025	0.087	0.165	27		62	
156-50	0.029	0.030	0.012	0.015	0.086	28		62	
A	0.014	0.013	0.013	0.009	0.049	4			93
B	0.003	0.015	0.008	0.050	0.076	42	7		44
C	0.010	0.026	0.015	0.008	0.059	10			81
R					0.40	91[a]			7
S					0.16	87[a]	6		6
S	0.006	0.020	0.020	0.16	0.206	57[a]	25	14	
T	0.020	0.10	0.10	0.16	0.38	74[a]	8		
T	0.020	0.08	0.12	0.17	0.39	72[a]	5		9
U	0.003	0.008	0.020	0.010	0.041	56[a]	14	15	15
V	0.005	0.020	0.030	0.080	0.135	60[a]	22	15	
1-11 C	0.001	0.007	0.006	0.019	0.033	45	30	18	5
179-7-1	0.004	0.007	0.004	0.024	0.039	57	3	6	28
179-6-1	0.002	0.007	0.006	0.020	0.035	48	28	12	11

[a]Mostly nitrogen.

of fused UO_2 could be significantly decreased and that the swelling problem could be eliminated by outgassing the oxide for 24 hr at 1000°C in vacuum prior to use.

Fuel Irradiation Tests

V. O. Haynes W. C. Thurber

Nonpelletized UO_2 fuel is being investigated relative to its suitability for use in a replacement core for the NS SAVANNAH. Irradiation tests are being conducted in the ORR pressurized-water loop. The test specimens are 0.5-in.-o.d. rods consisting of UO_2 clad with type 304 stainless steel of a nominal 0.035-in.-wall thickness. The fueled length of the specimens is about 16 in. The fabrication techniques being investigated are described in the preceding section of this chapter on "Fuel Development."

In the tests, a total of 24 fuel rods will be irradiated in clusters of three in the pressurized-water loop, with high-purity water at 1750 psi and 500°F flowing past the specimens at 10 fps. Typical irradiation specimens are shown in Fig. 4.29, which is a preirradiation photograph of assemblies for experiment No. 3.

The presently planned program for irradiation of nonpelletized UO_2 fuel in the ORR pressurized-water loop is summarized in Table 4.12. In experiments 1 and 3, specimens of hot- and cold-swaged fuel are being studied to determine the effects of swaging temperature, initial UO_2 particle size, UO_2 temperature, and irradiation time. Experiments 4, 5, 6, and 7, as mentioned in preceding sections, are for providing performance information for vibratory-compacted fuel. Two cold-swaged fuel rods are included to furnish information concerning the performance of vibratory-compacted fuel rods relative to swaged fuel rods and to extend the heat rating and burnup data for cold-swaged fuel.

Postirradiation examinations of experiment No. 1 specimens were performed at the GE Vallecitos Atomic Laboratory, and a report on the examinations is being prepared. The examinations have included gamma scans of each rod, dimensional measurements of the rods, analyses of crud adhering

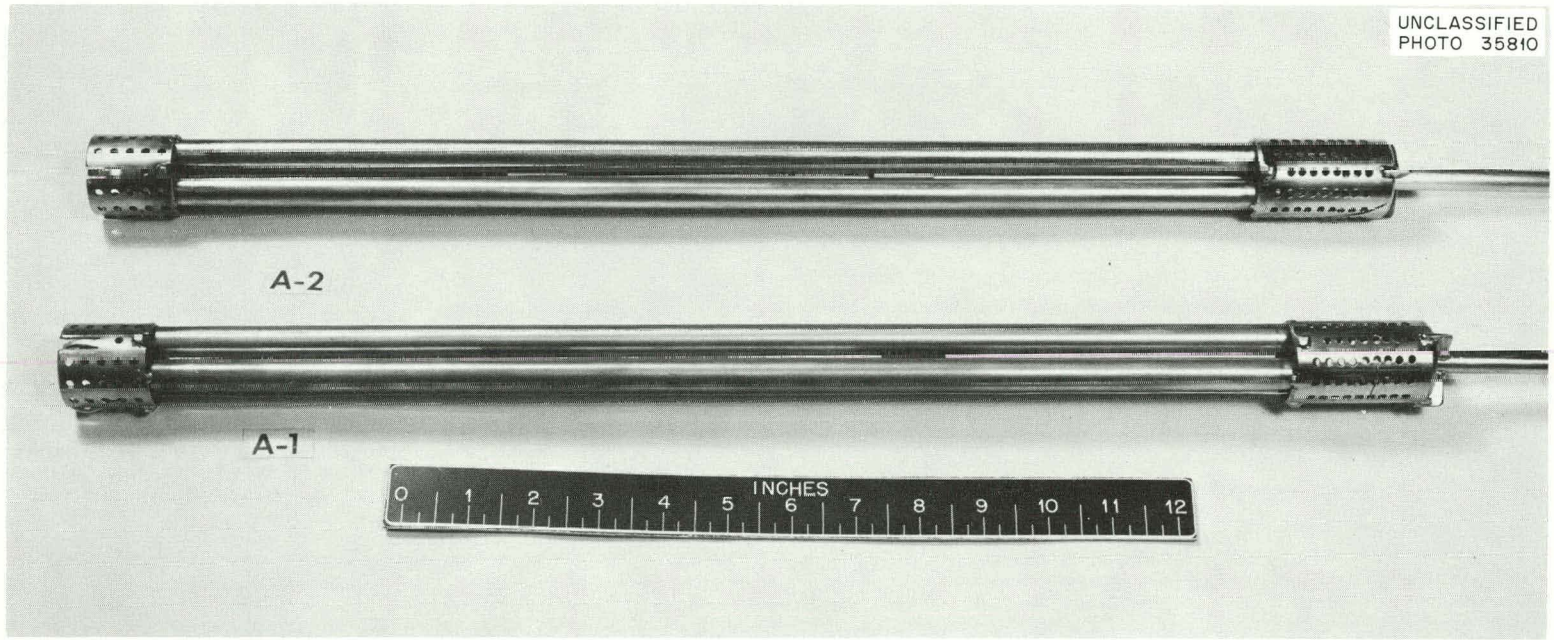

Fig. 4.29. Typical Fuel Rod Specimens for Irradiation in ORR Pressurized-Water Loop.

Table 4.12. Nonsintered UO_2 Fuel Irradiations in the ORR Pressurized-Water Loop

Experiment No.	Number of Rods	Fused-and-Ground UO_2 Fuel		Fuel Fabrication Method	Peak Heat Flux (Btu/hr·ft^2)	Peak Burnup (Mwd/MT of UO_2)	Status
		Particle Size	% of Theoretical Density				
1	2	-20	90	Hot swaged	115 000	1 050	Examination completed
	2	-20 +35	90	Cold swaged	90 000	900	
	2	-170 +325	88	Cold swaged	95 000	1 000	
3		Six rods identical with those for experiment 1			Slightly higher than for experiment 1	Greater than twice experiment 1	Examination started
4	1	-20 +35	89	Cold swaged	200 000	2 500	Irradiation completed
	2	(a)	89	Vibratory compacted	275 000	3 500	
5	1	-20 +35	89	Cold swaged	200 000	7 700	Irradiation in progress, to be completed 6/62
	2	(a)	89	Vibratory compacted	275 000	11 000	
6	3	(a)	89	Vibratory compacted	400 000	5 500	Irradiation in progress, to be completed 2/62
7	3	(a)	89	Vibratory compacted	550 000	7 500	Planned

[a]Distribution: 60% -10 +16 mesh, 15% -70 +100 mesh, 25% -200 mesh.

to rods, burnup analyses based on Cs^{137} and Ce^{144}, fission-gas-release analyses, and metallographic studies.

The gamma scans indicated a peak-to-average burnup of about 1.18 and showed numerous axial discontinuities. These discontinuities have been interpreted to represent small transverse cracks in the fuel body. A photograph of the gamma scan for the highest heat-rating fuel rod of experimental assembly No. 1 is presented in Fig. 4.30. The largest discontinuities were observed in this scan.

The only dimensional changes noted occurred in localized areas 1 to 2 in. from the bottom of rods 1N1, 101, and 1P1 and at 1 in. from the top of rod 1P1. The rod diameter measured about 1% larger after irradiation.

Considerable loose, black crud covered the specimens from end to end in a fairly uniform manner. The crud deposit was possibly heavier at the ends near the support clusters and in the more restricted coolant passages, and the A-2 cluster appeared to have a heavier deposit than the A-1 cluster.

Analyses were made of the Cs^{137}-to-U and Ce^{144}-to-U ratios of peak-burnup fuel sections. The peak burnup values computed from these data are given in Table 4.13.

Release of the fission gas Kr^{85} was measured, and the percentage release was computed based on the burnup values of Table 4.13. The release values are given in Table 4.14.

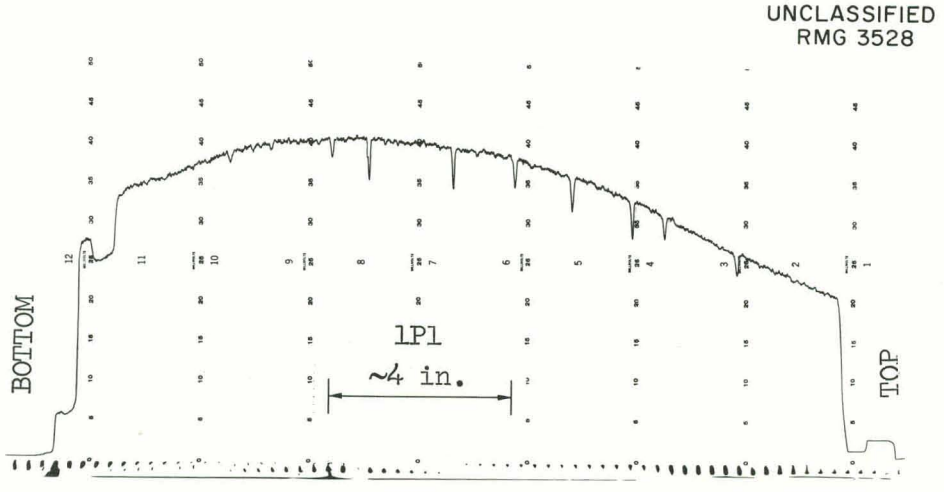

Fig. 4.30. Gamma Scan of Rod 1P1.

Table 4.13. Peak Burnup Values for Experiment No. 1

Rod	Peak Burnup (Mwd/MT of UO_2)	
	From Ce^{144}-to-U Ratio	From Cs^{137}-to-U Ratio
1A1	740	730
1B1	880	900
1C1	1010	950
1N1	840	810
1O1	860	790
1P1	1050	950

Table 4.14. Kr^{85} Release for Experiment No. 1

Rod	Kr^{85} Release (%)	
	From Ce^{144}-to-U Ratio	From Cs^{137}-to-U Ratio
1A1	0.7	0.7
1B1	4.9	4.8
1C1	5.7	6.0
1N1	5.8	6.1
1O1	2.5	2.7
1P1	3.4	3.7

Metallographic examinations were made of eight specimens selected from four rods (1B1, 1N1, 1O1, 1P1), as discussed in the following section, and little, if any, sintering of the fuel body could be detected. A section of the fuel rod having the highest heat rating is shown in Fig. 4.31, and the central portion of the fuel at the same section is shown in Fig. 4.32.

Two 16-rod bundles suitable for irradiation in the Vallecitos Boiling Water Reactor are being fabricated, as described in a preceding section. The proposed test conditions for these bundles include a peak heat flux of 325 000 Btu/hr·ft^2, a maximum burnup of 40 000 Mwd/MT of UO_2; a coolant temperature of 550°F, and a coolant pressure of 1000 psi.

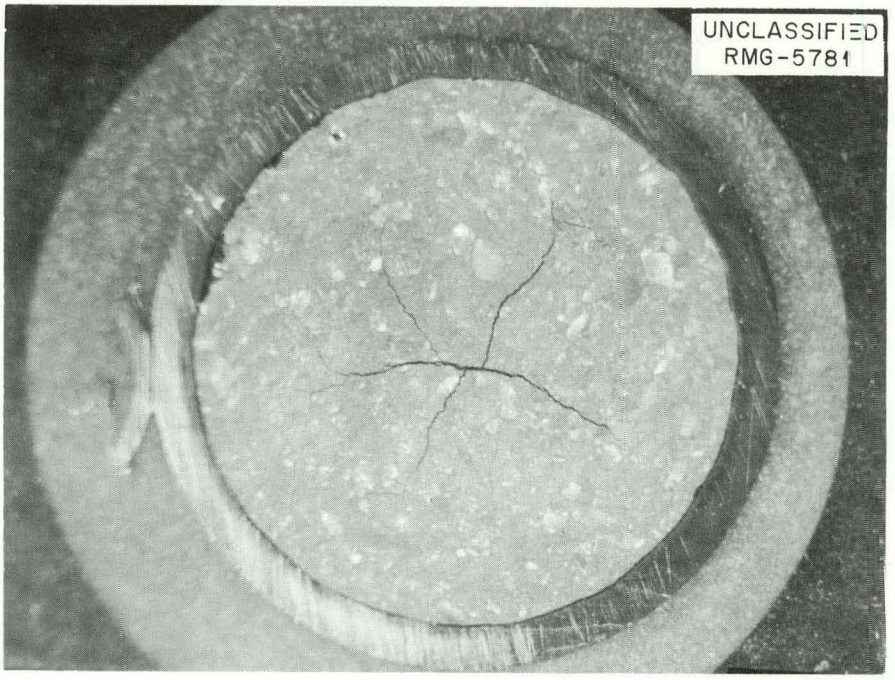

Fig. 4.31. Polished Cross Section of Fuel Rod 1P1. ~7X

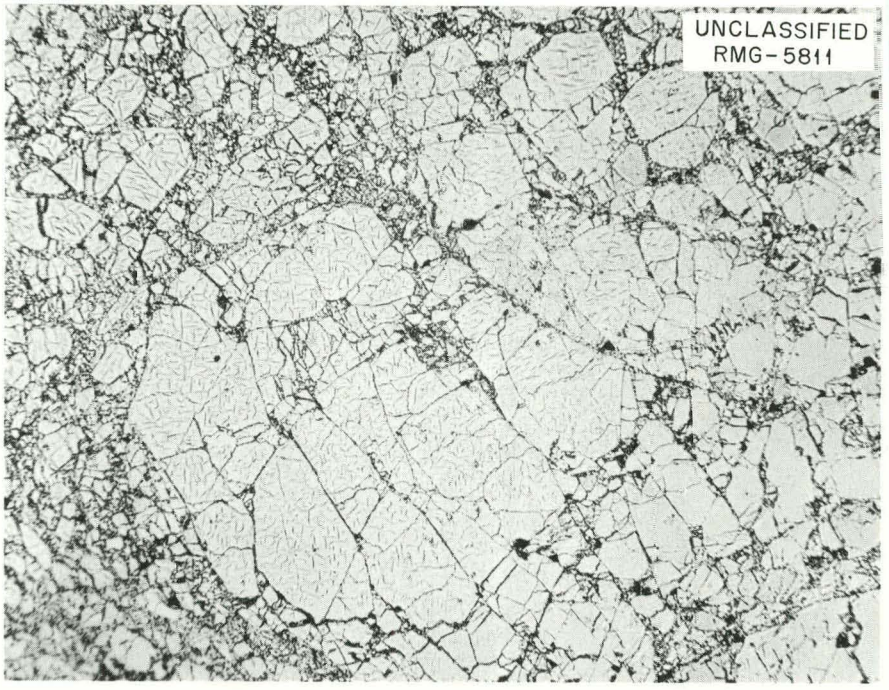

Fig. 4.32. Central Portion of Fuel Rod 1P1. Etchant: HNO_3-H_2O_2. 100X.

Postirradiation Metallographic Examination of Experimental Assembly No. 1

E. L. Long, Jr.

Metallographic examinations have been made of four fuel rods from experimental assembly No. 1, which was irradiated in the ORR pressurized-water loop. The rods were designated 1B1, 1N1, 101, and 1P1. Transverse sections were taken from near the points of maximum burnup, as determined from gamma scans. Top and bottom end plugs and ferrule-to-clad braze joints were also examined. The results of these postirradiation examinations were compared with results of examinations of unirradiated control samples.

The transverse sections from fuel rods 1B1, 1N1, and 101 were taken 8.6, 10, and 13 in., respectively, from the top of the fuel rods. The transverse sample from fuel rod 1P1 was not taken from the peak-flux zone but, rather, at a point 5 in. from the top end plug to include the top ferrule-to-clad braze joint. The sample from rod 1P1 thus represented a section of average burnup. All these samples included both fuel and cladding.

Fuel Rods

In the metallographic examination of the transverse sample from fuel rod 1B1, there was no evidence of corrosion at the outer surface of the type 304L stainless steel clad. A pearlitic structure was noted, however, on the inner surface that extended into the cladding to a depth of approximately 4 mils. The pearlitic structure was also present in the unirradiated control samples and therefore cannot be considered a direct or indirect effect of irradiation. An attempt to identify this phase by x-ray techniques is under way. A typical area of the pearlitic structure is shown in Fig. 4.33.

The UO_2 showed a greater amount of second-phase material (assumed to be uranium nitride) near the periphery than near the center of the fuel rod. There was no evidence of grain growth, recrystallization, or sintering of the UO_2; but, a void was noted along or near the UO_2-to-cladding interface, as can be seen in Fig. 4.33.

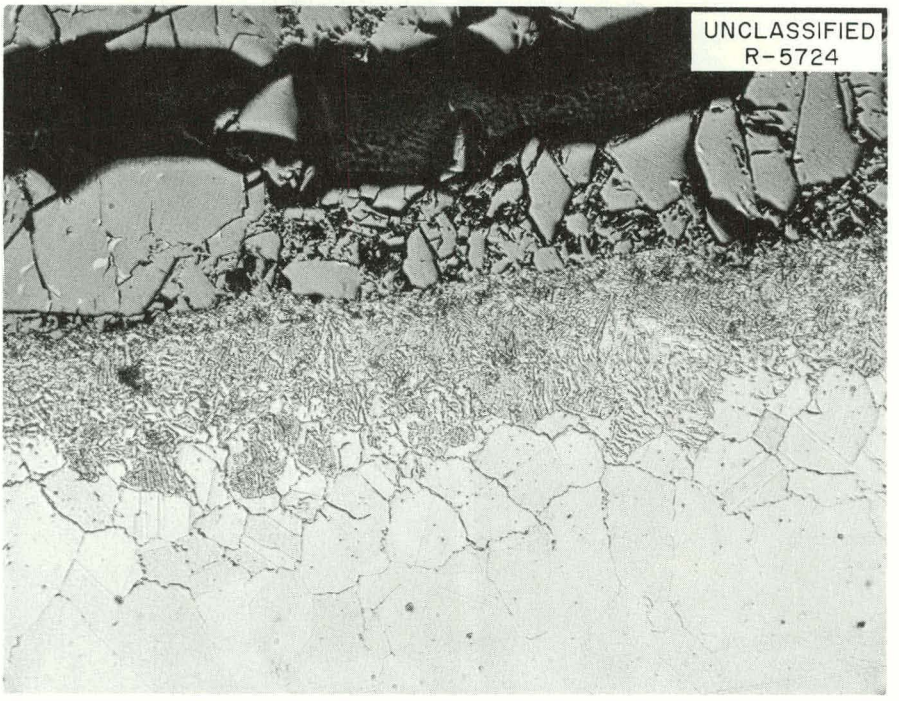

Fig. 4.33. Typical Area from Type 304L Stainless Steel Cladding–UO_2 Interface from Fuel Rod 1B1. Note pearlitic structure in inner surface of cladding. The light phase in the UO_2 is uranium nitride. Etchant: Marble's reagent. 250X

The pearlitic structure found in fuel rod 1B1 was also found in fuel rod 1N1 and varied in depth from 2 to 4 mils. There was no noticeable change in particle size of the UO_2, as compared with that of the unirradiated control sample. The second-phase material that was observed throughout the control was seen only in the outer third of the fuel section of the irradiated specimen. A slight difference noted in the etching characteristics of the UO_2 near the center of the fuel rod is suspected to be associated with the movement of the uranium nitride. The center and outer edge of the fuel are shown in Fig. 4.34.

Pearlitic structure typical of that described was also found in fuel rod 1O1. One important feature of this sample was that no void was found in the region of the UO_2-to-cladding interface for approximately three fourths of the circumference. Here again, the second-phase material was noted only at the outer region of the fuel. The globules that were seen were approximately three times the size of those in the control sample. No grain growth or evidence of sintering was noted.

Fig. 4.34. Representative Areas of the Fuel from Fuel Rod 1N1. Etchant: HNO_3 and H_2O_2. 100X. (a) Outer region of fuel near cladding. (b) Fuel near center.

The pearlitic structure in fuel rod 1P1 was found to an average depth of approximately 2 mils. Complete separation of the UO_2 from the cladding was noted. An acicular structure was present near the center of the fuel rod. This structure is not unlike that seen in many UO_2 pellets from the EGCR irradiation experiments and has been identified as uranium nitride.[29] This second-phase material was present as globules near the cladding. Typical areas at the cladding-to-fuel interface and the center of the fuel rod are shown in Fig. 4.35.

Welds and Cladding

None of the welds examined at the top and bottom end plugs showed any deleterious effects of irradiation; however, excessive penetration was found in one portion of the weld on the bottom end plug of fuel rod 1N1. Penetration of the weld metal into the fuel zone is shown in Fig. 4.36. Conversely, the weld on the top end plug of fuel rod 1N1 showed insufficient penetration. As may be seen in Fig. 4.37, the penetration of the weld metal was only approximately one third of the cladding wall thickness. The pearlitic structure shown penetrates into the weld zone, which indicates that it was formed after fabrication of the fuel rods. Since this structure was present in the unirradiated control samples, it can be concluded that the structure probably was formed during the brazing cycle.

Ferrule-to-Cladding Brazed Joints

The top ferrule-to-cladding brazed joint from the A-2 fuel rod bundle is shown in Fig. 4.38. The appearance of this brazed joint is similar to the appearance of those rated as acceptable in previous investigations of electroless-nickel brazed joints.[30] Cracks may be seen extending through the brittle eutectic in the braze and terminating in the nickel-rich zone. The bottom ferrule-to-cladding brazed joint from the same fuel bundle was also examined and was found to be similar in appearance to the top joint.

---

[29]GCR Quar. Prog. Rep. March 31, 1961, ORNL-3102, pp. 163–174.

[30]J. T. Lamartine and W. C. Thurber, Status Report – Application of Electroless-Nickel Brazing to Tubular Fuel Elements for the N. S. Savannah, ORNL CF-59-6-55, June 2, 1959.

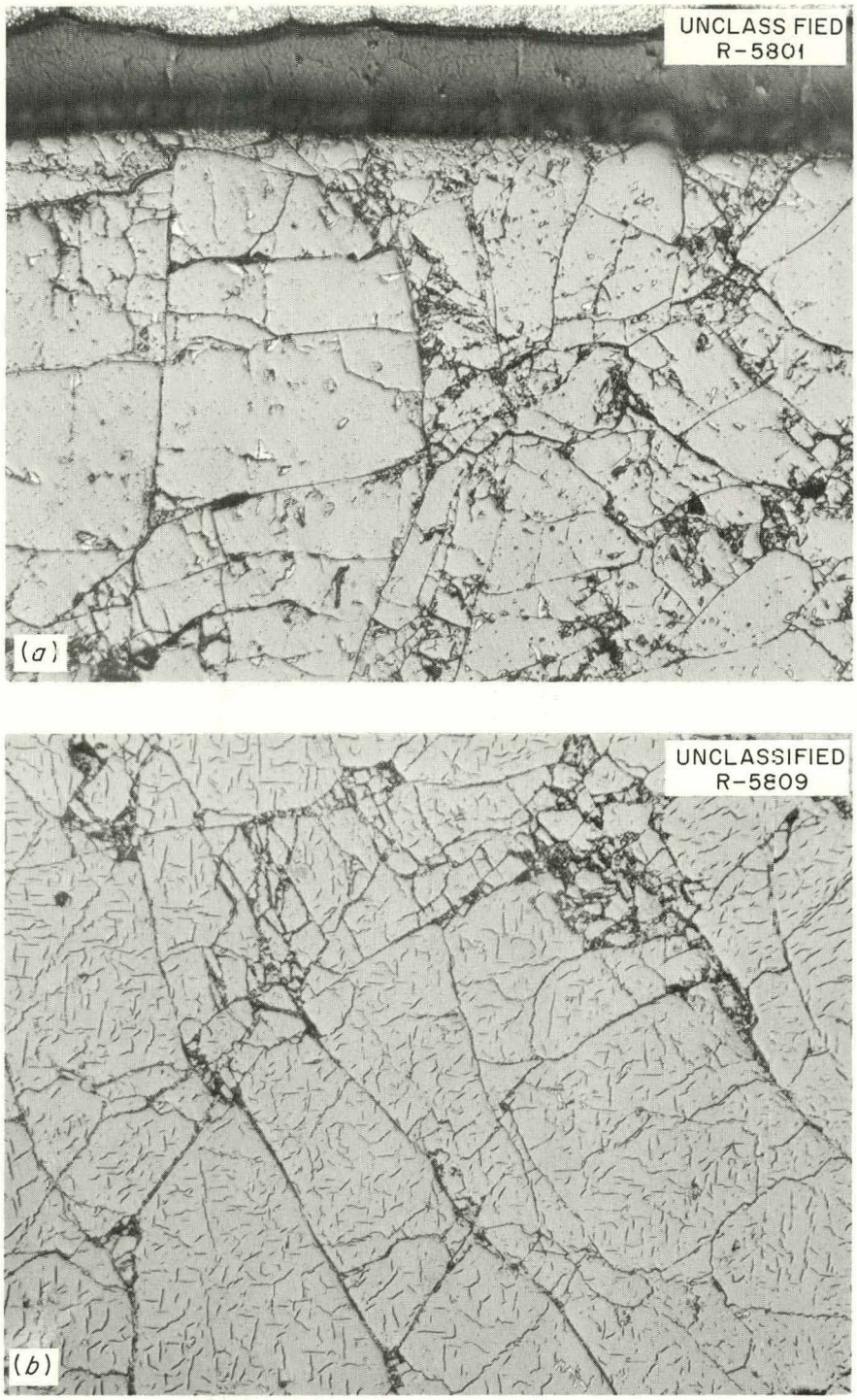

Fig. 4.35. Typical Areas from Fuel Rod 1P1. Etchant: HNO_3 and H_2O_2. 100X. (a) Outer region of fuel near cladding. (b) Fuel near center of rod.

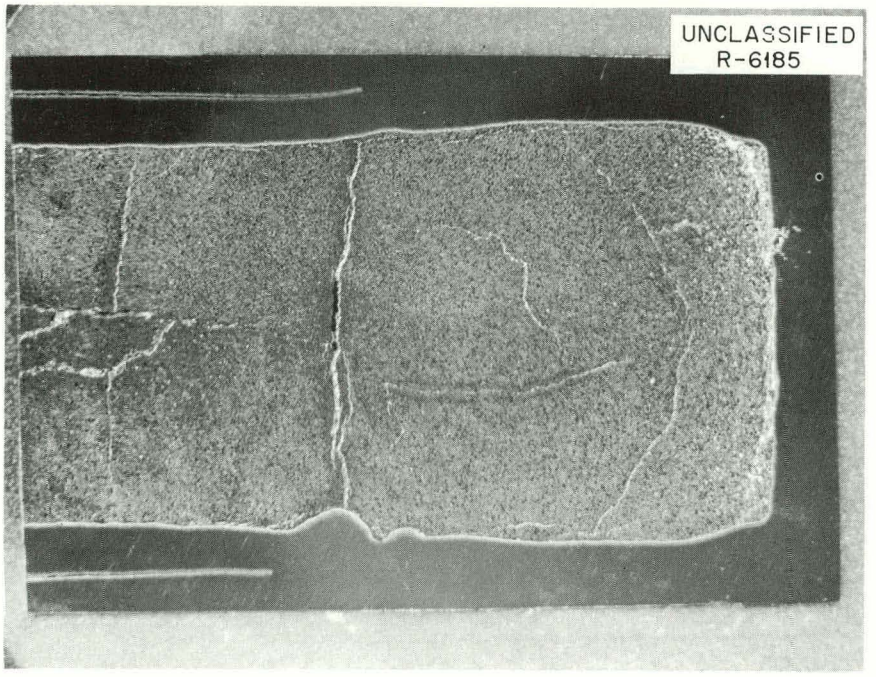

Fig. 4.36. Longitudinal Section of Bottom End Plug in Fuel Rod 1N1. Note excessive penetration of weld metal into fuel. As polished. ~6X

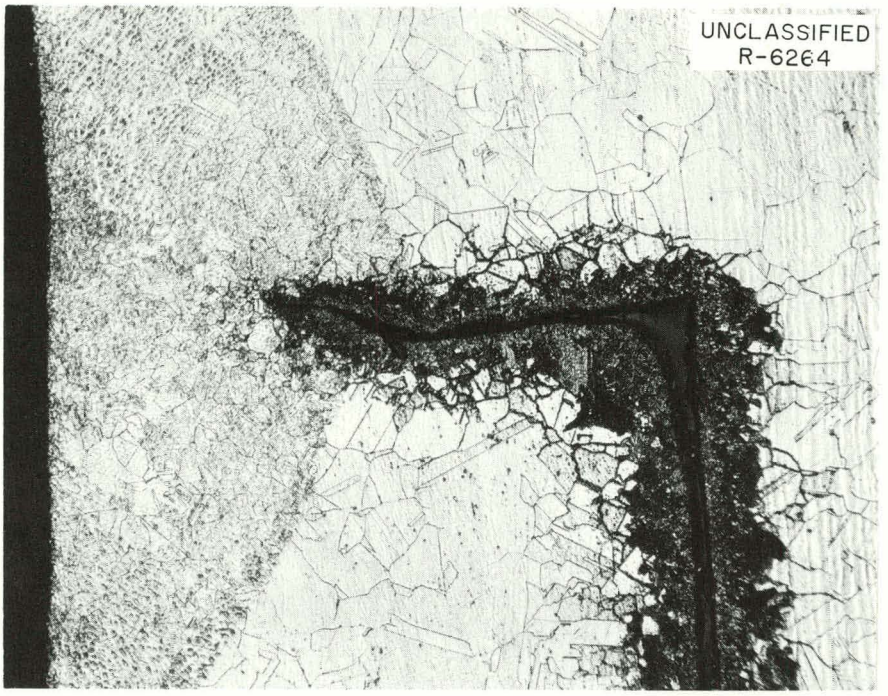

Fig. 4.37. Top End Plug and Cladding Weld Area. Note that pearlitic structure along cladding-to-plug interface extends into weld metal. Etchant: Marble's reagent. 100X

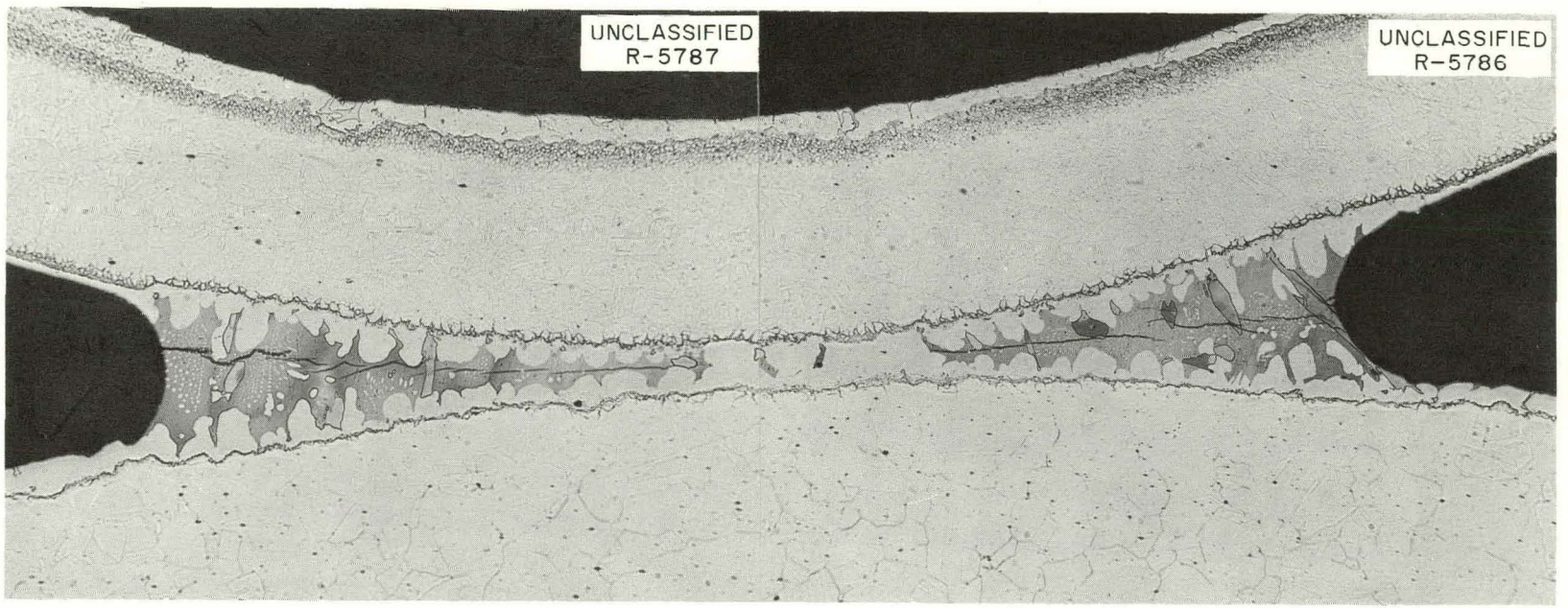

Fig. 4.38. Top Ferrule-to-Cladding Brazed Joint from the A-2 Fuel Bundle. Etchant: 5% chromic acid (electrolytic). 100X

ORNL-3238
UC-80 – Reactor Technology
TID-4500 (17th ed.)

INTERNAL DISTRIBUTION

1. R. E. Adams
2. T. D. Anderson
3. V. E. Anderson (K-25)
4. C. F. Baes, Jr.
5. S. E. Beall
6. R. J. Beaver
7. M. Bender
8. R. G. Berggren
9. D. S. Billington
10. R. E. Blanco
11. E. P. Blizard
12. T. V. Blosser
13. A. L. Boch
14. C. J. Borkowski
15. G. E. Boyd
16. W. E. Browning, Jr.
17. R. B. Briggs
18. F. R. Bruce
19. D. W. Cardwell
20. F. L. Carlsen, Jr.
21. T. E. Cole
22. B. W. Colston
23. J. A. Conlin
24. W. B. Cottrell
25. J. A. Cox
26. F. L. Culler
27. H. N. Culver
28. J. E. Cunningham
29. I. T. Dudley
30. E. P. Epler
31. W. K. Ergen
32. W. S. Ernst, Jr.
33. B. R. Fish
34. A. P. Fraas
35. J. K. Franzreb
36. J. H. Frye, Jr.
37. W. R. Gall
38. R. G. Gilliland
39. B. L. Greenstreet
40. J. C. Griess
41. W. R. Grimes
42. E. E. Gross
43. T. H. Handley
44. J. C. Hart
45. V. O. Haynes
46. M. R. Hill
47. H. W. Hoffman
48. W. H. Jordan
49. S. I. Kaplan
50. P. R. Kasten
51. G. W. Keilholtz
52. O. H. Klepper
53. R. B. Korsmeyer
54. P. G. Lafyatis
55. J. T. Lamartine
56. J. A. Lane
57. C. E. Larson
58. G. W. Leddicotte
59. E. L. Long, Jr.
60. R. N. Lyon
61. H. G. MacPherson
62. W. D. Manly
63. E. R. Mann
64. H. C. McCurdy
65. H. F. McDuffie
66. A. J. Miller
67. E. C. Miller
68. K. Z. Morgan
69. F. H. Neill
70. M. L. Nelson
71. W. R. Osborn
72. P. Patriarca
73. A. M. Perry
74. D. Phillips
75. M. E. Ramsey
76. J. T. Roberts
77. M. W. Rosenthal
78. G. W. Royster, Jr.
79. J. E. Rowe (K-25)
80. A. F. Rupp
81. G. Samuels
82. H. W. Savage
83. A. W. Savolainen
84. L. D. Schaffer
85. J. L. Scott
86. L. R. Shobe

87. O. Sisman
88. M. J. Skinner
89. G. M. Slaughter
90. A. H. Snell
91. I. Spiewak
92. P. E. Stein (Y-12)
93. J. A. Swartout
94. J. W. Tackett
95. W. C. Thurber
96. D. E. Tidwell
97. D. F. Toner
98. D. B. Trauger
99. G. M. Watson
100. A. M. Weinberg
101. M. S. Wechsler
102. C. L. Whitmarsh
103. G. D. Whitman
104. C. E. Winters
105. M. L. Winton
106-107. Central Research Library
108-110. ORNL-Y-12 Technical Library
Document Reference Section
111-132. Laboratory Records Department
133. Laboratory Records, ORNL RC

EXTERNAL DISTRIBUTION

134. Alco Products Inc. (Att: J. G. Gallagher)
135-136. Babcock & Wilcox Company, Atomic Energy Division (Att: W. R. Congdon)
137-139. Babcock & Wilcox Company, Atomic Energy Division (Att: R. T. Schomer)
140-141. Division of Reactor Development (Army Reactors), AEC, Washington (Att: W. C. Gribble)
142-151. Division of Reactor Development (Maritime Reactors), AEC, Washington (Att: E. K. Sullivan)
152. Ebasco Services, Inc., New York (Att: W. C. Stamm)
153. Martin Company, Nuclear Division (Att: J. F. O'Brien)
154. New York Operations Office, AEC (Att: Ira Adler)
155-157. New York Shipbuilding Corporation, Camden, N. J. (Att: M. M. Mann)
158-160. Reactor Division, AEC, ORO (Att: D. F. Cope)
161-162. Research and Development Division, AEC, ORO
163-167. States Marine Lines, Inc. (Att: R. O. Mehann)
168-170. Todd Shipyards Corporation, Nuclear Division (Att: B. W. Winchell)
171. R. W. McNamee, Manager, Research Administration, UCC
172-772. Given distribution as shown in TID-4500 (17th ed.) under Reactor Technology category (75 copies - OTS)